学位論文

Analysis of construction mechanism of medaka telencephalon by post-hatch neurogenesis.
（生後の神経新生を介したメダカ終脳の構築機構の解析）

平成 27 年 12 月博士（理学）申請

東京大学大学院理学系研究科
生物科学専攻

磯江泰子

Contents

Abstract

In vertebrates, the basic brain structure is established during embryonic development. Development of the brain, however, continues after birth/hatch, accompanied by rapid increases in the cell number and brain volume in many species. However, how postnatal/post-hatch neurogenesis contributes to brain construction and the organization of the neural network required for behavioral development remains largely unknown. To address this issue, I used medaka fish (*Oryzias latipes*), a model animal for molecular genetics that exhibits prominent post-hatch brain growth. In teleosts, at least 50% of the neurons in the adult brain are thought to be generated by neurogenesis after hatch. Various social behaviors also develop after hatch in medaka fish. Therefore, I thought that medaka could be an ideal animal model for investigating how post-hatch neurogenesis-mediated brain growth contributes to behavioral development.

In my graduate course studies, I first comprehensively mapped the proliferation zones (proliferation neurogenesis areas) in the medaka brain by bromodeoxyuridine immunohistochemistry using sexually immature fish and found that neurogenesis occurs in multiple brain areas (Chapter 1). I found that post-hatch neurogenesis is affected in *p53* mutants, indicating a role for *p53* in post-hatch neurogenesis. Next, to investigate how neurogenesis contributes to brain construction, I performed a cell-lineage analysis of newly born neurons in the medaka brain (Chapter 2). For this, I used a medaka transgenic (Tg) line (*HuC*:loxP-*DsRed*-loxP-*GFP*), in which the *HuC* promoter drives loxP-*DsRed*-loxP-*GFP* expression specifically in newly born neurons. This allowed me to visualize subsets of newly born neurons derived from a single progenitor neural cell labeled by DsRed. In this study, I focused on the telencephalon, which is considered to be a center for higher brain function, such as learning, memory, sensory

perception, and social cognition in teleosts. Induction of stochastic recombination (removing *DsRed*) by microinjection of Cre mRNA into Tg embryos at the one-cell stage allowed me to visualize single 'clonal units', subsets of newly born neurons derived from a single progenitor neural cell based on their expression of green fluorescent protein. Next, to more efficiently and easily induce stochastic recombination, I established a transgenic line (*HSP*:*Cre*), in which heat shock induces Cre/loxP-recombination in a temporally controlled manner. By mating these two lines (*HSP*:*Cre* and *HuC*:loxP-*DsRed*-loxP-*GFP*), I successfully induced stochastic Cre/loxP-recombination by exposing the Tg embryo to mild heat shock.

Using these Tg lines, I intended to systematically identify clonal units of newly born neurons in the whole telencephalon in medaka fish (Chapter 3). For this, I established an experimental procedure to three-dimensionally visualize the clonal units to compare the structure of the clonal units in multiple samples by observing transparent brains with light-sheet microscopy. Based on these experiments, I found that the telencephalon of medaka comprises approximately 40 clonal units. In addition, I found that individual brain regions that have been traditionally discriminated by anatomic observation comprise multiple clonal units. Importantly, the morphology of the clonal units differed between the dorsal (pallium) and ventral telencephalon (subpallium). In the pallium, clonal units were distributed exclusively to form each compartment (brain region), while in the subpallium, multiple clonal units existed in the same brain region in a mixed pattern. These findings suggest that post-hatch neurogenesis differentially contributes to the construction of the adult brain between the pallium and subpallium.

Next, to investigate possible molecular mechanisms involved in the formation of different clonal units between the pallium and subpallium, I performed an integrative and genome-wide epigenomic analysis (Chapter 4). By performing ATAC-seq, I compared genomic locations of open chromatin, which are associated

with DNA-binding transcription factors, using DNAs extracted from newly born neurons of the pallium and subpallium of the adult medaka brain. By listing possible target genes of the identified transcription factors, multiple genes involved in the axon guidance cascade were suggested to be differentially regulated between the pallium and subpallium. Therefore, it is likely that different molecular mechanisms are involved in neurogenesis-mediated brain construction between the pallium and subpallium in the teleost brain.

The future research plan of this study is to investigate how individual clonal units contribute to behavioral development in medaka fish. For this, it is necessary to induce somatic recombination in a temporally and spatially controlled manner in the medaka brain. To approach this issue, I established a novel experimental procedure to induce Cre-loxP recombination in the medaka brain using the infrared laser-evoked gene operator (IR-LEGO) system (Chapter 5). Using this procedure, I successfully induced Cre/loxP recombination in a single clonal unit by exposing medaka embryos to heat shock.

Finally, to investigate how individual clonal units contribute to behavioral development in medaka fish in future studies, I established a novel behavioral assay to investigate the development of a certain social behavior during the growth from larva to adult (Chapter 6). In the present study, I constructed a behavioral assay system to evaluate visually-mediated approach behavior to conspecifics and showed that the ability to recognize homospecifics/heterospecifics develops during growth from larva to adult in medaka fish.

I expect that my doctoral course studies will contribute to uncover the mechanisms of brain and behavioral development that are mediated by post-hatch/birth neurogenesis and to deepen our understanding of the construction mechanism of the vertebrate brain from the ontogenic and phylogenic viewpoints.

Abbreviations

A: nucleus anterioris of diencephalon

AOT: tractus opticus (optic tract) axialis

Cb: corpus cerebelli

CbSg: stratum granulare of corpus cerebelli

CbSm: stratum moleculare of corpus cerebelli

CbSp: stratum Purkinje of corpus cerebelli

CM: corpus mamillare

D: area dorsalis telencephali

Dc: area centralis of D

Dl: area lateroposterioris of D

Dld: area laterodorsalis of D

Dlp: posterior subdivision of dorsolateral telencephalon

Dlv: ventricular subdivision of dorsolateral telencephalon

Dm: area medialis of D

DOT: tractus opticus (optic tract) dorsalis

Dp: dorsal posterior telencephalon

DT: nucleus tegmentalis dorsalis

ECL: external cell layer of olfactory bulb

EP: epiphysis

ep: ependyma

Fll: fasciculus longitudinalis lateralis

Flm: fasciculus longitudinalis medialis

Flt: fasciculus longitudinalis lateralis telencephali

GL: glomerular layer of olfactory bulb

gc: griseum centrale

Hc: hypothalamus caudalis

Hd: nucleus dorsalis of habenula

HD: hypothalamus periventricularis dorsalis

Hv: nucleus ventralis of habenula

IQ: inferior oblique of nucleus of nervus oculomotorius

IR: inferior rectus of nucleus of nervus oculomotorius

MC: commissural minor

MOT: tractus opticus (optic tract) medialis

MR: medial rectus of nucleus of nervus oculomotorius

NCILP: nucleus centralis posterioris of lobus inferiosis

NDIL: nucleus diffusus of lobus inferioris

NDTL: nucleus diffusus of torus lateralis

NGp: nucleus glomerulosus medialis

ON: nervus olfactorius

OT: optic tectum

Pc: nucleus pretectalis centralis

PGc: nucleus preglomerulosus centralis

PGm: nucleus preglomerulosus medialis

PGZ: periventricular grey zone

PMp: nucleus preopticus magnocellularis pars parvocellularis

PPa: nucleus preopticus periventricularis, anterioris

PPp: nucleus preopticus parvocellularis posterioris

PSi: nucleus pretectalis superficialis pars intermedialis

PSm: nucleus pretectalis superficialis pars medialis

rp/V3: recessus preopticus of ventriculus tertius

RT: nucleus tegmentalis rostralis

SC: nucleus suprachiasmaticus

SGZ: subgranular zone

SVZ: subventricular zone

SR: superior rectus of nucleus of nervus oculomotorius

TA: nucleus tuberis posterioris

TCT: tractus cerebellotectalis

TIT: tractus isthmotectalis

TP: nucleus tuberis posterioris

TS: torus semicircularis

v3: ventriculus tertius

v4: ventriculus quartus

V: area ventralis of the telencephalon

VC: valvula cerebelli

Vd: area dorsalis of V

Vi: area intermedialis of V

Vl: ventral telencephalon, lateral subdivision

VL: nucleus ventrolateralis

VM: nucleus ventromedialis

vm: ventriculus mesencephali

VOT: tractus opticus (optic tract) ventralis

Vp: ventral telencephalon, posterior subdivision

Vv: area ventralis of V

General introduction

Development of social behavior during the growth period after birth/hatch is commonly observed among various vertebrates, from fish to mammals (Mason, 1979; Ball et al., 1993). Adult animals exhibit various social behaviors after sexual maturation, such as mating behaviors (intersexual relationship) and/or male-male competition for mating partners (intrasexual relationship) (Kaidanovich-Beilin et al., 2011; Maekawa et al., 2014). Observations of many species of vertebrates, teleosts (Higashijima et al., 2004), and birds (Bottjer and Arnold 1986) indicate that the social behavior repertoires of larval and sexually immature individuals are much less complex than those of adults. Development of these social behaviors is coordinated with social factors, such as the presence of conspecifics (Engeszer et al., 2007), as well as physiologic and environmental factors (Engeszer et al., 2004; de Kort et al., 2009; Green et al., 2012; Croft et al., 2012; Mangiamele et al., 2013; Snoeren et al., 2014). For example, the shoaling preference of zebrafish is affected by their early social experience with conspecifics (Engeszer et al., 2007). How brain growth and neural development after birth/hatch contribute to the development of social behaviors, however, remains largely unknown.

Most studies of the neural basis underlying brain construction and neural development focus on the embryonic stages. At the embryonic stage, the structure of the vertebrate brain is anatomically subdivided into five parts: the telencephalon, diencephalon, mesencephalon, metencephalon, and myelencephalon (Kandel et al., 2012). The expression of a combination of genes regulates the development of individual subdivisions, which appears to be conserved among vertebrates: *Otx2, Pax6,* and *Six3* in the telencephalon (Cobos I, et al., 2001; Abellán A, et al., 2009; Moreno N et al., 2009; Fernandez AS, et al., 1998; Medina L, et al. 2014); *Otx2, Pax6* and *Irx3* in the diencephalon (Martinez-Ferre A et al., 2012); and *Gbx2, Pax2* and *Irx3* in the

mesencephalon (Zervas M et al., 2005); For ventro-dorsal regionalization, *Wnts* and *Fgf8 are* expressed in the dorsal region, while *Shh and Nkx2.1* are expressed in the ventral region (Huang X et al., 2007). In contrast to the vast number of studies of embryonic neural development, little attention has been payed on the molecular mechanisms underlying brain and neural development during growth.

Some studies of the neural development after birth/hatch have focused on postnatal neurogenesis, which may have an important role in the development of social behavior after birth. For example, in mice, adult neurogenesis is restricted to two areas, the subventricular zone (SVZ), whose neurons integrate into the hippocampus, and the subgranular zone (SGZ), whose neurons integrate into the olfactory bulb (Oosumi et al., 2010; Seki et al., 2010). Female mice with genetic impairment in postnatal neurogenesis cannot discriminate a dominant male (Mak et al., 2007) and a familiar male (Wu et al., 2013). Also, mice reared in a socially poor environment exhibit poor neurogenesis and deficient social behavior (Fowler et al., 2002). Postnatal neurogenesis is suggested to be necessary for restoration and maintenance of the fine neural network in the olfactory bulb (Cummings et al., 2014). However, the neural networks required for the development of social cognition are unknown.

In the teleost fish, the brain volume and cell number dramatically increase after hatch. For example, the brain cell number of the adult zebrafish is 5~10 times greater than that of larval fish just after hatch, indicating that post-hatch neurogenesis prominently contributes to brain construction during the growth period after birth/hatch. To study the significance of post-hatch neurogenesis for the development of social cognition, we focused on medaka fish (*Oryzias latipes*) as an animal model, because adult medaka fish exhibit complex social behaviors and the development of social behaviors during the growth period after birth/hatch can be easily observed. For example, the adult female medaka can visually discriminate individual males and demonstrate a preference when they mate (Okuyama et al., 2014). In addition, medaka

brains show prominent post-hatch brain growth. A previous study identified 17 brain regions in which postnatal neurogenesis occurs, and as many as 5 of these regions are located in telencephalon (Kuroyanagi and Okuyama T et al., 2010). Therefore, I thought that these characteristics would make medaka fish a suitable animal model to study the relation between post birth/hatch neurogenesis and social behavior development.

In this doctoral thesis, I focused especially on the telencephalon. Based on a comprehensive study of gene expression from fish to mammals (88 species), the "social neural network (12 brain regions important for social decision-making)" is suggested to be conserved among vertebrates. Six brain regions of the "social neural network" are located in the telencephalon (O'Connell LA and Hoffmann, 2011, 2012). The small volume of the fish telencephalon simplifies the investigation of the social neural network in the whole telencephalon, compared with mammals.

First, to investigate areas of post-hatch neurogenesis in the telencephalon in juvenile fish during the growth period, I mapped areas of proliferation by bromodeoxyuridine immunohistochemistry. I also performed a mutant analysis to search for genes required for post-hatch neurogenesis and found that *p53* mutants were deficient in post-hatch neurogenesis (Chapter 1). However, investigating the relation between post-hatch neurogenesis and behavioral development using this mutant alone was difficult, because *p53* is broadly expressed in the whole body of medaka fish. Therefore, in my doctoral course, I established a genetic tool to induce the expression of an exogenous gene only in newly born neurons in the adult brain. Here I used a transgenic medaka fish (*HuC*:loxp-*DsRed*-loxp-*GFP*) that drives the expression of an exogenous gene (DsRed) in newly born neurons with a pan-neuronal marker gene (*HuC*) promoter. In addition, Cre/loxP recombination enabled us to drive the expression of another exogenous gene (green fluorescent protein) in a subpopulation of newly born neurons. Using this transgenic line, I found that clonal units

(subpopulations of newly born neurons derived from the same neural stem cell) could be visualized by the induction of random Cre/loxP recombination during embryogenesis (Chapter 2). Interestingly some clonal units seemed compartmentalized in the telencephalon. This finding led me to hypothesize that the adult brain is formed by a composition of clonal units of newly born neurons that are generated during the growth stage. To further test this hypothesis, I conducted a systematic analysis of the structure of clonal units in the whole telencephalon (Chapter 3). Then, I performed genome-wide mapping of locations of open chromatin to examine the regulation of gene expression of newly born neurons in the telencephalon (Chapter 4).

Finally, I established two methods to further investigate how individual clonal units contribute to behavioral development during the growth stage. First, I established a novel genetic tool to induce Cre/loxP recombination in neural stem cells at the single-cell level with an infrared laser (Chapter 5). Next, I established a novel behavioral system to compare social cognition of medaka fish among larval, juvenile, and adult medaka and evaluated the development of social cognition during the growth stage (Chapter 6). These methods will contribute to the identification of clonal units required for development of social cognition and clarify the neural basis underlying the contribution of post-hatch neurogenesis to the development of social cognition, which has been poorly understood.

Chapter 1

Post-hatch neurogenesis pattern description and *p53* mutants in medaka fish (*Oryzias latipes*).

Introduction

In the adult brain of teleosts, most proliferating cells are observed in well-defined zones of the brain (called proliferation zones) (Chapouton P et al., 2007). The whole brain of teleosts, such as medaka (*Oryzias latipes*) (Kuroyanagi Y et al., 2010), zebrafish (*Danio rerio*) (Zupanc GK et al., 2010), gymnotiform fish (*Apteronotus leptorhynchus*) (Zupanc GK et al., 1995), and three-spined stickleback (*Gasterosteus aculeatus*) (Ekstrom P et al., 2001), contains a large number of proliferation zones. A previous study identified 17 proliferation zones (Zones A–Q) in the adult medaka brain using sexually mature fish (age, more than 3 months) and demonstrated that there is persistent cell proliferation in these brain regions in the adult brain, irrespective of sex, body color, or growth environment (Kuroyanagi Y et al., 2010). Further, the distribution of proliferation zones is largely conserved among some fish species (Kuroyanagi Y et al., 2010), suggesting that this distribution in the adult teleost brain is important for the maintenance and development of the fundamental structure of fish brains (Kuroyanagi Y et al., 2010). In Chapter 1, I mapped areas of neurogenesis in the whole brain of juvenile medaka fish during the growth stage and compared the proliferation zones with those in adult fish. I found that the post-hatch neurogenesis required the presence of *p53*.

Materials & Methods

Fish

Medaka fish (*Oryzias latipes*), Cab strain and p53 mutants (Taniguchi Y et al., 2006), were maintained in groups in plastic aquariums (12 cm × 13 cm × 19 cm). Juvenile medaka fish (~1 month after hatching, body length 15 mm) selected according to the previously described definition (Kinoshita M et al., 2009) were used for immunohistochemistry and *in situ* hybridization studies.

Detection of mitotic cells in the juvenile medaka brain

The detection of mitotic cells was performed as described previously (Kuroyanagi Y, et al. 2010). Dividing cells were labeled with 5-bromo-29-deoxyuridine (BrdU), by exposure to water containing 1 g/L BrdU (Sigma Aldrich, Tokyo) for 4 hours. BrdU-positive cells were detected by anti-BrdU immunohistochemistry. Paraffin sections (10-mm thick) were cut with a microtome (LR-85, Yamato Kohki, Tokyo). Immunostaining was performed following standard procedures. Cell nuclei were detected with DAPI staining (Invitrogen, Tokyo). BrdU-positive cells were counted as described previously (Kuroyanagi Y et al., 2010).

TUNEL (TdT-mediated dUTP-biotin nick-end labeling) staining

Medaka brains were fixed in 4% paraformaldehyde (prepared in phosphate buffer saline) overnight and embedded in paraffin. Each brain was sliced into 10-μm sections. Apoptotic cells were detected using a DeadEnd^{TM} Fluorometric TUNEL System (Promega, Tokyo), according to the manufacturer's protocol.

In situ hybridization

In situ hybridization of tissue sections was performed as described previously (Okuyama T et al., 2011; Suehiro Y et al., 2009). The p53 cDNA fragment was amplified with forward primer 5′-TGTTACATTTTATAGCTGTGGAGCA-3′ and reverse primer 5′-TTGGGCTGAAAACAGCACAACCATAGTT-3′ using cDNA clone number orbr44c15 (Medaka National BioResource Project, Sasado T, et al. 2010) as a template. The digoxigenin (DIG)-labeled riboprobes were synthesized by T7 or SP6 polymerase with a DIG labeling mix (Roche, Tokyo) from a template containing the p53 cDNA fragment. Micrographs were obtained with a BX50 optical microscope (Olympus, Tokyo). The micrographs were processed with Photoshop software (Adobe, San Jose, CA).

TUNEL (TdT-mediated dUTP-biotin nick-end labeling) staining

Medaka brains were fixed in 4% paraformaldehyde (prepared in phosphate buffer saline) overnight and embedded in paraffin. Each brain was sliced into 10-μm sections. Apoptotic cells were detected using a DeadEndTM Fluorometric TUNEL System (Promega, Tokyo), according to the manufacturer's protocol.

Results

Distribution of proliferation zones in brains of juvenile medaka fish

The cell proliferation zones in the whole brain of juvenile medaka have not yet been described in detail. I mapped the proliferation zones in juvenile medaka (~1 month old, body length 15 mm) by identifying mitotic cells incorporating BrdU. Based on the distribution of DAPI staining and the medaka brain atlas (Anken R et al., 1998), I identified the locations of the paraffin sections in the whole brain. I then mapped the BrdU-positive cells and identified 18 proliferation zones, A–L and N–S (**Figure 1, 2**). Sixteen zones (A–L and N–Q), were identical to those previously identified in sexually mature medaka (Kuroyanagi Y and Okuyama T et al., 2010). In the present study, I could not confirm that there is a proliferation zone in the pituitary gland (zone M) previously identified in mature fish, as the pituitary gland is likely to be separate from the whole brain in the juvenile fish. The 16 zones (A–L and N–Q) were mapped to the telencephalon (zones A–D), preoptic area (zones E and F), pineal body (zone G), habenular nucleus (zone H), ventromedial nucleus (zone I), optic tectum (zones J and K), marginal zone of the third ventricular zone (zone L), hypothalamus (zone N), and cerebellum (zones O–Q) (**Figure 3**). The 2 additional zones (R and S) were identified in the periventricular grey zone (layer 3) and ependyme, respectively, which were not previously found in the mature fish (Kuroyanagi Y and Okuyama T et al., 2010), suggesting that these 2 proliferation zones might disappear or integrate into the surrounding proliferation zones during the sexual maturation (**Figure 1**).

Distribution of p53-expressing cells in brains of juvenile medaka fish

To elucidate the molecular basis underlying cell proliferation in the medaka brain, I

focused on medaka p53 (Taniguchi Y et al., 2006). p53 is expressed in proliferating and newly formed neurons of the adult murine brain (Campagne MV et al., 1998). To examine whether medaka p53-expressing cells were present in the proliferation zones, I performed in situ hybridization for detecting p53 transcripts and demonstrated that medaka p53 was expressed selectively in at least 12 zones (zones A–E, H–K, N, P, and Q) (**Figure 4**).

The p53 mutation had no effect on either the distribution of the proliferating zones or the number of proliferating cells

To examine whether p53 is involved in cell proliferation in the medaka brain, I mapped proliferation zones using two p53 mutant strains (Taniguchi Y et al., 2006). The p53E241X allele has a G to T substitution that changes Glu241 to a stop codon, and the p53Y186X allele has a T to A substitution that changes Tyr186 to a stop codon (Taniguchi Y et al., 2006). The two mutated p53 genes encode truncated proteins that terminate within a DNA-binding domain. These proteins lack the nuclear localization signal and tetramerization domain required for full activity. Thus, these nonsense mutations probably lead to a null phenotype (Taniguchi Y et al., 2006). I found the 18 proliferation zones in the two mutant strains, p53Y186X/Y186X (**Figure 5**) and p53E241X/Y186X (data not shown), indicating that loss of p53 has no effect on the distribution of proliferation zones. To examine whether the number of proliferating cells was affected by the p53 null mutation, I counted the number of BrdU-positive cells in the entire telencephalon (zones A–D). There was no significant difference in BrdU-positive cells between the wild-type (WT) (average ± SE, 2316 ± 598; n = 4), p53Y186X/Y186X mutant (1849 ± 248; n = 4), or p53E241X/E241X mutant (1728 ± 366; n = 3) (**Figure 6D and F**).

The p53 mutation led to decreased numbers of differentiated progenitors 1 week after BrdU exposure

To determine whether p53 mutation affects survival and/or proliferation of progeny cells, I compared the distribution pattern of differentiated newborn cells in the brains of WT (Cab strain) and p53Y186X/Y186X mutant medaka. One week after BrdU exposure, BrdU-positive cells migrated from the proliferation zones (**Figure 6E**) in the telencephalon of both WT and mutant strains, suggesting that there is no significant difference in the migration pattern between the 2 strains. However, in some brain regions, such as the telencephalon (zone C) (**Figure 6E**) and hypothalamus (zone N) (**Figure 7B**), the number of BrdU-positive neurons seemed to reduce in the mutant strain compared to the WT. Next, I quantified the number of BrdU-positive cells in WT (Cab strain), p53E241X/E241X, and p53Y186X/Y186X in the telencephalon (zones A–D). In the WT, the number of BrdU-positive cells 1 week after BrdU exposure (6300 ± 535, average ± S.E, n = 4) increased over two-fold (**Figure 6F**), suggesting proliferation of the migrated progenitors. In contrast, there was no significant increase in BrdU-positive cells 1 week after BrdU exposure in p53Y186X/Y186X or p53E241X/E241X mutants (3596 ± 572 and 2378 ± 560, respectively). These results raised two possibilities: (1) the p53 mutation enhanced cell death of differentiated progenitors (neuroblasts) or (2) the p53 mutation repressed neuroblast proliferation and/or repressed differentiation of stem cells to an active, proliferating, neuroblast subpopulation. To examine whether cell death was enhanced in the p53 mutant strains, I compared TUNEL-positive cells in the telencephalon of WT and p53 mutants. The number of TUNEL-positive cells was far less than the number of BrdU-positive cells in both WT and p53 mutants, with no difference between the WT and p53 mutants (**Figure 8**). I confirmed that TUNEL-positive signals were localized in nuclei stained with DAPI (**Figure 8A**), and numerous

TUNEL-positive cells were detected when using medaka pancreas sections, which are known to be susceptible to apoptosis (Sarela AI et al., 2002) (**Figure 9**).

Discussion

In the present study, I confirmed that neurogenesis broadly occurs in the telencephalon of juvenile medaka, suggesting that post-hatch neurogenesis contributes to development of the telencephalon. I also demonstrated that the p53 mutation did not affect the number of BrdU-positive cells immediately after BrdU exposure. In the SGZ of murine brains, adult neurogenesis originates from radial glia-like stem cells (Type 1 cells) through a proliferating stage (Type 2 cells) generating neuroblasts (Type 3 cells) and dentate granule interneurons (Seri B et al., 2004). This finding strongly suggests that loss of medaka p53 did not affect highly proliferating progenitors, which correspond to Type 1 and 2 cells. This seems inconsistent with a previous study indicating that genetic ablation of p53 enhanced proliferation of stem cells in the adult murine brain (Meletis K et al., 2006). There was no defect in stem cells in the p53 mutant medaka brain. Most mice, zebrafish, and medaka with p53 function defects develop without any obvious morphological defects (Tanigushi Y et al., 2006; Seri B et al., 2004; Jacobs WB et al., 2006; Danilova N et al., 2008. Zupanc GK et al., 2011, 2005), as p53 family proteins are redundant and can compensate for each other in various organs. These results imply that other p53 family members may compensate for a p53 deficiency in medaka brain stem cells.

Furthermore, I showed that the number of newborn cells that migrate from the proliferation zones increased during the 1-week period after BrdU exposure in a p53-dependent manner. These data suggested that p53 positively regulated the number of migrating progenitors, which may correspond to Type 3 cells (neuroblasts). Dividing neuroblasts are also found in the cerebellum (zone Q) of the zebrafish adult brain (Zupanc GK et al., 2011). The shift in the distribution of BrdU-positive cells from the proliferation zone into the granule cell layers is accompanied by an increase in the number of labeled cells (Zupanc GK et al., 2005). In the murine brain, there is

some evidence for the proliferation of migrating neuroblasts (Saghatelyan A et al., 2004), which originate from stem cells located in the SVZ of the lateral ventricles, moving along the rostral migratory stream. To determine which subpopulation of progenitor cells was regulated by p53, it will be crucial to characterize the subtype and maturation sequence of progenitor cells in the medaka brain.

Positive regulation of p53 in adult medaka brain neurogenesis appears to be the opposite of what is observed in murine p53 mutants (Meletis K et al., 2006; Jacobs WB et al., 2006), where p53 negatively regulates neurogenesis. One possible explanation is that the p53 N-truncated isoform, which has the opposite effect, may function in the medaka brain. In mice and zebrafish, the p53 family genes (including p63 and p73) have 2 isoforms—full length and N-truncated—with an alternative transcriptional start site (Gil-Perotin S et al., 2011; Meltis K et al., 2006; Talos F et al., 2010). Because the latter isoform lacks a transactivation domain, it is thought to function in a dominant-negative fashion to inhibit the transcriptional activity of full-length p53 family members. In the murine brain, p53 family proteins interact with each other in a cell-type/stage-specific manner and coordinated expression of the 2 isoforms is required for stem cell maintenance in adult neurogenesis (Gil-Perotin S et al., 2011; Meltis K et al., 2006; Talos F et al., 2010; Fletcher RB et al., 2011). As positive regulation of p53 in neurogenesis has not been reported in the murine brain, a p53 study using medaka may shed a light on a novel mechanism underlying adult neurogenesis. Gene mutation effects on post-hatch neurogenesis only using mutants are generally difficult to investigate. To study the relationship between post-hatch neurogenesis and behavior, it is necessary to focus the defect only in the brain. Therefore, in the following chapters, I used genetic tools to modify the gene expression in newly born neurons and focused on post-hatch brain development.

Chapter 2

Visualization of clonal units of newly born neurons in the telencephalon of medaka fish (*Oryzias latipes*).

Introduction

Genetic mosaic analysis is a powerful tool in the fields of neuroscience and developmental biology for labeling a subset of neurons, tracing cell-lineage, and modulating neuronal function (Nakazawa N et al., 2012; Kao CF et al., 2012; Lee T et al., 2001; Fox DT et al., 2008). The recent combination of Cre/loxP recombination and optogenetic tools allows for specific modulation of selected neurons within complex neural tissues (Yizhar O et al., 2011; Luo L et al., 2008). *Cre* recombinase induction can be spatially controlled by cell type-specific promoters/enhancers and site-specific viral infection (Suehiro Y et al., 2010; Kawakami K et al., 2010). Site-specific viral infection requires, however, invasive surgical procedures, which also limits free access to the entire brain.

Thus, the development of noninvasive methods for Cre/loxP recombination will increase neural population available for mosaic analyses of the vertebrate nervous system. To address this issue, I adopted a heat-inducible Cre/loxP gene induction system in medaka fish. Medaka embryos have high temperature tolerance (4–35°C) compared to zebrafish (25–33°C) (Westerfield M., 2010), allowing for various temperature-mediated treatments (Wittbrodt J et al., 2002). In addition, an artificial heat-shock promoter (HSP) comprising multimerized heat shock elements has very low background activity and no leak in medaka fish (Bajoghli B et al., 2004). To my knowledge, however, there are no reports of its application to neural tissues in medaka fish.

To examine whether the heat-inducible Cre/loxP gene induction system works in the medaka nervous system, I used transgenic (Tg) medaka, generated by Mr. Hoki and Dr. Okuyama, in which neural progenitors and young neurons are labeled by fluorescent signals using the promoter regions of medaka *HuC*. *HuC* belongs to a family of vertebrate neuronal-specific genes homologous to the Drosophila *elav* and

serves as an early marker of differentiating neurons (Good PJ, 1995; Hinman MN et al., 2008). Zebrafish *HuC* is expressed in neuronal precursor cells during embryogenesis, and then high expression levels persist in most regions of post-hatching and larval brain (Kim CH et al., 1996; Grandel H et al., 2006). Thus, the zebrafish *HuC* promoter is widely used for visualizing and/or modifying the function of neural circuits in juvenile fish (Sato T et al., 2006). The *HuC* promoter is also applicable for visualizing the differentiation process during adult neurogenesis, as *HuC* expression is restricted to newborn and differentiating neurons in the adult zebrafish brain (Grandel H et al., 2006; Kizil C et al., 2012).

In this chapter, I demonstrated that stochastic Cre recombination during embryogenesis allowed for visualization of clonally-related cells in compartmentalized regions of the telencephalon of the adult medaka brain. Then I showed that heat-inducible Cre/loxp recombination worked in the medaka fish nervous system.

Materials & Methods

Ethics statement

All experiments in this chapter were conducted using protocols approved by the Animal Care and Use Committee of the University of Tokyo (permit number: 12-07). All surgery was performed under cold anesthesia, and all efforts were made to minimize suffering.

Fish and breeding conditions

Medaka fish (*Oryzias latipes*, drR strain) and all Tg lines, Tg (*HuC*:loxP-*DsRed*-loxP-*GFP)* and Tg (*HSP*:*Cre*), were maintained in their respective groups in plastic aquariums (12 cm X 13 cm X 19 cm). All fish were hatched and bred in our laboratory. The water temperature was maintained at ~28°C and the light was provided by fluorescent lamps for 14 h per day (08:00 to 22:00).

Tg (HuC:loxP-DsRed-loxP-GFP)

The medaka *HuC* promoter was estimated by comparing the medaka genome with the *HuC* promoter of zebrafish. The medaka *HuC* promoter fragments were polymerase chain reaction-amplified from bacterial artificial chromosome containing the medaka *HuC* genomic region (clone name; ola1-o12-D12, NBRP medaka) with KOD DNA polymerase (TOYOBO) and the following sets of primers carrying the indicated restriction enzyme sites (underlined): 5'-CCGCTCGAGCGGTTTTGTTGCACCGCTAATGTTAGG-3' and 5'-TCCCCGCGGGGAGTACAATGAAAGAAATCTAGGTCC-3', which contain the recognition sites for *Xho*I and *Sac*II, respectively. ploxP-*DsRed*-loxP-*EGFP* plasmid was obtained from Prof. Tanaka (National Institute for Basic Biology) (Nakamura S et al., 2010).

Tg (HSP:Cre/Crs:BFP)

The dual expression vector, pPBIS19-*mgfc*:Tag*BFP*-8xHSE:*Cre* containing fused gene of Cre recombinase with N-terminal nuclear localization sequence and the red fluorescent protein mCherry under the control of artificial heat shock inducible promoter (Bajoghli B et al., 2010). This plasmid also had TagBFP (Wako Junyaku Kogyo Co. Ltd., Osaka, Japan) gene under the control of a mouse *gamma F crystalline* promoter (Vopalensky P et al., 2010) for selecting the proper transgenic lines. It allowed me to select the embryos carrying *HSP*:*Cre* transgene by blue fluorescence of their eyes without heat treatment. Insulators were inserted between the polyA sequence under the control of *HSP* promoter and TR3 and also inserted into the boundary region of the two promoters, *HSP* and *Crystalline* to prevent position-effects of the transgenes (**Figure 16**). The F1 embryos from wild type and vector-injected F0 were raised to sexual maturity and screened for germline transmission by a fluorescent microscopy examining BFP expression.

Observation of fluorescent signals in brains slices of Tg line (HuC:loxP-DsRed-loxP-GFP)

Fixed brains were washed in phosphate buffered saline (PBS) containing 0.5% Triton (PBST) and incubated in Sca*l*eA2 solution (4 M urea, 10% (wt/vol) glycerol and 0.1% (wt/vol) Triton X-100 (Hama H et al., 2011)) at room temperature for 3 h. The brains were washed again in 0.5% PBST and embedded in 4% agarose gel/PBS. Coronal slices (120 μm thick) were then cut with Vibroslicer (VT 1000S, Leica). Fluorescent signals were imaged using a confocal laser-scanning microscope (LSM710; Zeiss). Volume-rendered images were displayed using FluoRender (http://www.fluorender.com).

Immunohistochemistry

Immunostaining was performed on 14-μm cryosections. Whole brains were embedded in OCT compound (Sakura Tissue Tek) and cut using Cryostat (Leica, CM 1850). The sections were blocked with 0.2%Triton, 1% dimethylsulfoxide, and 2% bovine serum albumin in PBS at room temperature for 1 h, then incubated in the primary antibodies diluted in the blocking buffer at 4°C overnight. Primary antibodies used in this study were mouse anti-HuC/D (1:500, Molecular Probes), rabbit anti-DsRed (1:500, Clontech). Primary antibodies were detected by subclass-specific secondary antibodies labeled with Alexa 488/548 (1:1000, Molecular Probes), respectively.

mRNA microinjection and microscopy

Cre-SV40 was cloned into a pGEM-T easy vector (Promega, Madison, WI). Template preparation and *in vitro* synthesis of mRNAs were performed as described previously (Hiratani I et al., 2001). Confocal and fluorescence microscopy analyses were performed using a Zeiss confocal microscope (LSM710; Carl Zeiss, Oberkochen, Germany) and a Leica epifluorescence microscope (MZFLIII; Leica, Tokyo, Japan). The micrographs were processed with Photoshop software (Adobe, San Jose, CA) and the projection of a confocal stack was rendered using FluoRender (http://www.fluorender.com).

Heat-induction in the whole body

Ten embryos were placed into a tube with 200 μl medaka hatching buffer (Yasumasu S et al., 1989) and heated at 39°C for the prescribed number of hours in a thermalcycler (TProfessional Basic; Biometra).

Results

Generation and characterization of the HuC:loxP-DsRed-loxP-GFP Tg medaka line

Tg medaka line that expresses loxP-*DsRed*-loxP-*GFP* under the control of a 3.3-kb medaka *HuC* promoter (*HuC*:loxP-*DsRed*-loxP-*GFP*) was generated by Dr. Okuyama. *DsRed* expression in the Tg embryo was first detected as early as stage 27 in the anterior brain vesicle-intermediate brain vesicle (Ant-Int; **Figure 10A** and **Figure 11A**). After stage 34, DsRed fluorescence was observed in the whole brain (**Figure 10B, C** and **Figure 11B, C**). In 3-month-old adult fish, DsRed-expressing cells were prominently detected in the superficial layer of the telencephalon, cerebellum, posterior edge of the optic tectum, and the left side of habenular nucleus (**Figure 10D**). To determine the details of *DsRed* expression, I prepared coronal sections of the Tg whole brain (*HuC*:loxP-*DsRed*-loxP-*GFP*; **Figure 10E, F**). The surface of the telencephalon and the left side of habenular nucleus exhibited prominent DsRed expression (**Figure 10F** panel I - VII). In addition, DsRed expression was detected in the olfactory bulb (panel II - IV), preoptic area (panel V), ventromedial nucleus (panel VII), optic tectum (panel VIII - XIV), marginal zone of the third ventricular zone (panel VIII - XI), hypothalamus (panel X - XII), and cerebellum (panel XIV - XV). Ms. Kuyoyanagi and Dr. Okuyama previously mapped "proliferation zones" comprising stem cells in the adult medaka brain (Kuroyanagi Y et al., 2010) and found a large number of HuC-positive neural progenitors situated at or near the "proliferation zones" (**Figure 12**). DsRed-positive axons were observed near the olfactory bulb, fasciculus longitudinalis medialis (Flm), nucleus glomerulosus posterioris (NGp), and corpus interpeduncularis (Ci), to which the habenular nucleus neurons project (Agetsuma M et al., 2010). Taken together, these findings indicated that DsRed expression in the Tg (*HuC*:loxP-*DsRed*-loxP-*GFP*) labeled neural progenitor cells normally expressing

HuC. Furthermore, to confirm that DsRed is expressed in HuC-positive neural progenitors, I performed co-staining with antibody against HuC/D and DsRed by immunohistochemistry. The pattern of HuC/D expression overlapped with that of DsRed, including the habenular nucleus (**Figure 10G-I**).

Stochastic Cre/loxP recombination by injection of a low concentration of Cre mRNA

I examined whether stochastic recombination can be induced by injection of Cre mRNA into the Tg embryos at the 1-cell stage, which would allow us to label a certain cell lineage. First, I confirmed that Cre recombination was induced in most cells of various tissues, including muscle and brain, by Cre mRNA injection (100 ng/μl) into Tg (*beta actin*:loxP-*DsRed*-loxP-*GFP*) under the control of a ubiquitous beta-actin promoter (Suehiro Y et al., 2010) (**Figure 13A-E**). Next, a small amount of Cre mRNA (0.2, 2 and 20 ng/μl) was injected into the Tg (*HuC*:loxP-*DsRed*-loxP-*GFP*) at the 1-cell stage (30 min after fertilization). Recombination by Cre mRNA injection led to changes in the expression of DsRed to that of GFP (**Figure 14A**). The mosaic expression of DsRed and GFP (white arrowhead) was detected at the adult stage (**Figure 14B, C**). The induction of GFP expression increased dose-dependently. The distribution of GFP-expressing cells differed among individuals (**Figure 15**), indicating that stochastic recombination can be induced in some stem cells by injection of Cre mRNA. I was, however, unable to precisely determine the number of stem cells where recombination occurred, because it takes at least 12 h to express mature GFP during which cell divisions may have occurred.

To visualize the three-dimensional distribution of the DsRed- and GFP-expressing cells, I obtained optical images of vibratome sections (120 μm) and generated three-dimensional images of the telencephalon of the Cre mRNA (20 ng/μl)-injected fish (**Figure 14C** white dashed line and **Figure 14D**). Interestingly,

subpopulations of GFP-expressing cells were detected in spatially distinct segments. These findings suggest that that subpopulations (defined as clonally-related cells) derive from a single or a few adjacent cells.

Heat induction of Cre/loxP recombination in the nervous system

To induce the recombination by heat treatment, Dr. Shimizu established a Cre-inducible Tg (*HSP*:*Cre*/*Cry*:*BFP*) with an artificial *HSP* promoter containing eight consecutive artificial heat-shock response elements and beta-globin minimum promoter derived from *Xenopus laevis*. Expression of Cre in the Tg (*HSP*:*Cre*) was reported to be inducible by a brief heat shock treatment. The construct expressed blue fluorescent protein (BFP) under the control of the mouse *Crystallin* (*Cry*) promoter as a screening marker, and an insulator sequence was inserted between *HSP*:*Cre* and *Cry*:*BFP* (**Figure 16A**) (Shimizu A et al., 2012) to avoid cross talk between the artificial *HSP* and *Cry* promoters which are located in the same construct of the vector. Dr. Okuyama generated Tg (*HuC*:loxP-*DsRed*-loxP-*GFP*/*HSP*:*Cre*/*Cry*:*BFP*) by genetic crossing.

I examined the efficiency of the heat-inducible recombination during embryonic development. I exposed the embryos to heat shock (39°C, 3 h) at the early blastula stage (stage 9-10, 0~1 days post fertilization [dpf]) (**Figure 16D**). GFP fluorescence was detected at the time of hatching in the whole brain of Tg (*HuC*:loxP-*DsRed*-loxP-*GFP*/*HSP*:*Cre*/*Cry*:*BFP*) embryos (**Figure 16B**, upper panel). In contrast, no GFP fluorescence was detected in either heat-exposed Tg (*HuC*:loxP-*DsRed*-loxP-*GFP*) (**Figure 16B**, middle panel) or non-treated Tg (*HuC*:loxP-*DsRed*-loxP-*GFP*/*HSP*:*Cre*/*Cry*:*BFP*) embryos (**Figure 16B**, lower panel). These findings indicated that Cre protein expressed by HSP in response to heat induction led to the recombination. In addition, the efficiency of the heat-induced

recombination apparently decreased with development (**Figure 16C**).

Discussion

First I showed that injection of a low concentration of Cre mRNA induces stochastic Cre/loxP recombination. There are two possible causes for the stochastic Cre/loxP recombination. One is that distribution of injected mRNA may be sparse. The other is that low concentration in the cells may cause stochastic recombination, which is consistent with previous reports to show that low transcriptional Cre activity led to stochastic recombination. In the present study, I was unable to demonstrate the recombination at a single cell level, because it may take more time (>12h) for cells to express detectable GFP than cell cycle time of neural progenitors. Thus we cannot exclude a possibility that GFP-expressing cells comprises more than one clonal unit that derived form a single stem cell.

Next, I established a noninvasive method for controlled Cre/loxP site-specific recombination in the nervous system during medaka embryogenesis, which allowed us to visualize and/or modify the formation of a lineage-dependent structure. Recent studies with an advanced Gal4-UAS system in zebrafish promoted the genetic dissection of neural circuits (Asakawa K et al., 2008), revealing how a subpopulation of neurons produces behaviors in juvenile fish (Wyart C et al., 2009). The relationship between functional neural circuits and clonally-related neurons has, however, remained largely unknown. In the adult fruit fly brain, many areas of the brain neuropil are formed by the combination of distinct clonal units (Ito K et al., 2008). Recently, in the mouse visual cortex, clonally-related neurons derived from the same radial glia were found to have similar electrophysiologic properties (orientation selectivity) in response to a visual stimulus, in contrast to the response of the nearest-neighbor non-clonally related neurons (Li Y et al., 2012; Yu YC et al., 2012). These findings suggest that clonally-related neurons, rather than identifiable macroscopic brain structures, constitute the functional modules of neural circuits.

Several behavioral systems to assess optomotor response, schooling, shoaling, and mating partner preference were recently established in medaka fish (Imada H et al., 2010). Combinations of these behavioral systems and the present gene manipulation method will contribute to our understanding of how a subset of clonally-related neurons (a lineage-dependent structure) is involved in behavior.

Furthermore, in the adult brain, medaka *HuC* promoter activity is restricted to newborn and differentiating neurons. Thus, heat-inducible Cre/loxP site-specific recombination is also applicable for investigating adult neurogenesis in medaka fish. In contrast to mammals with limited neurogenesis in the adult brains, teleost fishes such as medaka fish and zebrafish constitutively generate newborn neurons in numerous proliferating zones across the whole brain throughout life (Kizil C et al., 2012; Kuroyanagi Y et al., 2010; Isoe Y et al., 2012; Zupanc GK., 2008; Chapouton P et al., 2007). As the distribution of proliferation zones in the adult brain is mostly conserved among teleost fishes, adult neurogenesis is believed to be important for the maintenance and development of the fundamental structure of the fish brain throughout life (Kizil C et al., 2012; Zupanc GK., 2008). Here I showed that stochastic and/or site-specific Cre/loxP recombination led to labeling of clonally-related neural progenitors that seem to form compartmentalized blocks in the telencephalon (**Figure 17**).

Chapter 3

Systematic clonal unit analysis of medaka telencephalon based on post-hatch neurogenesis.

Introduction

In vertebrates, the telencephalon is a brain region critical for learning (Saito K, et al., 2006; Pfenning AR, et al. 2014), memory (Frankland PW, et al., 2005; Strange BA et al., 2014), sensory perception (Cohen DH et al., 1973; Sur M et al., 2005), social cognition (such as courtship and aggressive behaviors of various vertebrates, fish, bird, and mammals; O'Connell LA, et al., 2011, 2012), and innate emotional behaviors (such as freezing behavior or anxiety in mice; LaBar KS, et al., 2006; Janak PH et al., 2015). The telencephalon is divided into two parts, the pallium and subpallium. The pallium is the outermost brain structure that covers underlying structures such as the cerebellum and hippocampus. In fish to mammals, the pallium is subdivided into multiple compartmentalized anatomic regions. The number and structure of compartmentalized structures in the pallium are diverse among vertebrates (Rakic P., 2009; Ganz J et al., 2014). The subpallium, including the basal ganglia, is located under the pallium. The function and structure of the subpallium seems relatively conserved among vertebrates (Moreno N, et al., 2009; Ebbesson SO., 2012). Several lines of evidence indicate that the molecular mechanisms defining the pallial and subpallial divisions are conserved among vertebrates. Expression patterns of some genes involved in the divisions are broadly conserved among vertebrates during the embryonic stage (Puelles L, et al., 2000; Wilson SW, et al., 2000; Bachy I, et al., 2002; Jarvis ED, et al., 2005; Sugahara F, et al., 2011). However, how the compartmentalized structure of the pallium emerges in the adult brain and the mechanisms that define the structural differences between the pallium and subpallium remain unknown.

In Chapter 2, I reported that clonal units of newly born neurons constitute the compartmentalized structure in the adult telencephalon. This finding led me to hypothesize that the compartmentalized structure of the pallium is generated via

post-hatch neurogenesis during a period of growth. In Chapter 3, I comprehensively investigated the structure of clonal units in the whole telencephalon.

Material and Methods

Ethics statement

The work in this chapter was conducted using protocols specifically approved by the Animal Care and Use Committee of the University of Tokyo (permit number: 12–07). All surgeries were performed under anesthesia using MS-222, and all efforts were made to minimize suffering, following the NIH Guide for the Care and Use of Laboratory Animals.

Fish

The transgenic (Tg) line (HuC:loxp-DsRed-loxp-GFP, HuC line) and Tg line (HSP-Cre/Crystallin-CFP , HSP line) were generated as previously described in Chapter 2. Sexually mature female fish of the HuC line and male fish of the HSP-line were paired and crossed (**Figure 18A**).

Induction of Cre/loxP recombination

Embryos of the double transgenic line, the HuC x HSP line, were mildly heated at 38°C for 15 min. Heat shock was applied using a thermal cycler to polymerase chain reaction tubes containing two eggs each. After the heat shock treatment, the embryos were maintained at 26°C until they hatched. The resulting fish were kept in a regular tank with a light: dark cycle of 14:10 hours.

Fluorescent signal detection

Adult fish brains were dissected by the usual procedure (Kinoshita M et al., 2009). After dissection, the brains were fixed in 4% paraformaldehyde/phosphate-buffered saline (PBS) overnight. The brains were then washed twice with PBST (0.5% Triton-X100 in phosphate buffered saline) and immersed into Sca/eA2 solution for about three hours on

ice (Hama H, et al. 2011). When the brains were confirmed to be transparent (**Figure 19A**), they were transferred into new Sca/eA2 solution with DAPI (0.5 ul/2ml) overnight at 4°C. The next day, the brains were transferred into new Sca/eA2 solution and washed with PBST. To prepare samples for signal detection, the brains were embedded in 0.75% gelatin with Sca/A2-Triton solution and fixed on glass coverslips (**Figure 19B**). Fluorescent signal detection was performed using a Digital Scanned Light-sheet Microscope (National Institute Basic Biology, Aichi, Japan) (Ichikawa T et al., 2013).

Image processing

To compare fluorescent signals of multiple brain samples, I performed image registration with CMTK registration GUI in Fiji (Ostrovsky A et al., 2013; for details, please see: https://github.com/jefferislab/BridgingRegistrations), as described in a previous report (Ito M et al., 2013). I used the DAPI signals of the best images obtained by light-sheet microscopy with Gaussian blur as the normalized brain. Three-dimensional reconstruction images were made with FluoRender (Wan Y et al., 2009).

Immunohistochemistry

The procedure was performed as previously reported (Okuyama T et al., 2013). Briefly, after cutting 14-um thick cryosections of adult brains of Tg (*HuC*:loxP-*DsREd*-loxP-*GFP*) fish, sections were incubated overnight with the primary antibody (anti-glial fibrillary acidic protein [GFAP], Sigma-Aldrich), antiSV2, DSHB, 1:2000) in 1% BSA/DMSO/Triton-X1000/PBS. After washing several times with DMSO/Triton-X1000/PBS, the sections were incubated with fluorescent Alexa488 (1:1000) and DAPI (1:4000) in 1% BSA/DMSO/Triton-X1000/PBS. After washing, fluorescent signals were detected using a fluorescence microscope.

Results

3D-imaging of the whole telencephalon of the adult fish brain with fluorescent signals

Generally, it is difficult to analyze the 3D structure of brain subdivisions and to compare the distribution of fluorescent signals among many samples using brain slices. Therefore, I established a system to perform 3D-imaging of clonal units labeled with fluorescent signals from a large number of samples. First, I established a new system to induce stochastic Cre/loxP recombination in a more efficient way than by Cre mRNA injection. By crossing with the Tg (HSP-Cre) line, in which Cre recombinase is expressed by heat shock, Cre/loxP recombination can be easily induced by heat shock at an early developmental stage (st.17) (**Figure 18A, B**). When mild heat shock was applied to embryos of the Tg (HuC) line x Tg (HSP) line, stochastic Cre/loxP recombination was induced, resulting in random patterns of DsRed and GFP (**Figure 18C, D**). I next established a method to perform 3D imaging of the whole telencephalon using fluorescent signals. Recently, many brain-clearing solutions were developed using other types of vertebrate brains (Ke MT et al., 2013; Yang B et al., 2014). Here I used Sca/eA2 to clear the brains of medaka fish, because they are smaller than rodent brains and Sca/eA2 is easier to prepare (Hama H et al., 2011) (**Figure 19A**). After clearing and staining with DAPI, brains were bonded to glass slides and aligned (**Figure 19B**), and fluorescent signals were detected by light-sheet fluorescence microscopy, which allowed for 3D-visualization of the fluorescent signals at the brain-wide level.

Identification of clonal units by registration of fluorescent signals to the normalized brain

To investigate how individual clonal units of newly born cells contribute to the construction of the telencephalon, I systematically identified 3D structures of all the clonal units in the whole telencephalon. In particular, I examined whether traditional anatomic brain regions could be defined by combinations of clonal units. To this end, it is necessary to compare individual structures with a DAPI reference signal. It was very difficult to obtain images with the same angle due to differences in the sample preparation. Therefore, I collaborated with Dr. Kei Ito to use the image registration method, which was recently used to identify the structure of clonal units in *Drosophila* brain (Ito M et al., 2013) and allows for geometric alignment of a dataset of 3D images and for comparison of datasets across subjects. I used one of the best image-sequences obtained of DAPI signals with image processing using Gaussian blur as the normalized brain (**Figure 20**). First, anatomic regions of transverse sections in the normalized telencephalon were defined based on the boundary of the DAPI signals. Second, the anatomic regions of horizontal sections were defined by checking the orthogonal view of the normalized brain (**Figure 19C, 20**). Also, I made a 3D medaka brain atlas by subdividing the anatomic regions according to the DsRed signals in the Tg line (several examples shown in **Figure 21**, summarized in **Figure 22**). Then, to identify the structure of a single clonal unit, I analyzed almost 70 brains of the Tg line with induction of stochastic Cre/loxP recombination. By registering the DAPI signals onto the normalized 3D-brain, other fluorescent signals from GFP and DsRed were transformed to match the normalized brain (**Figure 23**). The result is shown in **Table 1**. In most samples, GFP-positive cells were partially detected. Also, I found that the same structures of GFP-positive neurons were detected multiple times inside the identical anatomic brain region. Therefore, I re-defined the structure of the subdivisions of anatomic regions (**Figure 24**), and analyzed the structures of the GFP-positive clones one by one (**Table 2**). When an identical GFP-positive pattern was detected in more than three brains, the GFP-positive pattern was manually

identified as a clonal unit (**Figure 24**). I identified almost 40 clonal units in one hemisphere of the telencephalon (**Figure 25**). I did not detect differences in the structure of the clonal units between females and males. In some brain regions, such as the Dc and AC, expression of the fluorescent proteins DsRed and GFP was not driven by the HuC promoter, and therefore I could not perform clonal analysis in these anatomic regions.

Structural differences in clonal units between the dorsal and ventral telencephalon

In the dorsal telencephalon (pallium), I found that clonal units comprised compartmentalized blocks, as described in Chapter 2 (Okuyama T et al., 2013). Also, each anatomic region comprised multiple clonal units that are localized in a mutually exclusive manner (**Figure 26**). I also observed that axons of some clonal units project to the same brain regions (Dp to olfactory bulb; **Figure 26-2)**. On the other hand, mixed patterns consisting of DsRed and GFP signals were observed in the ventral telencephalon, the subpallium (Vd, Vs, Vp, and Vv; **Figure 27, 28**). When I checked multiple samples from different sections using the re-section method in 3D-image processing software (Fiji), I observed that mixed patterns were distributed along multiple anatomic regions (**Figure 29**). Axons of cells in the ventral telencephalon projected to neighboring brain regions (**Figure 28B** right). I also found that there were two layers in the ventral telencephalon, a superficial part and an interior part (**Figure 28C**). In both parts, a mixed pattern was detected. The ventral telencephalon of zebrafish can be divided into two layers based on the expression of genetic markers (Ganz J et al., 2012), which might be consistent with my data.

Structural relationship of neurons in clonal units and radial glia in the telencephalon

A previous study of cryosections in the adult zebrafish brain showed that GFAP-positive radial glia cells distribute radially in the pallium and neural progenitors migrate along the fibers of the radial glia (Dirian L et al., 2014). To examine whether the structure of clonal units is related to the polarity of the radial glial cells, I checked the distribution of GFAP-positive cells in the Tg (HuC) line with immunohistochemistry. I found that GFAP-positive fibers had an apical-basal polarity with aligned fibers projections, surrounded by the DsRed-positive regions in the pallium (**Figure 28**). By contrast, in the subpallium, a relatively lower density of GFAP-positive fibers was detected in the DsRed-positive regions and GFAP-positive fibers project without any clear alignment of their projections (**Figure 30B**, right). This suggests that radial glia cells in the dorsal telencephalon (pallium) might be used as a scaffold for the migration of newly born neurons.

Discussion

Postnatal neurogenesis just after birth occurs broadly in the brain, and is referred to as a growth spurt in humans (Dobbing J, et al. 1973). Several previous studies demonstrated that postnatal/post-hatch neurogenesis plays a critical role in functional maturation after birth/hatch (Sahay A, et al., 2011; Clark PJ, et al., 2012; Inokuchi K., 2011; Kitamura T, et al., 2014; Imayoshi I, et al., 2008; Ming GL, et al., 2011; Sakamoto M, et al., 2011). In contrast, little attention has been paid to the contribution of postnatal/post-hatch neurogenesis to the brain-wide architecture. Here I analyzed labeled clonal units in transparent adult medaka brains using light-sheet fluorescence microscopy, which provides a systematic overview of the architecture of the whole telencephalon. It is very difficult to trace the 3D structure using brain slices, but 3D imaging allowed me to demonstrate that clonal units exclusively constitute the anatomic region of the pallium. By systematic analysis, I found differences in the architecture of clonal units between the pallium and subpallium. Individual clonal units in the pallium were distributed exclusively in a single compartment (a specific brain region), while in the subpallium, multiple clonal units comprised a mixed pattern in the same brain region. This is the first study to uncover how individual anatomic regions comprise clonal units in teleosts. I also demonstrated that axons of some clonal units in the pallium (Dp) project to the same brain regions. In contrast, in the subpallium, the axons of the clonal units project apparently randomly to adjacent anatomic regions. Furthermore, there were differences in the colocation of GFAP-positive glia fibers with DsRed-positive newly born neurons and the projection pattern of their fibers between the pallium and subpallium. My findings strongly suggest that, at least in teleosts, post-hatch neurogenesis mediates the emergence of a compartmentalized structure in the pallium and generates differences in the brain architecture between the pallium and subpallium.

Previous studies, not only in teleosts but also in other vertebrates, suggested differences in the developmental process between the pallium and subpallium. In mammals, GABAergic neurons migrate into the subpallium region (Mayer C et al., 2015; Harwell CC et al., 2015) and glutamatergic neurons exhibit vertical migration guided by fibers of radial glia cells in developing cortex at the embryonic stage (Luhmann HJ et al., 2015). In the mammalian cortex, long fiber tracts of glia cells function as a scaffold for neuronal migration (Cerri S et al., 2010). The results of the immunohistochemistry experiments implied that newly born cells in the pallium were partially guided by radial glia cells near the dorsal surface. In zebrafish, the direction of fibers of radial glia cells differ between two major anatomic regions in the pallium, Dl and Dm (Than-Trong E et al., 2015), consistent with our data in the medaka telencephalon (**Figure 30**, #2). Differences in the direction of the fibers were not observed among individual clonal units, suggesting that migration of newly born cells along radial glia cells may generate the structural differences among larger anatomic regions such as Dl and Dm, rather than sub-compartments defined by the clonal units. In addition, parallel alignment of radial glia fibers may allow for the development of newly born neurons independent of other clonal units, which are assumed to lead to the generation of compartmental structures in the pallium.

A critical and interesting question remains regarding the functional meaning of the structural differences in the pallium and subpallium. In invertebrates, *Drosophila melanogaster* studies suggested that clonal units are connectional units in the neural network of the central brain (Rooke JE et al., 2000; Bonaguidi MA et al., 2011; Ito M et al., 2013; Yu HH et al., 2013). Also, in vertebrate studies, sister neurons derived from same neural stem cells show the same electrophysiologic properties (Yu YC et al., 2009, 2012), the same response to stimuli (Li Y et al., 2012; Ohtsuki G et al., 2012; Muldal AM et al., 2014), and tend to connect with each other (Yu YC et al., 2009; Gao P et al., 2013). Taken together, I would like to propose a possible model of

the generation of differences in the clonal unit architecture: (1) newly born neurons in the pallium develop independently of other clonal units and function within individual clonal units, (2) newly born neurons in the the subpallium develop by closely interacting with newly born neurons in the other clonal units and form cooperative connections over clonal units (**Figure 31**). Evaluation of the neural activity of individual clonal units will elucidate this model.

Clonal analyses in other vertebrate brains suggest that the structural patterns of clonal-units are more complicated in avian and mammalian brains (**Figure 32**). In the chick telencephalon, subsets of compartmentalized clones are located in rostrocaudal arrays (Szele FG et al., 1996). In the reptile dorsal cortex, the avian hyperpallium, and the mammalian cerebral cortex, newly born neurons migrate on radial glia cell fibers during development, forming a columnar structure (Montiel JF et al., 2015). In the avian and mammalian cortex, however, neurons of the subpallium also migrate tangentially (Cobos I et al., 2001; Gelman DM et al., 2009), thus the avian and mammalian cortices comprise a combination of compartmentalized and mixed structures. It would be interesting to know whether this structural difference among vertebrates can be explained by differences in earlier developmental stages. In teleosts, the pallium and subpallium are closely located because the brain develops by lateral eversion. In contrast, the pallium and subpallium of birds and mammals are separated by ventricles because the brains develop in an inverted manner (**Figure 32**). It may be that neurons of the subpallium must migrate to the pallium and connect in birds and mammals, but not in teleosts.

Structural diversity of the telencephalon among teleost fish species has been reported (Northcutt RG., 2008). For example, the number of anatomic regions in the pallium differs among teleost fish species (Northcutt RG, 2006; Burmeister SS et al., 2009; Harvey-Girard E et al., 2015; Ganz J et al., 2015). In addition, social teleost species exhibit different types of social behavior, especially mating behavior. How can

this diversity of brain and social behavior be explained? It would be interesting if individual clonal units works as a functional neural-network unit and differences in the combination of clonal units generates the diversity of the structure and the function of the pallium. My findings may provide clues to clarify how cell-lineage diversity generates the diversity of the pallium among teleost fish.

Chapter 4

Genome-wide regulatory region analysis of the medaka telencephalon

Introduction

In Chapter 3, I demonstrated that newly born neurons of clonal units derived from the same neural stem cells during the growth stage have a different architecture between the pallium and subpallium. In the pallium, individual subcompartments of anatomic regions comprise only a single clonal unit, and the newly born neurons within individual clonal units interact with each other. In the subpallium, an anatomic region comprises multiple clonal units in a mixed pattern, and the newly born neurons interact with neurons of other clonal units. Taken together, the molecular mechanisms underlying the interactions of newly born neurons with other neurons are assumed to differ between the pallium and subpallium in the adult teleost brain. However, the molecular mechanism that causes this difference is unknown.

Therefore, in this Chapter, to investigate the possible molecular mechanisms that underlie the different construction mechanisms between the pallium and subpallium, I examined whether gene expression of newly born neurons is regulated differentially between the pallium and subpallium (**Figure 33A**). For this purpose, I performed an assay for transposase-accessible chromatin with sequencing (ATAC-seq), which is a recently-developed highly sensitive technology to examine the dynamics of the genome structure by inserting adaptors into open chromatin (**Figure 33B**). Although there are many techniques available to examine chromatin-accessibility data, such as DNase-seq (Song L et al., 2010) and FAIRE-seq (Giresi PG et al., 2009), which need larger amounts of cells (1-50 million cells), ATAC-seq allows us to identify open chromatin sites with only 500–50,000 cells and examine the interplay between genomic locations of open chromatin at the nucleotide-base resolution (Buenrostro JD et al., 2013; Lara-Astiaso D et al., 2014). Furthermore, ATAC-seq enabled me to investigate the open chromatin regions that regulate not only current gene expression, but also past and future gene expression, because the regulatory regions are stably opened before and

after gene expression if those regions were, are, or will be strongly regulated. In addition to my investigation of gene regulation, I examined differences in the gene expression using RNA-seq. By combining ATAC-seq and RNA-seq, I analyzed the molecular mechanisms underlying the structural differences between the dorsal and ventral telencephalon.

Materials and Methods

Ethics statement

The work in this chapter was conducted using protocols specifically approved by the Animal Care and Use Committee of the University of Tokyo (permit number: 12–07). All surgery was performed under anesthesia using MS-222, and all efforts were made to minimize suffering, following the NIH Guide for the Care and Use of Laboratory Animals.

Brain slicing and collecting DsRed-positive neurons in the dorsal and ventral telencephalon

Adult medaka fish were anesthetized using tricaine methanesulfonate (MS222) solution (0.4%). After brain dissection, brains were immersed into artificial cerebral spinal fluid on ice. Then, brains were embedded in 2.5% low-melting agarose in artificial cerebral spinal fluid and frozen at -20℃ for 8 min. After removing the excess agarose gel, 130-μm thick brain slices were cut using a vibrating blade microtome (Leica VT1000S). The slices were collected, placed onto the slide glass, and dissected using a razor blade under a fluorescence microscope based on the DsRed signal (Leica MZ16F) (**Figure 34AB**).

ATAC-seq

For the ATAC-seq, sample preparation, nuclei extraction, adaptor insertion, amplification, sequencing, and mapping were performed according to the previously described protocol (Buenrostro JD et al., 2015). Briefly, after collecting the dorsal and ventral telencephalon in a 1.5-ml tube with phosphate-buffered saline, the nuclei were extracted in lysis buffer. Then, adaptors were inserted with transposase. After purifying the DNA with Ampure XP (Beckman Coulter), adaptor-inserted genome regions were

amplified using adaptor-specific primers and then again purified. The quality of the purified libraries was checked using a Bioanalyzer High-Sensitivity DNA Analysis kit (Agilent Technologies, US) (**Figure 34CD**). The sequence was read using Illumina. Peaks of the open chromatin regions were identified by Macs2 (Model-based Analysis of ChIP-Seq; http://liulab.dfci.harvard.edu/MACS/).

Gene ontology (GO) and pathway enrichment analysis

For Gene ontology (GO) and Kyoto Encyclopedia of Genes and Genomes (KEGG) pathway enrichment analysis, I used the Database for Annotation, Visualization and Integrated Discovery (DAVID) Bioinformatics Resources (Huang da W et al., 2009). Genes of the closest 5'UTR of "specific peaks" were identified as candidate regulated genes. Then, human homologs of candidate genes were searched using BioMart. For background, human homologs of all medaka genes were used. (https://david.ncifcrf.gov/)

Identification of predictive regulatory sequences by Support Vector Machines (SVM)

To identify predictive regulatory sequence of the dorsal and ventral telencephalon, kmer-SVM (http://kmersvm.beerlab.org/) was used as previously described (Fletez-Brant C et al., 2013). Briefly, a null sequence was generated using random sampling from genomic DNA. The SVM was trained on some of the sequences of the dorsal-specific peaks or ventral-specific peaks, and receiver operating characteristic curves and precision-recall curves were plotted.

MEME (Multiple Em for Motif Elicitation)

To search for the most enriched motif in the dorsal- or ventral-specific peaks, the motif-based sequence analysis tool MEME (http://meme-suite.org/tools/meme) was used.

RNA-seq

After slicing the brain, the dorsal or ventral telencephalon was cut and collected. Five fish were used for each sample. RNA extraction was performed using an RNeasy Mini Kit (Qiagen). The quality of RNA was checked using a Bioanalyzer with an Agilent RNA 6000 Pico Kit (Agilent Technologies). Then, construction of the stranded mRNA-Seq library was performed using KAPA Stranded mRNA-Seq Kit (KAPA Biosystems). After verifying the quality of the library, sequencing was performed, and mapped to the medaka fish genome (Hd-rR). Analysis with SAMMate (Xu G et al., 2011) allowed me to compare the gene expression level between the pallium and subpallium samples.

Results

Open chromatin profiles in the dorsal and ventral telencephalon

To investigate differences in the molecular mechanisms underlying post-hatch neurogenesis between the pallium and subpallium, I performed ATAC-seq, in collaboration with Dr. Nakamura and Dr. Takeda at the University of Tokyo (please see the "Contribution" section). There are some reports of ATAC-seq using mammalian samples (Buenrostro JD et al., 2013; Lara-Astiaso D et al., 2014). Thus, I examined whether ATAC-seq could work with samples from the medaka adult brain. In ATAC-seq, bacterial (Tn5) transposase integrates adaptors into regions of accessible chromatin (open chromatin). Therefore, genome regions that could be mapped as high peaks in ATAC-seq are maintained open, and thus it is estimated that transcription factors bind to these genomic regions. After tagmentation with the adaptors, polymerase chain reaction (PCR) was performed using the adaptors as primers. Amplifiable PCR fragments were used as a library for high-throughput sequencing to identify the integrated locations in the whole genome. The size distribution of the PCR fragments from the dorsal and ventral telencephalon had clear periodicity (**Figure 34CD**) equal to the helical pitch of DNA (Buenrostro JD et al., 2015), suggesting that the library was successfully prepared. Next, sequencing of the library using Illumina high-throughput sequencing instruments was conducted. The majority of reads (read density) were within the peaks derived from intersections of ATAC-seq peaks (**Figure 35**). To infer differences in open chromatin regions between the dorsal and ventral telencephalon (pallium and subpallium, respectively), high ATAC-seq peak regions were identified by peak-calling algorithms for ChIP-Seq, MACS. By scanning the whole genome, 108,466 peaks and 72,798 peaks were identified in the dorsal and ventral samples, respectively; 940 peaks were identified as "dorsal-specific peaks" and 536 peaks were identified

as ”ventral-specific peaks” (**Figure 36**).

Axon guidance pathway identified as the candidate pathway for the difference

To identify the differences in the biologic functions and pathways between the dorsal and ventral telencephalon, I identified human homologs of candidate genes within and/or adjacent to the specific peaks, as described in the Materials & Methods. Next, I used the DAVID and KEGG pathways to test for enrichment of functionally annotated gene sets among the identified genes. The most enriched annotation and GO term was “Axon guidance pathway” in both the dorsal and ventral telencephalon (**Table 3**). The mapping viewer of the axon guidance pathway showed that dorsal and ventral specific peaks were associated with all of the axon guidance signaling pathways (**Figure 37**). Interestingly, gene bodies for gene families for *EphA, EphB, UNC-5* family*, Sema5,* and *NRP1* included dorsal- and ventral-specific peaks. Thus, a set of genes belonging to the same family was prominently regulated in a different way between the dorsal and ventral telencephalon.

Next, to examine differences in the transcriptional expression level between the pallium and subpallium, I performed RNA-seq. A total of 35,166,176 reads for the dorsal telencephalon and 31,488,710 reads were obtained. I compared the reads per kilobase of exon per million mapped reads (RPKM). First, I identified the genes whose RPKM in the dorsal telencephalon was twice as high as that in the ventral telencephalon, and vice versa. Among 20,459 genes, 545 genes were identified as “dorsal-preferential expressed genes” and 519 genes were identified as “ventral-preferential expressed genes” (**Figure 38**). Next, I examined whether the genes of axon guidance pathways are included among those ventral- or dorsal-preferential expressed genes, and found that many genes were both specifically regulated and preferentially expressed in either the dorsal or ventral telencephalon (**Figure 39**). These findings further supported the notion

that axon guidance pathways are important for the structural differences between the dorsal and ventral telencephalon. Next, I examined the genes whose expression was both restricted and strong, that are assumed to characterize the nature of neurons. By identifying genes expressed five times higher than in other parts of the telencephalon, 86 were identified as "dorsal-specific genes" and 145 were identified as "ventral-specific genes" (**Figure 40**). I then checked the expression level of axon guidance pathway transcripts, which is a candidate pathway for the differences (**Table 4**). **Figure 41** shows the expression level of genes of the netrin family (**Figure 41A**), Eph/ephrins (**Figure 41B**), cytokine-cytokine receptor interaction (**Figure 41C**), Slit/Robo system (**Figure 41D**), and semaphorins (**Figure 41E**). As shown **Figure 41** and **Figure 44A**, *EPHA5* (**Figure 41B**) is preferentially expressed in the dorsal telencephalon, and *unc5a* (**Figure 41A**), *EPHB1* (**Figure 41B**), and *CXCL14* (**Figure 41C**) are strongly expressed in the ventral telencephalon. No genes in the Slit/Robo system or semaphorins were identified as "dorsal preferentially-expressed genes" nor "ventral preferentially-expressed genes".

Predictive regulatory sequence for gene expression specifically in the dorsal and ventral telencephalon

Open chromatin regions are considered to be DNA regulatory elements, including enhancers, repressors, insulators, and promoters (Boyle AP et al., 2008) and to be bound by transcription factors or co-activators (Buenrostro JD et al., 2015; Davie K et al., 2015). I examined if there were common regulatory elements in specific open chromatin regions of the dorsal or ventral telencephalon. First, I applied kmer-SVM, a recently developed computational method (Ben-Hur A et al., 2008; Lee D et al., 2011; Fletez-Brant C et al., 2013). Surprisingly, the accuracy of the classifier was quite high (AUROC=0.972, AUPRC=0.982), suggesting that open chromatin is regulated by

common transcription factors with several regulatory elements (**Figure 42AB**). I also applied MEME to find enriched motifs in the dorsal or ventral specific peaks (**Figure 42C**). I found that some motifs are detected in both SVM and MEME (AGTGG in dorsal, CTGTCA in ventral). This suggests that those sequences could be good candidate transcription factor binding sites.

Therefore, I examined whether those genes are expressed specifically in the pallium and subpallium (**Table 5, Figure 43A**). I found that *meis2 (meis homeobox 2)* is prominently expressed in the subpallium (~30 fold) (**Table 5, Figure 43B, 44B**). Also, as the motif candidate shown in **Figure 42** is a short sequence, I examined the paralogs of genes listed in **Table 5** (**Figure 43**). No genes were detected as preferential genes among *meis* paralogs. Additionally, *NeuroD* and *nfixa* are preferentially expressed in the pallium (expression level is 4 times higher than that in the subpallium) (**Table 5, Figure 43B, 44B**) and Sox3 is preferentially expressed in the subpallium (expression level is 4 times higher than that in subpallium).

Discussion

In this Chapter, I investigated how gene expression is differentially regulated in the pallium or subpallium at the whole-genome level using ATAC-seq and RNA-seq.

Discussion about gene expression of the axon guidance pathway.

First, I found that *unc5a (unc-5 netrin receptor A)* in the netrin pathway, *EPHB1 (EPH receptor B1)* in the Ephs/ephrin pathway, and *CXCL14 (chemokine (C-X-C motif) ligand 14)* in the cytokine-cytokine receptor pathway were preferentially expressed in the subpallium, and the *EPHA5 (EPH receptor A5)* in the Ephs/ephrin pathway was preferentially expressed in the pallium. UNC5 (netrin receptor) family proteins are widely known as transmembrane receptors that mediate both repulsion and attraction signals for axonal growth cones in embryonic development. In mammalian embryos at embryonic day 16.5, *Unc5A* is broadly expressed in the cerebellum, habenula, subventricular zone (SVZ), and ventricular zone (VZ). After birth, at postnatal day 5, *Unc5A* is strongly expressed in the hippocampus, although the expression level in the cortex decreases and it is no longer detectable in the habenula (van den Heuvel DM et al., 2013). The SVZ, VZ, and hippocampus are areas of neurogenesis in the mammalian brain. Thus, it is possible that *unc5a* in medaka fish also functions as an important factor in postnatal neurogenesis. Some studies in zebrafish report that *unc5a* and *unc5da* (zebrafish ortholog) are broadly expressed in the telencephalon during embryogenesis (Yang B et al., 2013). It is important to clarify whether *unc5a* expression in teleosts is restricted to immature newly born neurons during postnatal neurogenesis. Mammalian studies report that the chemokine *CXCL14, also named BRAK (BRAK; breast and kidney derived),* is highly expressed in many brain regions, including the cortex, basal ganglia, septum, and hippocampus (Banisadr et al., 2011),

and is assumed to regulate GABAergic synaptic inputs to adult neural precursor cells (Banisadr et al., 2011). *CXCL12*, which is a ventral specific candidate gene (Figure 5), binds a shared receptor, CXCR4 (Tanegashima K et al., 2013), and is considered to function in an opposing way in GABA release; CXCL14 inhibits GABA release and CXCL12 enhances it (Banisadr et al., 2011). *CXCL14* expression was strongly detected in the subpallium (**Figure 41C, Table 4**) where GABAergic neurons are enriched, suggesting that the involvement of CXCLs in the development of GABAergic neurons is conserved among vertebrates. In contrast, I also found bidirectional regulation in the expression of a gene family belonging to the ephrin pathway; *EPHA5* and *EPHB1* are preferentially expressed in the pallium and the subpallium, respectively. In the adult mouse brain, *EPHA5* is broadly expressed, but especially highly expressed in cerebral cortex (Cooper MA et al., 2009), which is consistent with my finding that EPHA5 is strongly expressed in the pallium (**Figure 41,B Table 4**). As *EPHA5* is considered to function in mapping axon terminals to the target field topographically (Yue Y et al., 2002; Feldheim DA et al., 2004), *EPHA5* in medaka fish may also contribute to the architecture of clonal units in the pallium of the medaka brain. In the mammalian adult brain, *EPHB1* is expressed in neural stem cells and progenitor cells in the dentate gyrus, and is suggested to regulate cell proliferation (Conover JC et al., 2000; Chumley MJ et al., 2007). The ligand of *EPHB1, ephrinb3a,* is also strongly expressed in the subpallium (**Table 4**), implying that *EPHB1/ephrinb3* signaling is involved in post-hatch neurogenesis in teleosts.

Here I identified some candidate genes (the subpallium: *unc5a* in the netrin pathway, *EPHB1* in Ephs/ephrin pathway, *CXCL14 and CXCL12* in a cytokine-cytokine receptor pathway; the pallium: *EPHA5*) selectively involved in the axon guidance pathway in the pallium and subpallium, respectively. Based on developmental studies, *EPHA5* and its ligand *ephrins* are expressed in the mammalian nervous system and function to determine brain region boundaries (Wilkinson DG et

al., 2001). It might be that *EPHA5/ephrin* signaling determines the boundaries of individual clonal-unit compartments in the telencephalon. Further studies using the conditional gene regulation method (see Chapter 5) are required to investigate how these factors generate differences in the architecture between the pallium and subpallium.

Discussion of transcription factor binding to regulatory sequences.

How is expression of the identified genes regulated? Finally, I investigated the candidate transcription factors by comparing the predictive regulatory sequences in the pallium and subpallium, and found preferential expression of *Meis2a (Meis homeobox 2a)* in the subpallium. *Meis2* is a member of TALE superfamily (alpha helixes 1 and 2 are separated by an extra three-amino-acid loop extension) of homeodomains with Pbx1 (Bürglin TR., 1997; Mukherjee K et al., 2007). In humans, Meis2 and Pbx1 homeodomain proteins interact with Klf4 (Krupple-like factor), which is a Yamanaka factor (Takahashi K et al., 2006) implicated in tumorigenesis and in maintaining stem cell pluripotency (Bjerke GA et al., 2011). Meis2 might regulate stem cell pluripotency via Klf4 in the subpallium. In addition, it is reported that Meis2 and Pbx1 bind to the regulatory sequence (5'-CGGTCA-3') of the enhancer region of ephA8 and regulate the expression of ephA8 in the developing mouse mesencephalon (Shim S et al., 2007); ephA8 affects the outgrowth of hippocampal neurons (Buchser WJ et al., 2010). Additionally, the predictive regulatory sequence of *meis2* (5'-CTGTCA-3') was identified in both SVM and MEME. I also found that one of the ventral-specific peaks included a regulatory sequence of *meis2* in the gene body of *ephb1*. Thus, it is possible that Meis2 regulates post-hatch neurogenesis in the subpallium via ephA8 and/or ephB1. My finding, for the first time, suggests the possible involvement of *Meis2* in gene-specific expression in the subpallium.

My RNA-seq analysis also demonstrated that one of the paralogs of *atoh1*,

NeuroD2, was strongly expressed in the pallium (RPKM in dorsal: 435.50, RPKM in ventral: 98.55) (**Figure 43, Table 5**). NeuroD functions as a transcriptional activator by binding to E box-containing promoter consensus core sequences 5'-CANNTG-3' (Miyachi T et al., 1999). Based on MEME analysis, 5'-CAGTTGG-3' is one of the enriched sequences of open chromatin in the pallium (**Figure 42C**). Inside 5'-CAGTGG-3', I observed both 5'-CANNTG-3', which is a core binding sequence for NeuroD, and 5'-AGTGG-3', which is an Atoh1-binding motif. Therefore, it is possible that NeuroD2 regulates gene expression in the pallium. NeuroD2 is a basic helix-loop-helix transcription factor that enhances neuronal differentiation and neuronal survival (Olson JM H et al., 2001). In the mouse brain, NeuroD2 is also strongly expressed in the cerebral cortex and hippocampus (pallium) in the telencephalon (Farah MH et al., 2000), consistent with the strong expression of NeuroD2 in the medaka pallium. Taken together, NeuroD2 might function as a key regulator of the gene expression for neural differentiation in post-hatch neurogenesis in the pallium.

In future studies, it would be important to compare clonal units to investigate the molecular basis underlying "lineage diversity", which generates compartmentalized structures in the teleost pallium. To approach this issue, I am planning to establish a FACS method to isolate clonal unit-selective newly born neurons for further analysis with ATAC-seq and RNA-seq.

Chapter 5

Controlled Cre/loxP site-specific recombination in the developing brain in medaka fish *(Oryzias latipes)*.

Introduction

In Chapter 3, I showed that clonal units, subpopulations of newly born neurons derived from neural stem cells during the growth stage, constitute anatomic regions differentially between the dorsal and ventral telencephalon. In Chapter 4, by ATAC-seq and RNA seq, I found that the regulation of gene expression is also quite different between the dorsal and ventral telencephalon. However, whether individual clonal units also function differentially in the telencephalon remains unknown. To comprehensively investigate the function of individual clonal units, a system to modify gene expression in spatially controlled manner must be developed.

To modify gene expression in neuronal subsets in the vertebrate brain, I used a heat-inducible promoter, the HSP promoter, in transgenic medaka fish. Local heat treatment using a metal probe and an infrared laser results in ectopic *Cre* induction in a small number of cells in various tissues, such as the gonads and epidermal tissues, in medaka fish (Deguchi T, et al. 2009, Kobayashi K, et al. 2012, Nakamura S, et al. 2010). Here I used an infrared laser-evoked gene operator (IR-LEGO) system to induce highly regulated spatiotemporal *Cre* expression in neural precursor cells of medaka embryos. Medaka fish have a transparent chorion, which permits noninvasive observations of the nervous system throughout development (Wittbrodt J, et al. 2002), and allows for heating a small subpopulation of differentiating neurons in the neural placode using an infrared laser (IR, wavelength: 1480 nm). Based on the fate maps of neural placodes in the medaka embryo, I will be able to induce exogenous genes in clonal units of interest by irradiating a small population of neural stem cells for post-patch neurogenesis during embryogenesis. Here we examined whether irradiation of developing medaka embryo brains using an infrared laser would allow for visualization of clonally-related HuC-expressing cells in both juvenile and adult medaka fish.

Materials and Methods

Ethics statement

All experiments in this chapter were conducted using protocols approved by the Animal Care and Use Committee of the University of Tokyo (permit number: 12-07). All surgery was performed under cold anesthesia, and all efforts were made to minimize suffering.

Fish

Medaka Tg lines, Tg (*HuC*:loxP-*DsRed*-loxP-*GFP)* and Tg (*HSP*:*Cre*), were maintained in their respective groups in plastic aquariums (12 cm X 13 cm X 19 cm). All fish were hatched and bred in our laboratory. The water temperature was maintained at ~28°C and the light was provided by fluorescent lamps for 14 h per day (08:00 to 22:00). Female fish of Tg (*HuC*:loxP-*DsRed*-loxP-*GFP)* and male fish of Tg (*HSP*:*Cre*) were crossed to get embryos. To screen double positive Tg embryos, I checked the expression of DsRed in nervous systems and BFP in crystalline after heat induction.

Heat induction in the telencephalon

Embryos were mounted at stage 24, dorsal side up, in a drop of 2% methylcellulose (M-0387; Sigma Chemical Co., St. Louis, MO) and observed using the 20x custom made objective lens (mono-coated lens of UPlanSApo; Olympus, Tokyo, Japan) for an Olympus epifluorescence microscope with IR-LEGO unit (IR-LEGO 1000; Sigma-Koki, Saitama, Japan). Heat was induced in the telencephalon by 1480-nm light generated by a high-power single mode CW Raman fiber laser (Model PYL-3-1480-M; IRE-Polus Group, Sturbridge, MA), as previously described (Deguchi T, et al. 2009, Kamei Y, et al. 2009).

Results

Spatially controlled induction of Cre/loxP recombination using an IR-LEGO system

To control Cre/loxP recombination spatially, we used the infrared laser-evoked gene operator (IR-LEGO) system (**Figure 45A**) to induce local Cre expression by laser irradiation (Deguchi T, et al. 2009. Kamei Y, et al. 2009). We heated the surface of the right neural placode of the telencephalon in stage 24 Tg (HuC:loxP-DsRed-loxP-GFP/HSP:Cre/Cry:BFP) embryos (2 dpf, **Figure 45B**) by irradiation with an incident laser power of 21.6 mW for 1 sec. GFP fluorescence was detected in a subpopulation of neurons in the right telencephalon in the heat-exposed Tg (HuC:loxP-DsRed-loxP-GFP/HSP:Cre/Cry:BFP) juvenile and adult fish only in the right side (**Figure 46**). The juveniles were observed after hatching. In negative controls, GFP fluorescence was not detected in either heat-exposed Tg (HuC:loxP-DsRed-loxP-GFP) or non-treated Tg (HuC:loxP-DsRed-loxP-GFP/HSP:Cre/Cry:BFP) fish and also in the left side of the treated Tg (**Figure 46A**). Furthermore, when we made transverse slices of adult brain, we found that GFP fluorescence was detected exclusively in only one clonal unit in the telencephalon and not detected in other brain area (**Figure 46B**). These findings indicated that GFP-expressing neurons in both juvenile and adult brains were clonally-related cells derived from the micro area of neural placodes exposed to the infrared laser.

Discussion

The use of a low laser intensity to theoretically target a single cell would make it possible to induce recombination in a single or a few adjacent cells (Suzuki M et al., 2014; Miao G et al., 2015). Determining the distributions of GFP-expressing cells by repeated analysis would allow us to identify clonal units derived from the target micro area. The presence of identical subpopulations of clonally related cells in multiple samples could reveal clonal units. Considering that GFP-expressing cells comprise a single and more than one clonal unit, all the distribution patterns should be described by a combination of identified clonal units. Based on my finding in Chapter 3, the number of target neural stem cells that generate clonal units in the telencephalon is estimated to be ~40 cells/hemisphere. Further comprehensive analysis will reveal the distribution of neural stem cells in the medaka embryo and allow us to create a fate map of individual clonal units.

In future studies, I will induce exogenous genes in clonal units of interest using this method. For example, induction of genes for DREADD (Designer Receptors Exclusively Activated by Designer Drugs) will enable us to artificially control neural activity in clonal units of interest. In addition, further ATAC-seq with a single clonal unit (Chapter 4) will reveal candidate transcription factors that define cell lineages of post-hatch neurogenesis. Ectopic expression of the identified transcription factors in neural stem cells of interest will clarify the molecular mechanisms underlying the cell-lineage diversity of post-hatch neurogenesis. Thus, this work provides a promising method for lineage analysis of newly born neurons during the growth stage and allows for further investigation of the involvement of such a lineage-dependent structures in the formation of functional neural circuits mediated by post-hatch neurogenesis.

Finally, I will discuss the general importance of this method in the field of neuroscience. The development of methods to analyze neural subpopulations is

important. Among neural networks that express the same neuropeptides, specific subpopulations are reported to function as a neural network for specific behaviors (Hong W, et al., 2014; Wu Z et al., 2014). Analysis of neural subpopulations requires the appropriate promoters/enhancers. Enhancer trap lines are effective to limit the neuronal populations for investigation in zebrafish (Scott EK et al., 2007; Asakawa K et al., 2008; Otsuna H et al., 2015). However, comprehensive analysis is difficult unless the gene expression pattern is known. For site-specific gene modulation, viral injection has been performed in mouse studies (Kitamura T et al., 2015; Adhikari A et al., 2015). Injecting virus into intact brain, however, is not possible. The present study provides a noninvasive method of performing a comprehensive analysis of the neural system at clonal unit levels.

Chapter 6

Ontogeny and sexual differences in swimming proximity to conspecifics in response to visual cues in medaka fish (Oryzias latipes).

Introduction

The development of social behavior is commonly observed among various vertebrates from fish to mammals (Mason, 1979; Ball et al., 1993). Adult animals exhibit various social behaviors after sexual maturation, such as mating behaviors (intersexual relationship) and/or male-male competition for mating partners (intrasexual relationship) (Kaidanovich-Beilin et al., 2011; Maekawa et al., 2014). In contrast, observations of many species of vertebrates, teleosts (Higashijima et al., 2004) and birds (Bottjer and Arnold 1986), indicate that the social behavior repertoires of larval and sexually immature individuals are much less complex than those of adults. Development of these social behaviors is coordinated with social factors, such as the presence of conspecifics (Engeszer et al., 2007), as well as physiologic and environmental factors (Engeszer et al., 2004; de Kort et al., 2009; Green et al., 2012; Croft et al., 2012; Mangiamele et al., 2013; Snoeren et al., 2014). For example, the shoaling preference of zebrafish is affected by their early social experience with conspecifics (Engeszer et al., 2007). Therefore, the social motivation to interact with other individuals may change during growth and be affected by social factors. Investigating the neural/molecular basis underlying the development of complex social behaviors has been difficult, because of lack of simple behavioral paradigms to compare social behaviors throughout life using an animal model for molecular genetics.

Medaka fish, an animal model for molecular genetics, exhibit complex behavioral repertoires associated with mating under laboratory conditions; sexually mature females are able to visually discriminate conspecifics, prefer to mate with socially familiar males, and tend to reject unfamiliar males (Okuyama et al., 2014). In a triadic relationship (male, male, and female), one male robustly exhibits mate-guarding behavior toward the female and rival male (Yokoi et al., 2015). Two

adult fish exhibit schooling behavior (Imada et al., 2010), which is elicited by movement of a visual background (optomotor response). By contrast, larval fish do not exhibit visually-elicited schooling behaviors (Imada et al., 2010). Therefore, medaka fish could be a useful animal model for studying the development of social behaviors, especially visually-mediated social behaviors. Until recently, however, no behavioral paradigm existed for assessing visually-mediated social behaviors throughout life using medaka fish.

Here, I established a novel behavioral paradigm to quantify the proximity to visual cues of conspecifics from larval/juvenile to adult fish, as proximity to conspecifics is the first and essential step in various social behaviors, schooling (Imada et al., 2010; Ohicai et al., 2013), mating (Okuyama et al., 2014), and aggressive behaviors (Kagawa 2014; Yokoi et al., 2015). This paradigm allows me to compare the effect of the growth stage, sex, reproductive status, and social familiarity on visually-mediated proximity to conspecifics.

Materials and methods

Ethics statement

The work in this paper was conducted using protocols specifically approved by the Animal Care and Use Committee of the University of Tokyo (permit number: 12–07). All surgery was performed under anesthesia using MS-222 (tricaine methanesulfonate), and all efforts were made to minimize suffering, following the NIH Guide for the Care and Use of Laboratory Animals.

Animal maintenance

Medaka fish (Oryzias latipes) of the d-rR strain were maintained in groups (~10 fish, male and female mixed breeding) in a plastic tank (12x13x19 cm). Growth stages were categorized into three groups according to the previously described definition (Kinoshita et al., 2009). "Larval fish" included those ~1 month old and less than 1 cm long (Stage 41~42, second and third larval stages). "Juvenile fish" included those less than 2 months old, ~1.5 cm long, and sexually immature (Stage 43, first juvenile stage). "Adult fish" included those ~3 months old, longer than 2 cm, and sexually mature. Zebrafish of wild-type strain (RIKEN WT) were maintained in groups in a plastic tank of the same size. All groups were maintained at a temperature of 28°C and under a 14:10-h light-dark condition.

Quantification of the proximity to visual cues from other fish

The detailed procedure is explained in **Figure 47**. Two round transparent tanks (diameter: 15 cm, 10 cm) were used for juvenile and adult medaka fish. For larval fish, smaller transparent tanks (diameter: 10 cm, 7 cm) made of acrylic glass were used (**Figure 47A**). The thickness of the tank wall was 3-mm each. The water depth was maintained at ~2 cm. The fish in the Inside tank was softly placed in the middle of the

tank with hand. After placing the fish in each part ("Outside" and "Inside"), the water tanks were covered with a semi-transparent sheet to provide a clear visual background for assessing fish movement. A video was recorded from underneath the water tanks. 1 min after placing the fish, a 1-min video was recorded (**Figure 47C**). The video data were analyzed with software, Move-tr/2D (Library Co., Japan). The 1-min video was transformed into 1800 frames (30 frames/s). The position of the center of the fish body was automatically recorded, and the distance between the center positions of the two fish was calculated in each frame. For negative controls, only one fish was placed into either the Outside or Inside water tank, and videos were recorded (**Figure 47D**). The fish were able to freely swim and move around in the Outside tank (**Figure 48**). The two videos were then overlaid into a virtual composite and the virtual composite distances between the center positions of the two fish were calculated. "Percentage of time in each bin" (%) was calculated based on the number of frames in each bin (0.25 cm-width), divided by 1800 then multiplied by 100. To determine whether the medaka fish maintained proximity, "proximity frequency" (%) was calculated as the sum of the percentage of time in each bin in which distance was less than 6 cm (4.5 cm, for larval fish), and compared to that of the negative control using a Mann-Whitney U test (**Figure 47E**). To assess the proximity, I used "proximity frequency" instead of the inter-individual distance. The reason is that the deviation of the inter-individual distance was much higher in case that the two fish did not maintain close proximity (**Figure 49A**), which decreased detection sensitivity of the difference compared with the negative controls.

Optic nerve dissection

I performed the optic nerve dissection following the NIH Guide for the Care and Use of Laboratory Animals. Fish were anesthetized in MS222 solution. Fish were then placed on wet tissue paper and only the optic nerves were cut – the eyes were not

removed. Fish were placed into a fish tank containing 1% NaCl in water. After a few minutes, the fish began to swim. Optomotor response test confirmed visual system dysfunction. After 1 week of recovery, the optic nerve-cut medaka fish ("Cut fish") were used in experiments. Iconfirmed that 1 week after the surgery, the mortality rate of optic nerve-cut fish was 0% and all of them maintained fertility without any signs of starvation.

Optomotor response test

The optomotor response test was performed as described previously (Imada et al., 2010). One fish was placed into the tank and a striped paper cylinder was moved at a speed of 35.2 degrees/s.

Fish familiarization

Fish familiarization was accomplished as previously described (Okuyama et al., 2014). The detailed procedure is described in **Figure 57A**. Fish were maintained in pairs before this test. After verifying over several consecutive mornings that the females laid eggs, the pairs of fish were used in the test. To visually familiarize each other, the day before mating, a male fish was placed into a transparent cup so that the two fish could see each other (Okuyama et al., 2014). The two fish that had seen each other were used as "familiar". At the same time, I prepared "unfamiliar", which were swapped between two pairs that had undergone visual familiarization before mating. The next morning I performed behavioral test at around 11: 00 in the morning. For the "before mating" test, I transferred a male/female pair of fish into an apparatus to assess proximity to conspecifics. For the "after mating" test, a pair of fish was placed together in a single tank. After the female fish laid eggs, I used that male/female pair for assessing proximity.

Results

Assessment of visually-induced motivation to maintain proximity to conspecifics

I examined whether the proximity between a pair of adult female medaka fish (age, 2 months; length, 2.5 cm) could be detected with a transparent cylindrical partition between the fish. The peak of histograms of the distance between two fish was ~2.75 cm and the mean distance was 5.14 ± 0.27 cm (**Figure 49A**, left upper panel). In the present study, proximity was quantified as the frequency of a distance less than 6 cm (proximity frequency), as the histograms had an apparent inflection point at approximately 6 cm (**Figure 47E**). To determine statistically significant proximity, I prepared negative controls based on previous studies (Okuyama et al., 2014; Yokoi et al., 2015). I placed fish separately into either the Inside or Outside tank (**Figure 47D**), and made a virtual composite of videos of the two individuals, which represents two free-swimming fish without any inter-individual interaction (Okuyama et al., 2014; Yokoi et al., 2015). The swimming distances of the two fish did not differ from that of negative controls (**Figure 48**). When I calculated the proximity frequency of the two individuals of wild-type strain (d-rR), the proximity frequency of 72.39% ± 5.27% was significantly higher than that of negative control (42.27% ± 2.90%) (Mann-Whitney U=12, p=0.0005, sig≤0.05, 2-tailed). A significant difference in the proximity frequency compared with the negative controls indicated that the two fish maintained proximity to each other (**Figure 49B**, the left panel). Next, to examine whether a visual response of both fish is required to maintain proximity, one of the two fish was replaced by a fish with the optic nerve cut (Cut; **Figure 49AB**). When the Cut fish was placed in the Outside tank, proximity frequency (71.57% ± 6.40%) was significantly higher than negative controls (39.85% ± 1.81%) (Mann-Whitney U=5.5, p=0.0001, sig≤0.05, 2-tailed) (**Figure 49AB**). The peak of histograms of the distance

between the two fish was ~3.5 cm and the mean distance was 5.28 ± 0.39 (Mean ± SEM) cm. This result indicates that a fish in the Inside tank maintained proximity to the fish in the Outside tank. On the other hand, when the Cut fish was placed in the Inside tank, no significant proximity was detected (47.73% ± 2.83%, negative control; 41.05% ± 1.80%) (Mann-Whitney U=30, p=0.0841, sig≤0.05, 2-tailed) (**Figure 49AB**). This result was the same as when Cut fish were in both the Outside and Inside tanks (33.78% ± 2.39%, negative control; 37.51% ± 1.94%) (Mann-Whitney U=37.50, p=0.3630, sig≤0.05, 2-tailed). I additionally performed the same experiments with male fish and confirmed that there was no apparent difference between sexes (**Figure 50**). I also confirmed that there was no significant difference in the swimming distances between the Cut fish and normal fish in the Outside tank (**Figure 49C**). Thus, normal visual function in fish in the Inside tank was necessary and sufficient for these fish to maintain proximity based on visual cues from fish in the Outside tank. This behavioral paradigm can be used to quantify the visually-induced motivation of fish in the Inside tank as a focal fish.

Maintained proximity of larval fish with conspecifics and heterospecifics

To evaluate the development of visually-induced motivation to maintain proximity to conspecifics and/or conspecific recognition during growing stages, I used larval fish (age, ~1 month; length, <1 cm) and smaller water tanks (**Figure 47B**) and juvenile fish (age, ~2 months; length, ~1.5 cm). Larval (71.24% ± 3.54%, negative control; 43.88% ±4.01%) and juvenile fish (66.90% ± 5.78%, negative control; 33.99% ± 1.95%) maintained proximity to conspecifics, indicating that medaka fish have visually-induced motivation to maintain proximity already at the larval/juvenile stage (**Figure 51AB**, **Figure 52**). Next, to investigate whether medaka fish maintain proximity in a species-specific manner, I examined whether medaka fish maintain

proximity based on the visual cues of heterospecific fish. Most adult and juvenile medaka fish in the Inside tank did not maintain proximity to zebrafish in the Outside tank, irrespective of sex (adult male; 42.18% ± 4.80%, negative controls; 40.19% ± 2.33%, adult female; 43.31% ± 4.46%, negative controls; 39.15% ± 2.12%, juvenile; 42.72% ± 3.09%, negative controls; 39.32% ± 2.26%) (**Figure 51C, Figure 52A**). Thus, adult/juvenile medaka fish visually distinguished zebrafish from medaka fish and exhibited no motivation to maintain proximity with heterospecific fish. In contrast, larval medaka fish maintained proximity to heterospecific fish of the same size (59.28% ± 5.26%, negative control; 43.55% ± 4.05%) (Mann-Whitney U=62, p=0.0357, sig≤0.05, 2-tailed) (**Figure 51D, Figure 53**). The optomotor response experiments indicated that larval medaka fish have the ability to respond to visual stimuli (**Figure 54**). Thus, larval medaka fish may lack the ability to distinguish conspecifics and/or have visually-induced motivation to maintain proximity to heterospecific fish.

Effect of sexual difference/physiologic status on maintained proximity to conspecifics

The reproductive cycle of medaka females is 24 h and adult females spawn and lay eggs once every morning under laboratory conditions (Kinoshita et al., 2009). Endogenous physiologic conditions and hormonal states also change in close association with reproductive regulation in a time-of-day-dependent manner (Karigo et al., 2012). Here I examined whether the proximity of adult (sexually mature) fish of the same and opposite sex was affected by time-of-day. I performed the behavioral test in the morning (from AM10:00 to 12:00) and in the afternoon (from PM 17:00 to 19:00). Adult fish significantly maintained proximity with conspecifics irrespective of sex both in the morning (male & male, female & male, female & female, male &

female; 54.46% ± 5.91%, 66.96% ± 8.79%, 71.36% ± 5.54%, 65.55% ± 6.00%, negative control; 29.20% ± 2.60%, 31.59% ± 2.01%, 28.31% ± 4.49%, 36.61% ± 3.165%) and in the afternoon (male & male, female & male, female & female, male & female; 54.44% ± 4.97%, 75.75% ± 3.34%, 72.47% ± 5.56%, 84.15% ± 4.50%, negative control; 32.85% ± 1.97%, 41.31% ± 2.97%, 32.96% ± 2.79%, 34.68% ± 3.00%) (**Figure 55, Figure 56**). The standard error of the mean (SEM) of the proximity frequency, which described the variability within individual experimental groups, was relatively high in the morning (mating period, from 10:00 to 12:00) in an intersexual (female-male) relationship (**Figure 55** the upper panel, **Figure 56**). Next, I tested the types of social factors that affected proximity to the opposite sex during the mating period. As female medaka fish visually recognize familiar males and tend to reject unfamiliar males (Okuyama et al., 2014), I tested the effect of social familiarity on proximity before spawning. The proximity frequency of a female with a familiar male (75.90% ± 5.52%) was significantly higher than that with an unfamiliar male (55.75% ± 6.60%) before spawning (Wilcoxon matched-pairs signed rank test, $p=0.0181$, sig$\leq$0.05, 2-tailed) (**Figure 57B**). The proximity frequency of a female with an unfamiliar male (47.63% ± 5.48%) was not significantly different from its negative control (35.48% ± 1.28%) before spawning (Mann-Whitney $U=15$, $p=0.0865$, 2-tailed) (**Figure 58** the upper panel, **Figure 59** the left panel). Finally, I examined whether familiarity affected proximity after spawning. After spawning, the proximity frequency did not significantly differ between familiar (54.51% ± 6.31%) and unfamiliar males (47.82% ± 6.27%) (Wilcoxon matched-pairs signed rank test, $p=0.4548$, 2-tailed). In addition, male fish maintained proximity with females to the same degree, irrespective of social familiarity both before (familiar; 76.23% ± 6.54%, unfamiliar; 75.28% ± 5.95%) (Wilcoxon matched-pairs signed rank test, $p=0.7609$, 2-tailed) and after the female's spawning (familiar; 56.69% ± 8.01%, unfamiliar; 58.80% ± 6.09%) (Wilcoxon matched-pairs signed rank test, $p=0.9032$, 2-tailed) (**Figure 57B, Figure 58**,

Figure 59), which was consistent with previous reports that social familiarity and female reproductive status have no effect on male mating activity (Okuyama et al., 2014; Yokoi et al., 2015).

Discussion

I established a behavioral paradigm to quantify visually-induced motivation of a single focal fish to maintain proximity to a single target fish. This behavioral paradigm using only two fish makes it very easy and efficient to compare the same visual behavior under different developmental stages, different physiologic conditions, and different social status. In the present behavioral paradigm, medaka fish robustly and reproducibly maintained proximity to conspecifics. Furthermore, the visually-induced motivation of only a single fish in the Inside tank can be measured in this behavioral paradigm. This might be because target fish in the Outside tank are more likely to be in the visual field of the focal fish in the Inside tank. Additionally, fish in the Outside tank could not directly approach fish in the Inside tank due to the spatial restrictions in this behavioral paradigm, although the swimming behavior of fish in the Outside tank was normal (**Figure 48**). Due to the spatial restrictions, swimming behavior of fish in the Outside tank may less reflect maintenance of proximity than behavior of the fish in the Inside tank.

In the present study, swimming proximity to other fish was affected by the developmental stage, social relationship, and physiologic conditions. First, I demonstrated that larval fish tended to maintain proximity to heterospecifics. One possibility is that larval fish do not have the ability to discriminate conspecific fish. Visual function in medaka fish (such as spatial and temporal resolution) improves during growth (Carvalho et al., 2002), and thus the ontogenetic development of visual function may be necessary for perception and recognition of conspecific fish. Another possibility is that juvenile fish have visually-induced motivation to approach heterospecifics. In other species, young fish form a group with different species to avoid predation (Lightfoot et al., 1996; Ward et al., 2003). Further ecologic studies are needed to examine whether larval fish tend to shoal with heterospecifics under natural

conditions (Laegdsgaard and Johnson, 2001). Previous study demonstrated that visually-induced motivation to maintain proximity to heterospecifics declined with an increase in the growth stage. Thus, this behavioral paradigm will enable us to investigate the molecular/neural basis underlying development/changes in visually-mediated social behavior by focusing on the specificity of the proximity maintained with conspecifics. In addition, I demonstrated that adult medaka females prefer to maintain proximity to visually familiar males only when they are ready to spawn. The present findings strongly suggested that adult females decreased visually-induced motivation to maintain proximity to unfamiliar males. Previously Okuyama and I reported that females choose mating partners by rejecting courtship of unfamiliar males, which prolonged the latency to mate (Okuyama et al., 2014). Thus it had been unknown whether female positively approach familiar males. The present study, for the first time, demonstrated that females are motivated to positively approach familiar males rather than unfamiliar males. Based on the finding that proximity frequency with familiar and unfamiliar males did not differ after spawning, female medaka fish may lose selectivity for association partners after spawning.

Based on recent studies with mammals and humans, the molecular mechanism that controls social motivation may involve some neurotransmitters, such as dopamine and oxytocin (Takayanagi et al., 2005; Enter et al., 2012; Gunaydin et al., 2014; Bridges et al., 2015). The ontogeny of social behaviors using animal models has been well studied in rodents. For example, parental behaviors develop in close association with pregnancy, season, and presence of pups. Studies using these experimental animals revealed that hormonal changes (Bridges et al., 2015), adult neurogenesis (Sakamoto et al., 2011; Peretto et al., 2014), and epigenetic modifications (Branchi et al., 2009) are involved in the development of behavior. Social interaction in rodents, however, is mainly mediated by olfactory (Cheal et al., 1975; Avale et al., 2011) and/or auditory cues (Campbell et al., 2014). In humans, the ontogeny of the

ability to visually recognize individuals (ability of infants to perceive faces of adults) (Fants 1963) and social attention (Farronia et al., 2000) has been investigated by focusing on infant gazing. However, investigation of the molecular/genetic basis underlying the ontogeny of visually-mediated social behaviors is very difficult in human studies. My study provides a behavioral paradigm with medaka fish for investigating the development/changes in visually-mediated social behavior.

General Discussion

In this doctoral thesis, I investigated the mechanisms underlying construction of the telencephalon by neurogenesis during growth. In Chapter 1, I found that post-hatch neurogenesis occurs broadly in the telencephalon in medaka fish during growth. In teleost fish, post-hatch neurogenesis occurs more broadly in the whole brain, even after sexual maturation, than in any other vertebrate studied to date. The distribution of the regions of neurogenesis is highly conserved among teleost fishes, but the physiologic significance of the widespread neurogenic capacity throughout the brain remains obscure. Post-hatch neurogenesis in teleost fishes has been thought to contribute only to brain growth and regeneration after brain injury (Kizil C et al., 2012; Barbosa JS et al., 2015), and thus little attention has been paid to the cell-lineage diversity of neurogenesis involved in the development of the adult brain.

In the zebrafish telencephalon, neural progenitors contributing to post-hatch neurogenesis exhibit different characteristics between the pallium and subpallium. Progenitors positive for radial glia markers (e.g., glial fibrillary acidic protein [GFAP]) distribute to the pallium, while progenitors positive for epithelial markers (e.g., nestin) distribute in the subpallium (Ganz J et al., 2010, 2016). Prominent subdivisions in the expression pattern of conserved marker genes are observed in the telencephalon of zebrafish (Ganz J et al., 2014). For example, *tbr1* and *neurod* are expressed in the pallium, while *dlx2a* and *dlx5a* are expressed in the subpallium (Ganz J et al., 2012). The structure of a single cell-lineage at the brain-wide level had not been described previously in any teleost fish. Therefore, in my doctoral thesis (Chapters 2 and 3), I established a systematic clonal analysis method and found that anatomic regions in the pallium comprise multiple clonal units exclusively, while anatomic regions of the subpallium comprise multiple clonal units in a mixed pattern. This finding strongly suggested that the number and type of clonal units of post-hatch neurogenesis generate

the basic architecture of the pallium. My findings shed light on the mechanism underlying the structural diversity in the pallium among various fish species. If individual clonal units develop autonomously without interacting with each other in the pallium, the structure of the pallium could easily be modified by changes in the number and type of clonal units. Thus, my findings might provide a link between the cell-lineage diversity of post-hatch neurogenesis and the structural diversity of the pallium among teleost fish species. By contrary, the structural conservation of the subpallium is observed among vertebrates; basal ganglia, subdivided into two major parts, striatum and pallidum, are exist in all jawed vertebrates. According to my finding, newly born neurons in the subpallium seem to develop by closely interacting with those in other clonal units. I assumed that such a close interaction could result in a structural restriction, which might lead to the structural conservation among vertebrates.

Next, I investigated the molecular mechanisms contributing to the different construction by clonal units (Chapter 4). Using ATAC-seq to analyze the differences in gene expression regulation, I found that the axon guidance pathway is differentially regulated between the pallium and subpallium. Regulatory regions specific to the pallium and subpallium could be predicted based on the sequence data of open chromatin, and I used RNA-seq to confirm the expression of transcription factors that bind to the regulatory regions: *NeuroD2* in the pallium and *Meis2* in the subpallium. Using RNA-seq, I also identified some candidate genes (subpallium: *unc5a* in the netrin pathway, *EPHB1* in the Ephs/ephrin pathway, and *CXCL14* and *CXCL12* in the cytokine-cytokine receptor pathway; pallium: *EPHA5*) selectively involved in the axon guidance pathway in the pallium and subpallium. In mammals, *Meis2*, *EPHB1*, and *CXCL14* are strongly expressed in the postnatal regions of neurogenesis, the subventricular zone and/or the dentate gyrus (Conover JC et al., 2000; Banisadr G et al., 2011; Agoston Z et al., 2014). Previous findings together with my results suggest

that the molecular mechanisms of subpallium neurogenesis in the teleost brain are equivalent to those of postnatal neurogenesis in the mammalian brain.

What then is the equivalent molecular mechanism of neurogenesis between the teleost pallium and the mammalian brain? Given that the rapid increase in brain volume (brain spurt) mediated by neurogenesis occurs only during the neonatal period in mammals, I focused on the neonatal and/or late-stage fetal period in mammals to compare to the medaka. As described in Chapter 3, newly born neurons that were DsRed-positive in the Tg (*HuC*-loxP-*DsRed*-loxP-*GFP*) line were surrounded by GFAP-positive radial glia with apical-basal polarity, while newly born neurons in the subpallium were not. This GFAP distribution is also reported in the zebrafish brain (Lam CS et al., 2009; Schmidt R et al., 2013). In the developing mammalian brain, newly-born neurons in the cortex migrate along GFAP-positive radial glia, thus the mechanism of integration of newly born neurons into the neural circuit during growth in the teleost brain seems to have an underlying developmental process similar to that of the mammalian pallium. Consistently, the homologs of pallium-preferential genes in medaka fish are involved in neural development in the mammalian brain. *EPHA5* broadly functions in cell-cell recognition and in the topographic orientation of neuronal systems in the developing cortex (Cooper MA et al., 2009). *NeuroD2* has a critical role in neuronal differentiation and survival of neural progenitors. Interestingly, NeuroD2-KO mice exhibit small brains and early death. Functional analysis of pallium-preferential genes in post-hatch neurogenesis in medaka fish might also provide clues to compare the molecular basis of the brain architecture of the pallium between fish and mammals.

I found that the construction mechanism in certain anatomic regions might differ at both the structural and molecular levels, but whether individual clonal units function as “functional units” or whether the gene expression is unified in each clonal unit is unclear. Thus, to modify gene expression in a single clonal unit of interest, I

used the IR-LEGO system and induced Cre-loxP recombination at a single cell in a spatially controlled manner (Chapter 5). Combining a transgenic line in which neural inactivation (e.g., the DREADD system (Vardy E et al., 2015) or tetanus toxin (Kumar D et al., 2014)) can be induced by Cre/loxP recombination will facilitate functional analysis. Finally, for future behavioral analysis, I established a novel behavioral system to compare social interactions of medaka fish throughout life. Though many social behavior paradigms have been established in medaka fish, there has been no behavioral assay system to directly evaluate social cognition during growth. In Chapter 6, I quantified the swimming proximity to other fish among larval, juvenile, and adult medaka, and was able to evaluate the behavioral development of social cognition during growth. Future studies might uncover the novel mechanisms that underlie specialization of brain function, especially in the pallium.

The findings from my doctoral studies suggest how the cell-lineage diversity of neurogenesis contributes to regional specialization in the pallium, at least in teleosts. Specialization of brain function is assumed in human cortex based on studies of partial brain lesions (Riva D et al., 1993; Haaland KY et al., 1994) and functional magnetic resonance analysis (Wang D et al., 2014; Yeo BT et al., 2015). It remains unknown, however, whether the cell-lineage diversity of neurogenesis contributes to the specialization of brain function in the cortex in any species. It is likely that the cell-lineage diversity generates regional specialization as well as specialization of brain function in the vertebrate pallium. In teleost fishes such as the cichlid (Burmeister SS et al., 2009; Munchrath LA et al., 2010), comparative studies have demonstrated a positive correlation between the structural complexity of the pallium and behavioral complexity, especially social behavior. My research provides clues to explain how such complex social behaviors mediated by evolutionary changes of the pallium emerge. I expect that this study will contribute to our understanding of the mechanisms of behavioral development mediated by neurogenesis during growth as well as the

evolutionary mechanisms of complex behaviors from ontogenetic and phylogenic viewpoints.

Figures & Tables

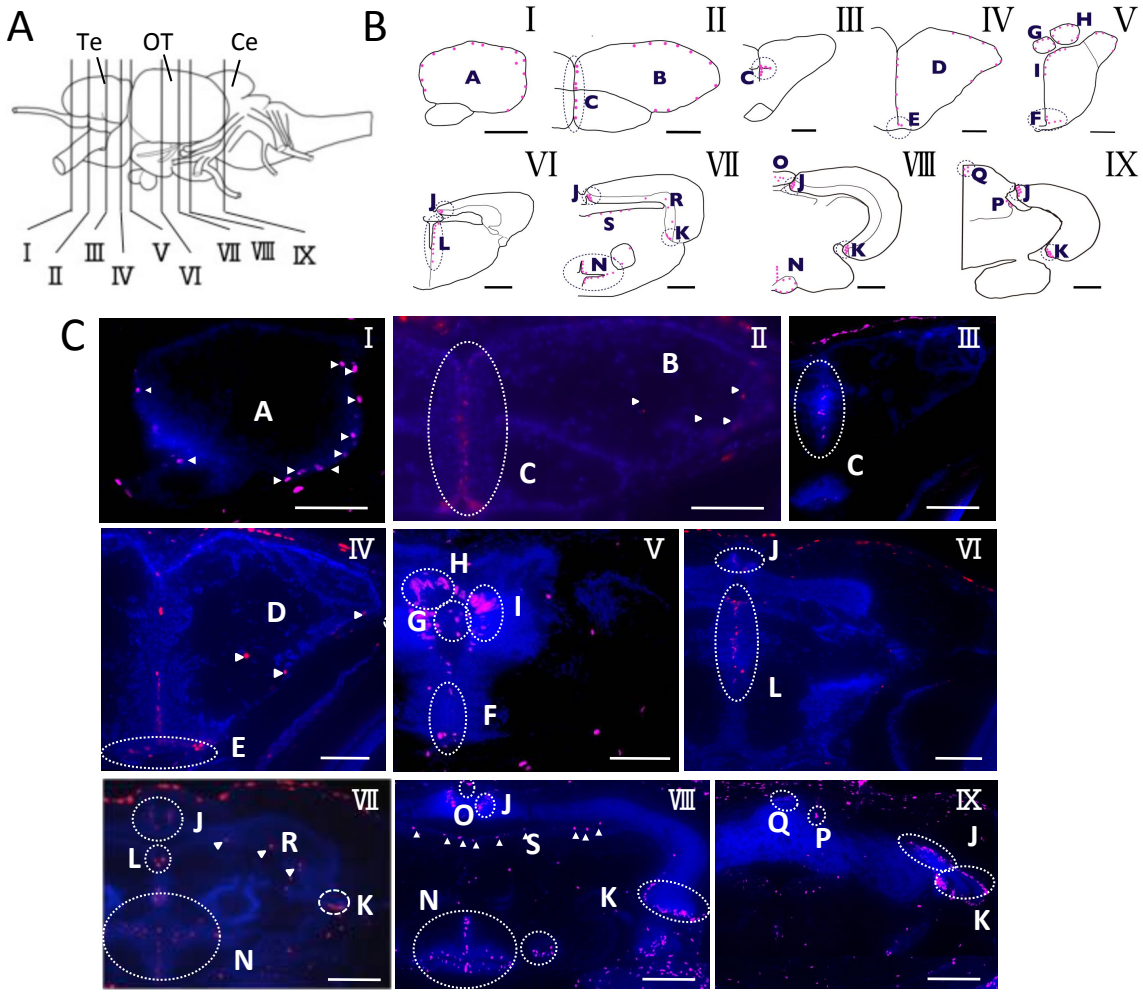

Figure 1. Mapping proliferation zones in the brain of young medaka.
(A) Schematic drawing of the lateral view of the medaka brain. The positions of sections I–IX are indicated by the lines. Te: telencephalon, OT: optic tectum, Cb: cerebellum. (B) Schematic representation of the distribution of the 18 proliferation zones. Red dots indicate proliferating cells. Zone A: marginal zones of the anterior part of the telencephalon, Zone B: marginal zones of the dorsolateral part of the telencephalon, Zone C: medial zones of the telencephalon, Zone D: dorsolateral part of the posterior part of the telencephalon, Zones E and F: preoptic area, Zone G: pineal body, Zone H: habenular nucleus, Zone I: ventromedial nucleus, Zones J and K: optic tectum, Zone L: anterior part of marginal zones of third ventricular zone, Zone N: hypothalamus, Zones O–Q: cerebellum, Zone R: periventricular grey zone (layer 3), and Zone S: Ependyme. Roman numerals in the panels correspond to section numbers shown in (A). Proliferation zones were determined according to the medaka fish brain atlas (Figure 2). (C) Distribution of BrdU-positive cells in the different proliferation zones. A magnified photo for zones P and Q (cerebellum) in panel XI is shown in Supplemental Fig. 2. Scale bars indicate 100 mm.

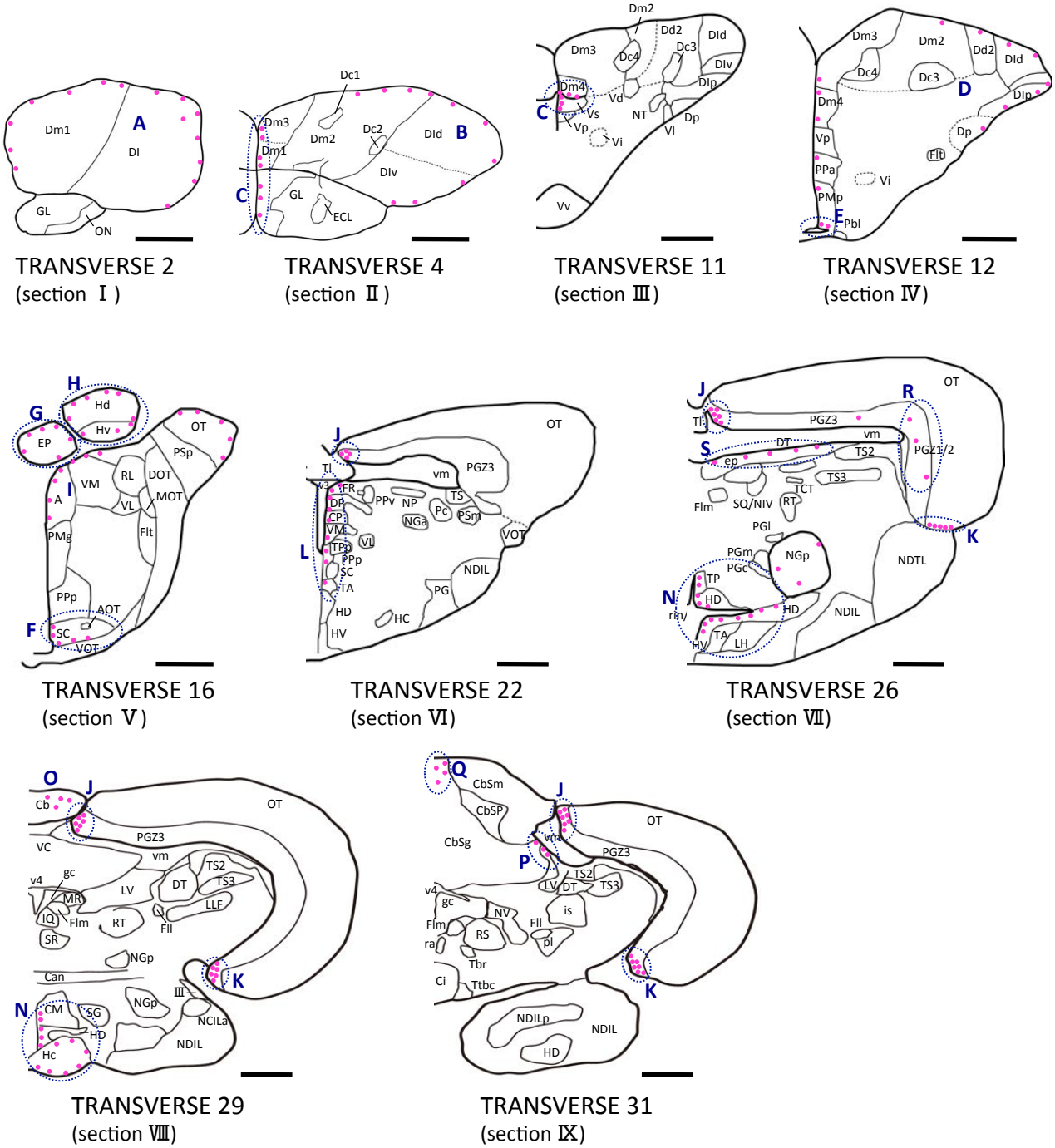

Figure 2. Determination of proliferation zones based on the brain atlas of the medaka fish

Scale bars indicate 100 mm.

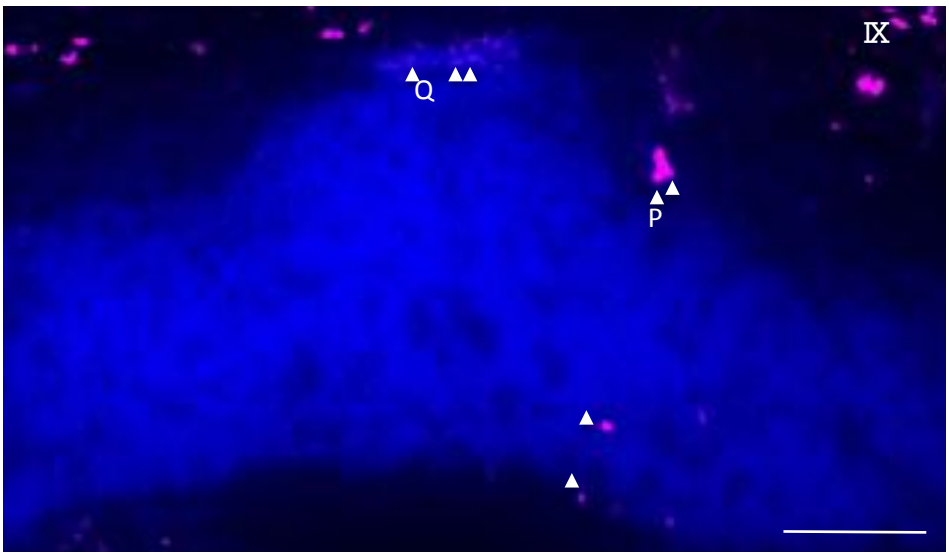

Figure 3. Distribution of BrdU-positive cells in the cerebellum (Zones P, Q).
Magnified figure of panel XI in Fig.1. Scale bars indicate 80 mm.

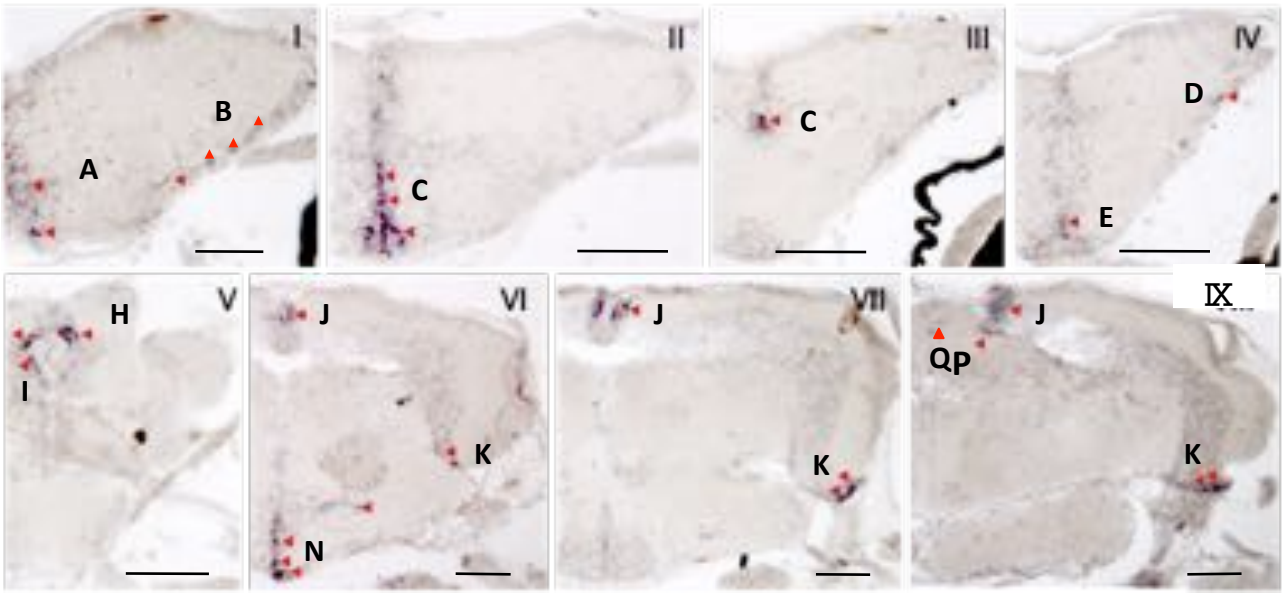

Figure 4. Distribution of medaka p53-expressing cells in the brain of young medaka. Zones A–D: telencephalon, Zones E: preoptic area, Zone H: habenular nucleus, Zone I: ventromedial nucleus, Zones J and K: optic tectum, Zone N: hypothalamus, Zones P and Q: cerebellum. Scale bars indicate 100 mm.

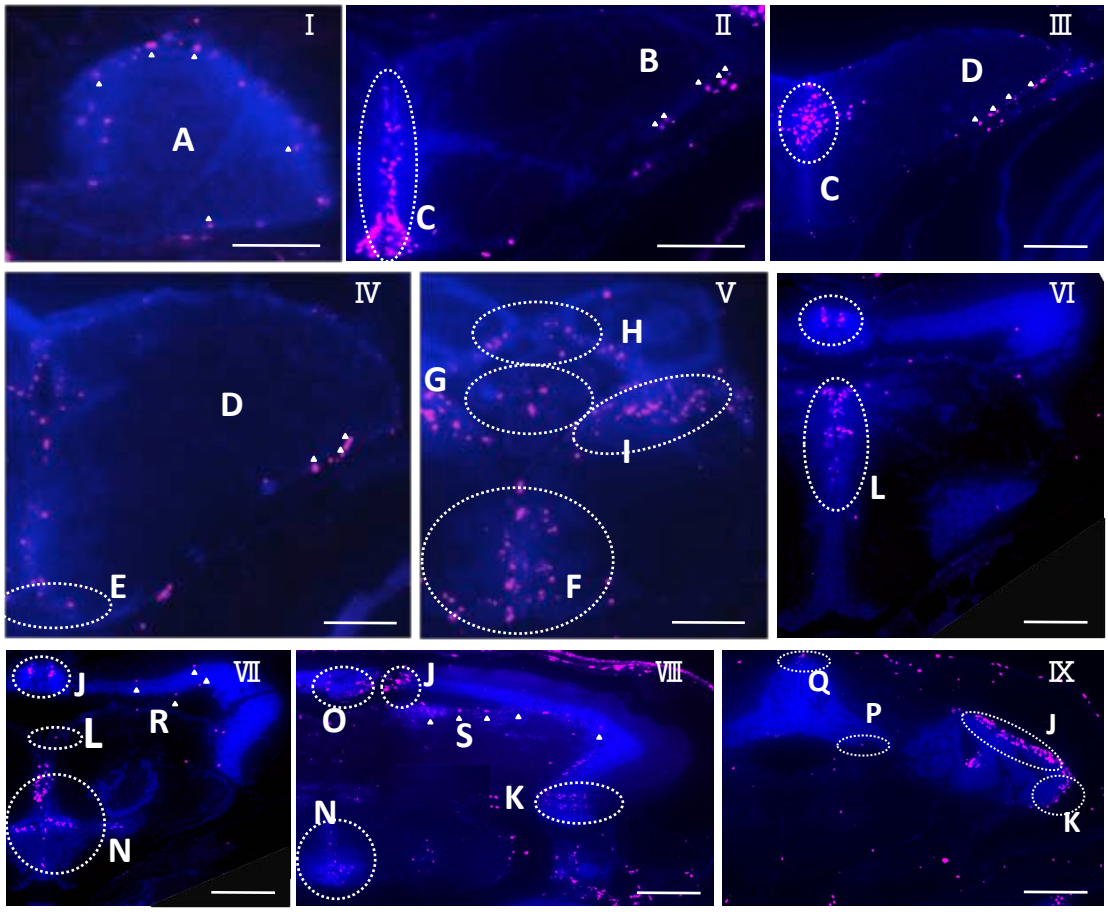

Figure 5. Distribution of BrdU-positive cells immediately after BrdU exposure in the *p53* mutant.

Zones A–D: telencephalon, Zones E and F: preoptic area, Zone G: pineal body, Zone H: habenular nucleus, Zone I: ventromedial nucleus, Zones J and K: optic tectum, Zone L: anterior part of marginal zones of third ventricular zone, Zone M: hypophysis, Zone N: hypothalamus, Zones O–Q: cerebellum, Zone R: periventricular grey zone (layer 3), and Zone S: Ependyme. Scale bars indicate 100 mm.

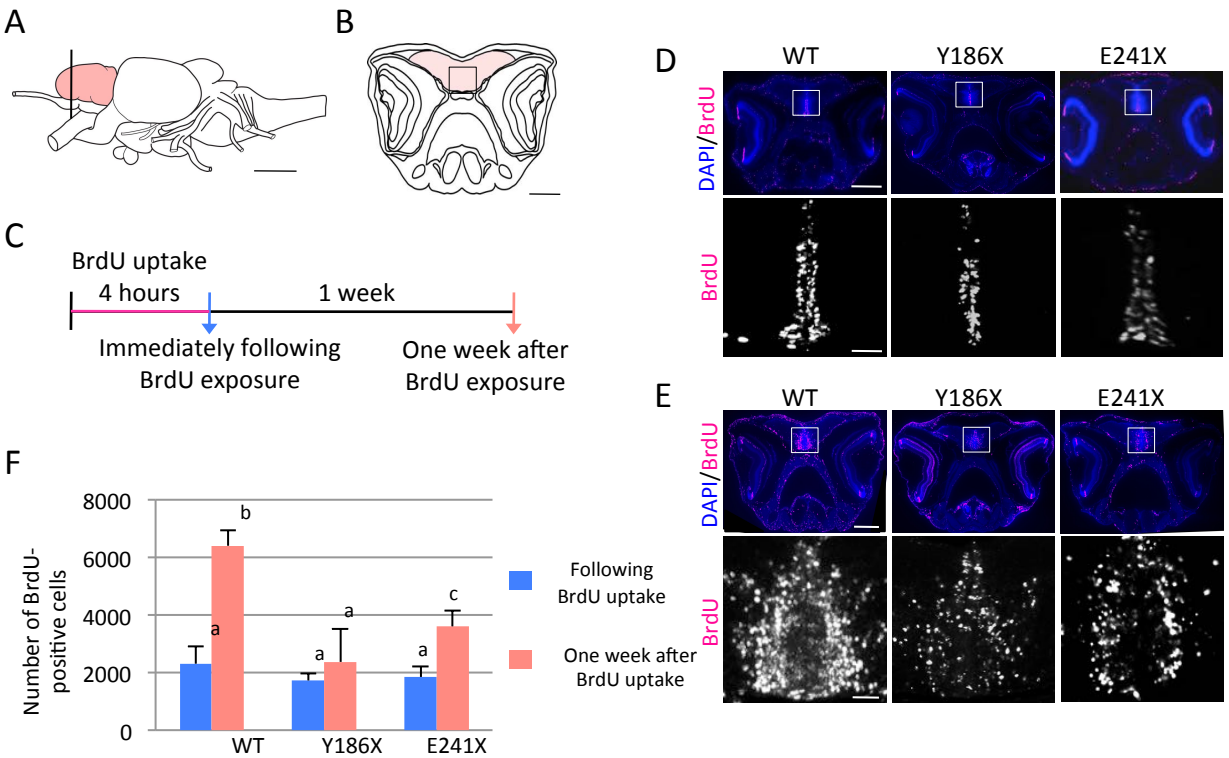

Figure 6. Comparison of the distribution and number of newborn cells in WT and p53 mutants.

(A) Schematic drawing of the medaka brain and position of the telencephalon in the brain. (B) Schematic drawing of the transverse section of the medaka head. The section of images in (D) and (E), are indicated by a line and a square in (A) and (B), respectively. The pink area represents the medaka telencephalon. (C) The time schedule of this experiment. (D and E) Anti-BrdU immunohistochemistry of paraffin sections from wild-type (WT) medaka (Cab strain) and p53 mutants (Magenta). Nuclei were stained with DAPI (Blue). The upper row indicates the transverse sections (Scale bars, 200 mm) and the lower row indicates the magnified view of the proliferation zone (Zone E; Scale bars, 40 mm), represented by the white rectangles in the upper row. (D) Immunohistochemistry was performed immediately after BrdU exposure. (E) Immunohistochemistry was performed 1 week after BrdU exposure. (F) Number of BrdU-positive cells in the telencephalon of WT and p53 mutants medaka brains. Significant differences were observed between a & b, and b & c ($p < 0.01$ and $p < 0.05$, respectively; ANOVA with Bonferroni-Dunn post-hoc test; n = 3–4 per group).

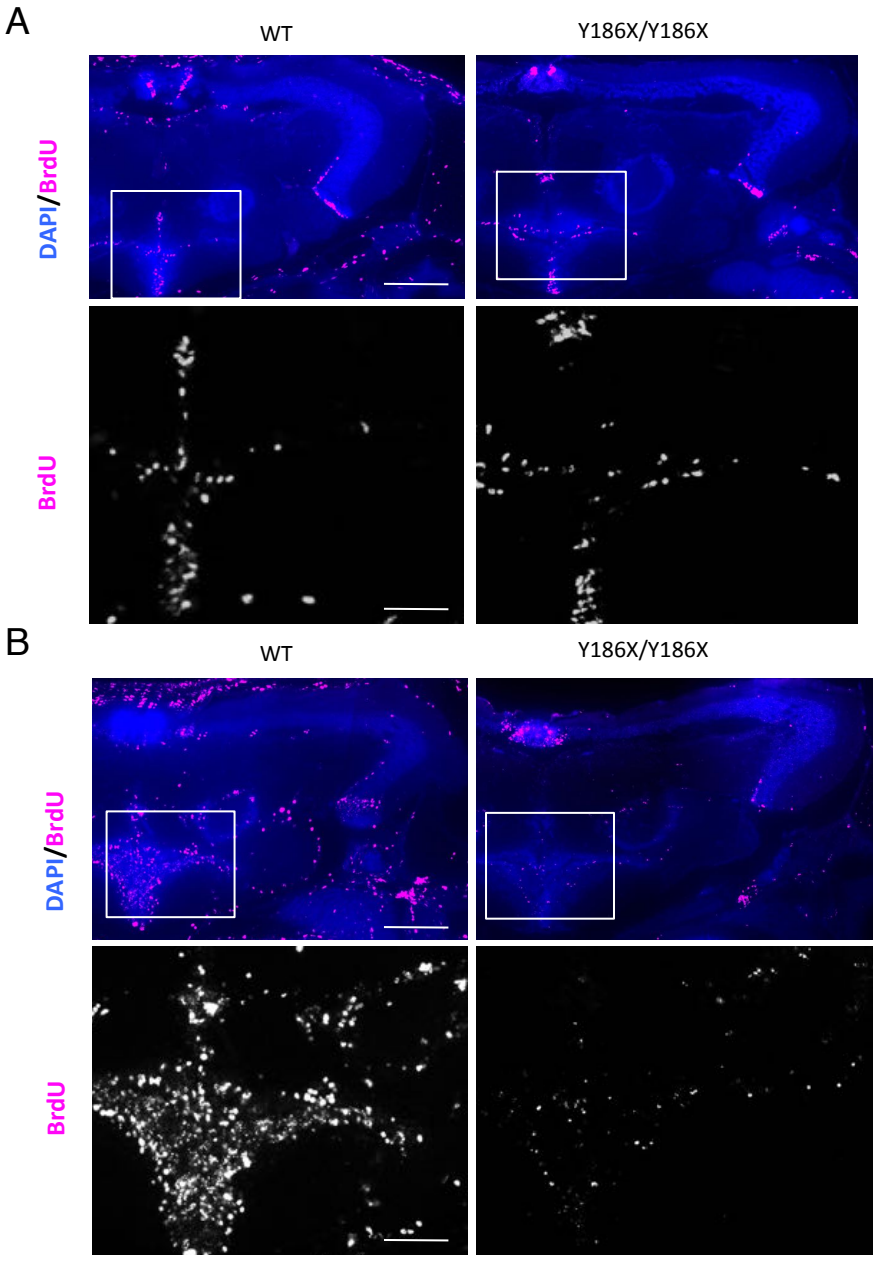

Figure 7. Comparison of the distribution of newborn cells in the hypothalamus (Zone N) between WT and p53 mutants.
Anti-BrdU immunohistochemistry of paraffin sections from wild-type medaka (Cab strain) and p53 mutants (Y186X/Y186X) (Magenta). Nuclei were stained with DAPI (Blue). Immunohistochemistry was performed immediately after BrdU exposure (A) and 1 week after BrdU exposure (B). The first row indicates the transverse sections (Scale bars indicate 100 mm) and the second row indicates the magnified view of the proliferation zone (Scale bars indicate 60 mm) (Zone N), represented by the white rectangles in the first row.

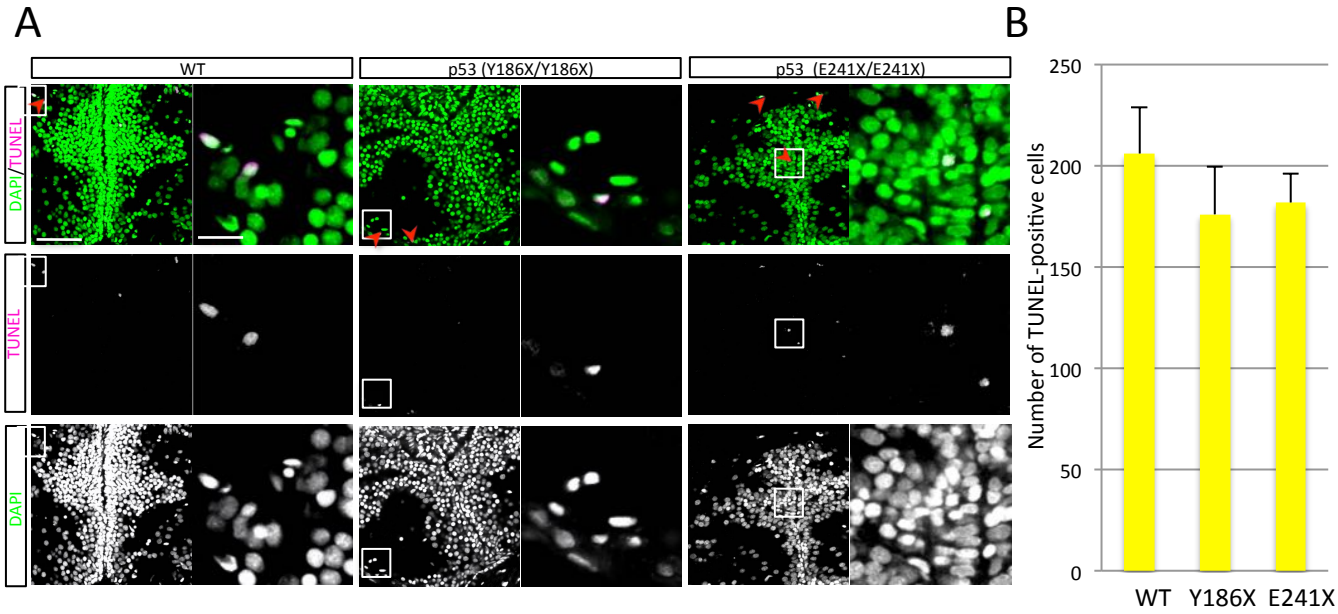

Figure 8. Cell death in the telencephalon of young medaka.
(A) Confocal images show double-labeling of TUNEL (Magenta) and DAPI (Green) in **Zone D**. Red arrow head indicate TUNEL-positive cells. For each strain, images in the right column are the magnified images of the region outlined by the white rectangle in the left column images. Scale bars indicate 80 mm (left) and 20 mm (right) (B) Quantification of TUNEL-positive cells. No significant difference was detected (ANOVA with a Bonferroni-Dunn post-hoc test; n =3–4 per group).

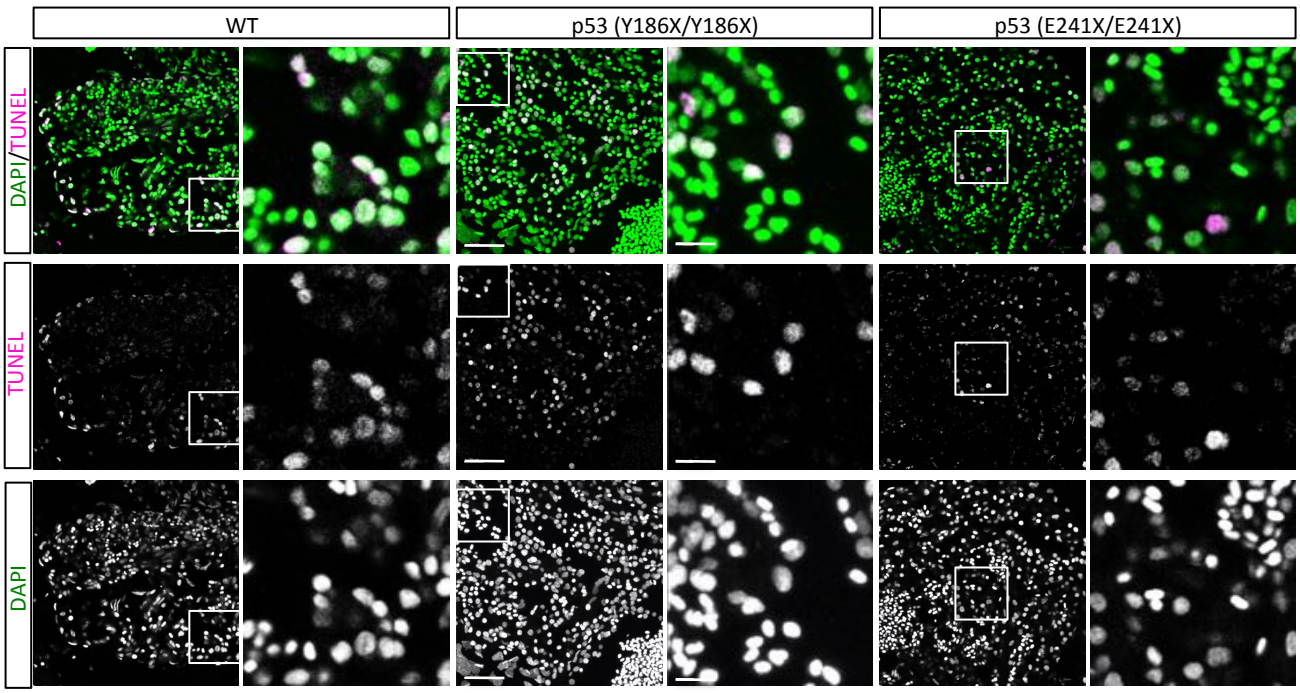

Figure 9. Detection of cell death in medaka pancreas sections using the TUNEL method.

Confocal images show double-labeling of TUNEL (Magenta) and DAPI (Green). For each strain, images in the right column are the magnified images of the region outlined by the white rectangle in the left column images. Scale bars indicate 80 mm (left) and 20 mm (right).

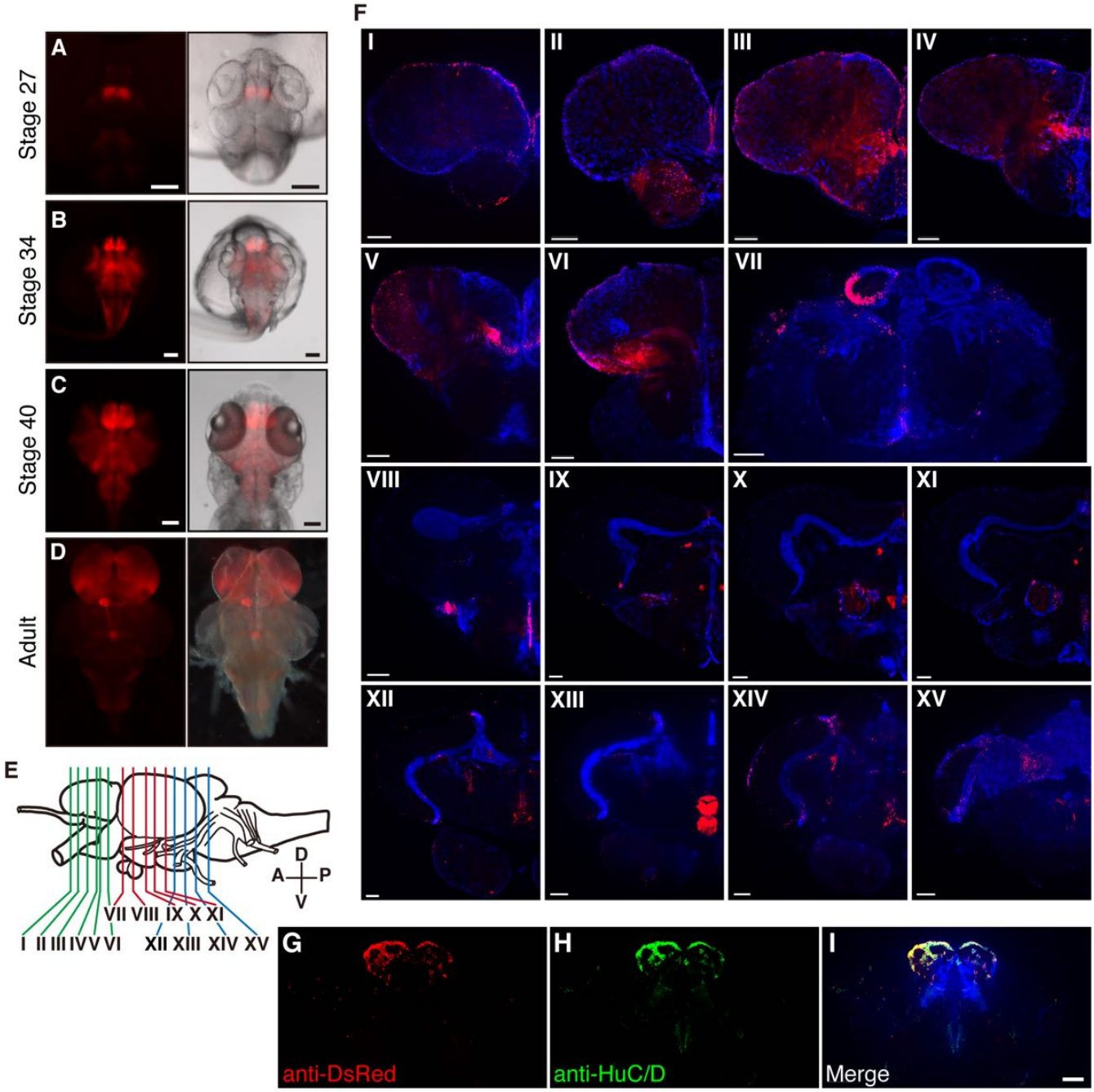

Figure 10. DsRed expression in *HuC*:loxP-*DsRed*-loxP-*GFP* Tg medaka at different stages. (A-D) Onset of DsRed expression in the brain from the dorsal view. DsRed expression was restricted to the anterior brain vesicle-intermediate brain vesicle (Ant-Int) at stage 27 (A). Additional DsRed-expressing neurons were observed in the entire brain at stages 34 (B) and 40 (C). At the adult stage (D), prominent DsRed expression was observed in the telencephalon and left side of the habenular nucleus. (E) Schematic drawing of adult medaka brain indicating the depth of each coronal section in (F). (F) Fluorescent images of coronal forebrain slices from an *HuC*:loxP-*DsRed*-loxP-*GFP* adult. Please see supplemental Fig.S1 for description of DeRed positive cells, by referring to the medaka brain atlas. (G-I) Photomicrographs depicting DsRed and HuC/D immunofluorescence within the habenular nucleus of the *HuC*:loxP-*DsRed*-loxP-*GFP* Tg brain. White arrow indicates a double-labeled neuron, which is shown separately below for DsRed (G) and HuC/D (H) immunofluorescence with DAPI (blue) staining, as well as in a composite (I). Scale bars 100 μm.

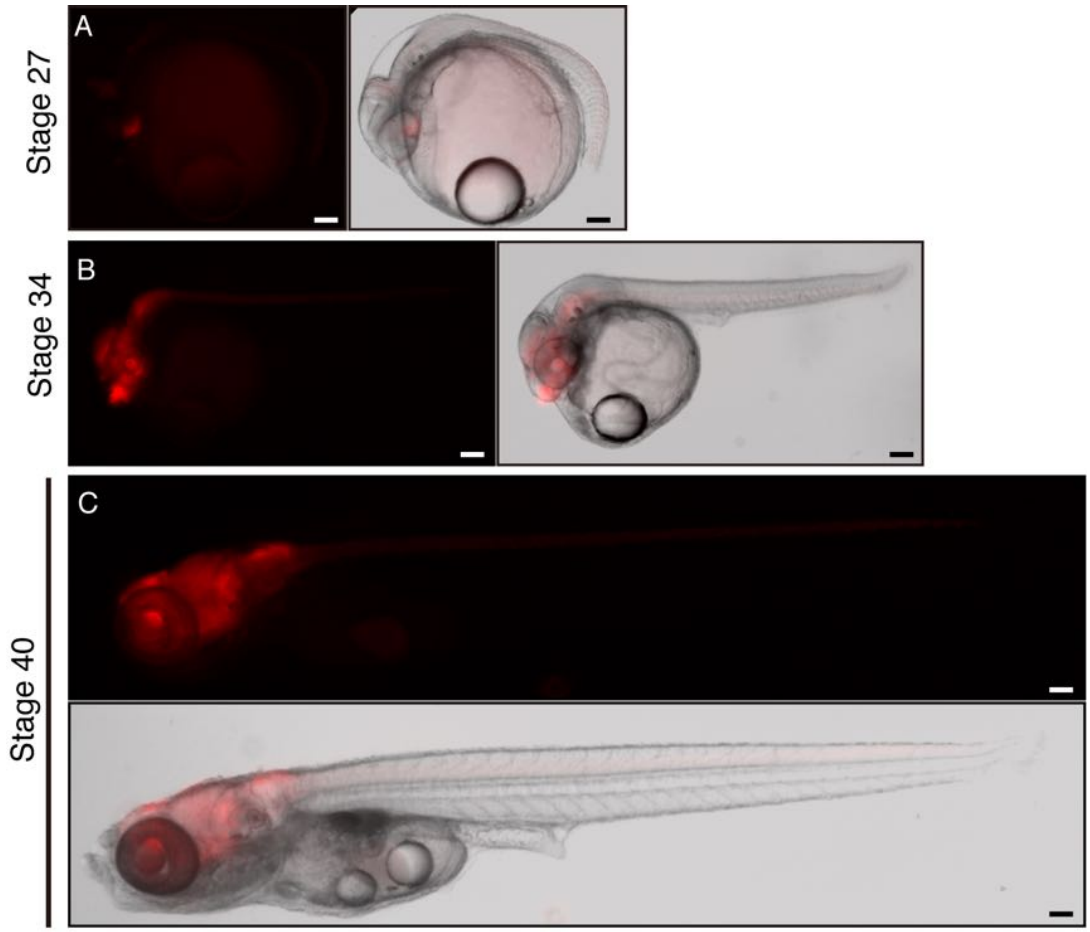

Figure 11. DsRed expression in *HuC*:loxP-*DsRed*-loxP-*GFP* Tg medaka. (A-C) Onset of DsRed expression in the brain from the lateral view at Stages 27 (A), 34 (B), and 40 (C). (D-G) Photomicrographs depicting DsRed (red), HuC/D (green), DAPI (blue), and their merged image immunofluorescence in the *HuC*:loxP-*DsRed*-loxP-*GFP* Tg brain in the preoptic area (D), optic tectum and hypothalamus (E, F), and cerebellum (G). Scale bar, 100 μm.

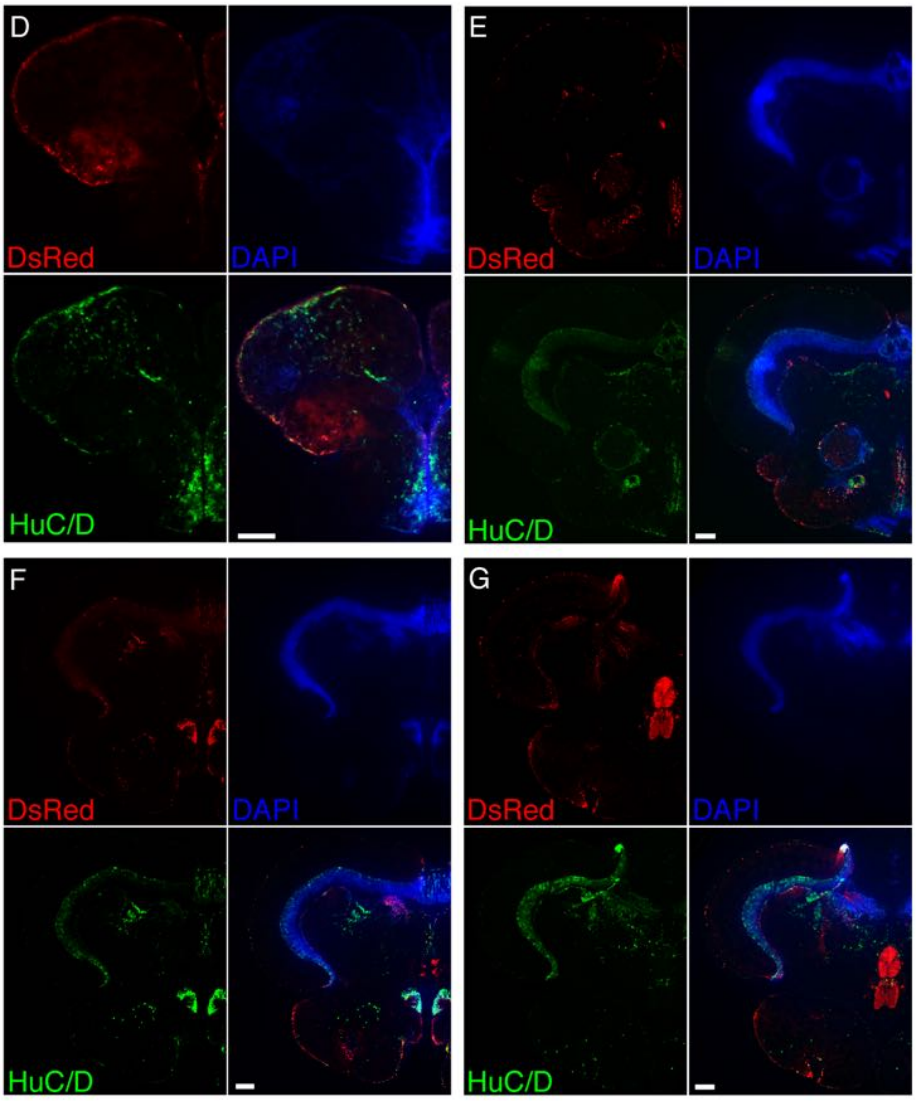

Figure 11. (Continued.)

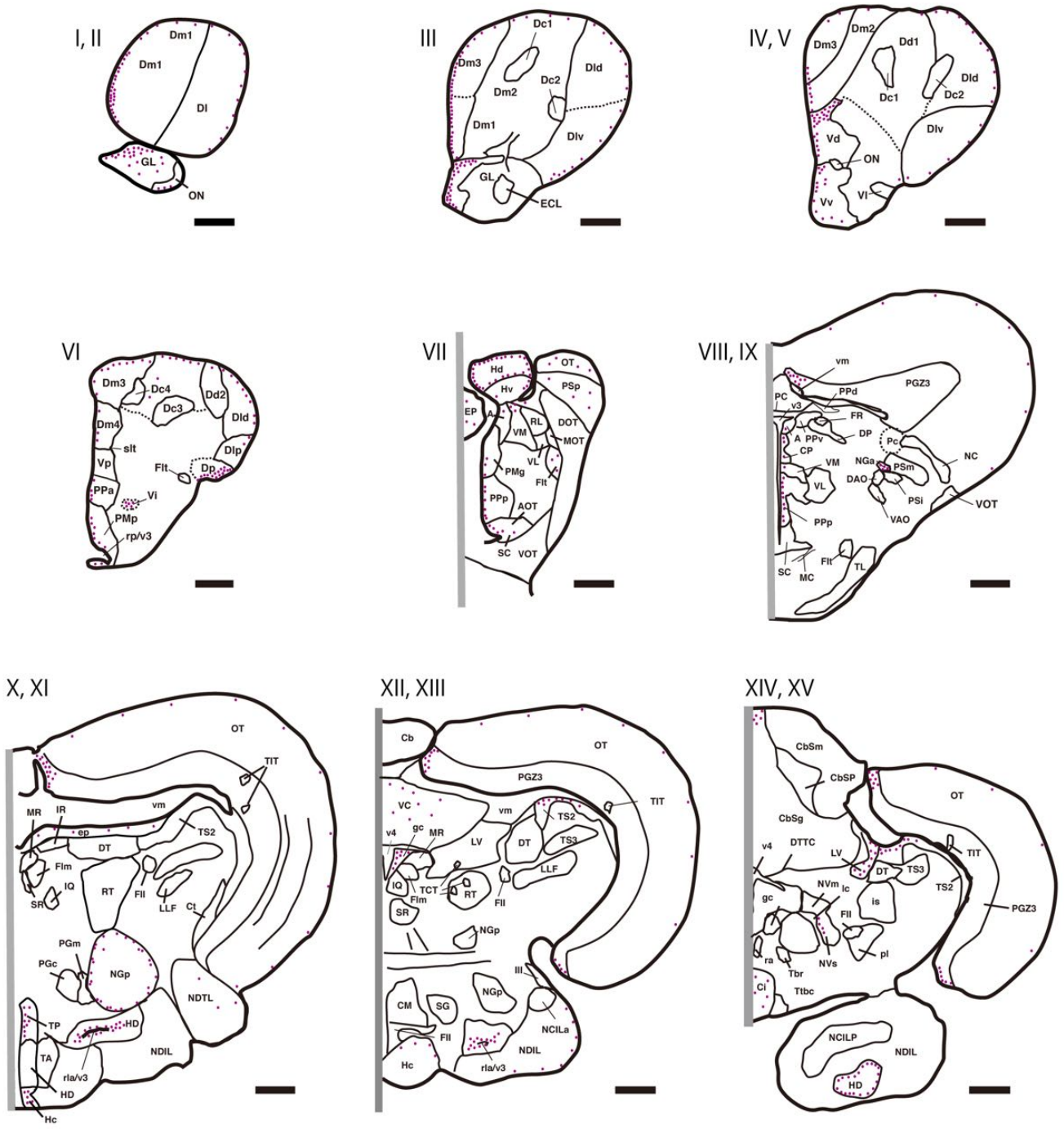

Figure 12. Schematic drawing of HuC-expressing neurons. Magenta dots indicate the position of the HuC-expressing neurons.

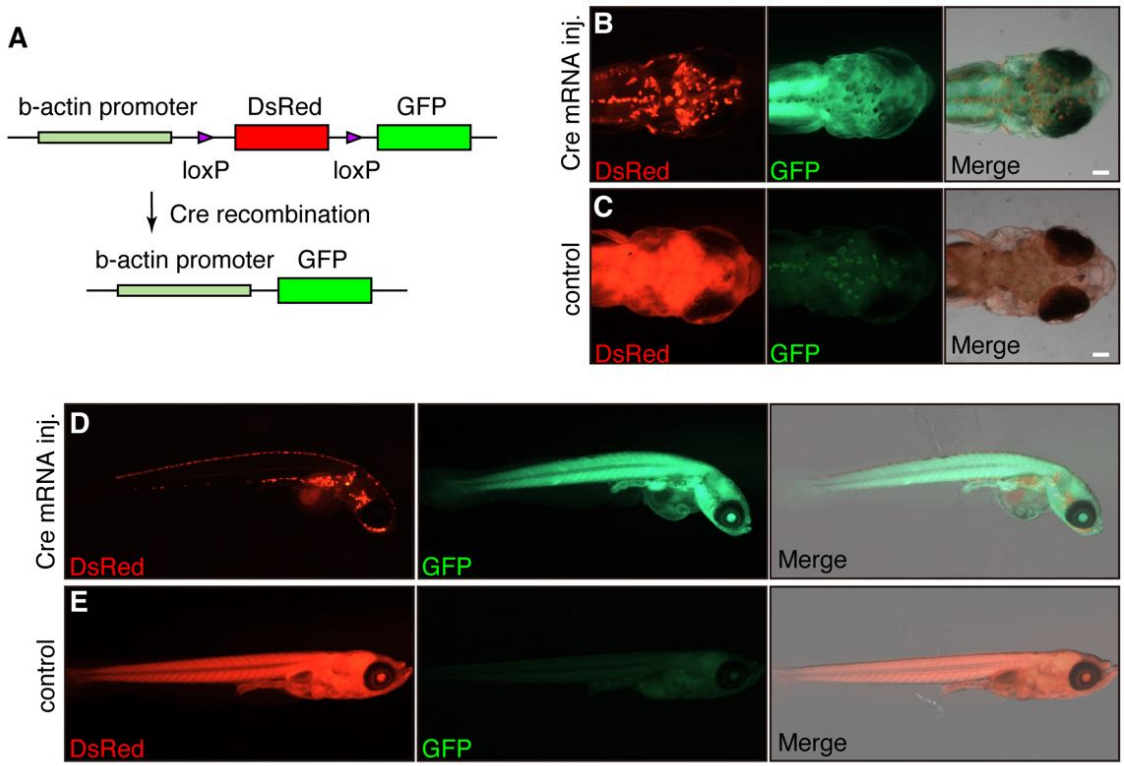

Figure 13. Cre/loxP recombination by Cre mRNA injection. (A) Schematic drawing of Cre/loxP recombination in Tg (*beta actin*:loxP-*DsRed*-loxP-*GFP*). (B-F) Prominent GFP expression was observed in the whole body of Cre mRNA-injected embryos. Cre mRNA-injected embryos (B,D) and negative control embryos (C,E) are shown from dorsal (B,C) and lateral (D,E) views. Scale bar, 100 μm.

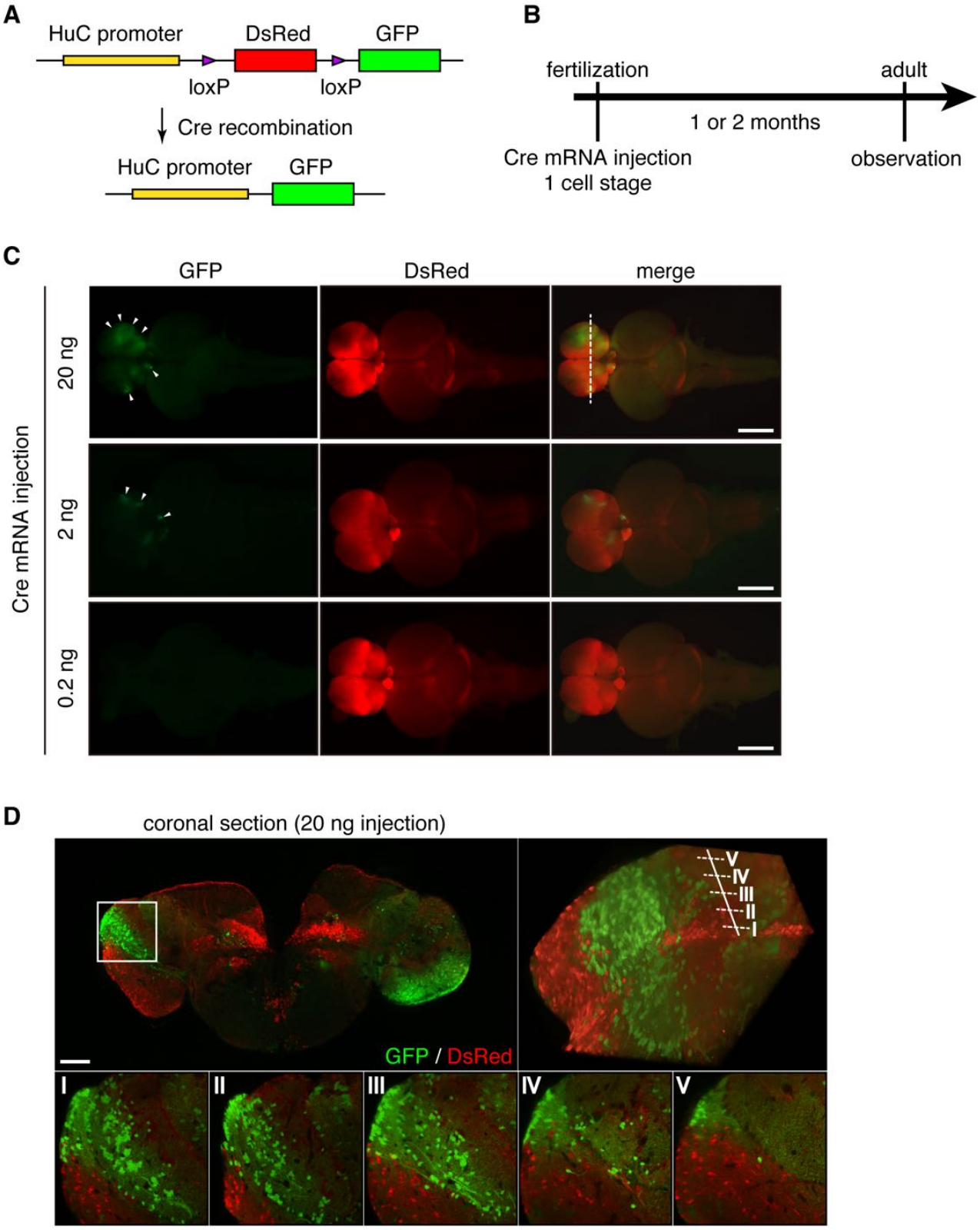

Figure 14. Cre mRNA-mediated gene recombination in the *HuC*:loxP-*DsRed*-loxP-*GFP* Tg brain. (A) *HuC*:loxP-*DsRed*-loxP-*GFP* construct. The gene recombination converts DsRed expression to GFP. (B) Experimental procedure. Cre mRNA was injected at the 1-cell stage and the fluorescence pattern was observed at the adult stage. (C) Fluorescent images of adult Tg embryos brain with Cre mRNA (20, 2, and 0.2 ng/μl, respectively) at the 1-cell stage. DsRed, enhanced GFP (EGFP), and merged images of embryos. Anterior is to the left, and right is toward the top. Scale bar, 1 mm. (D) Coronal fluorescent images of Cre mRNA (20 ng/μl)-injected brain. Merged images of DsRed and GFP in the posterior telencephalon. A magnified view of the lateral telencephalon (white box) shows the spatial compartmentalization of GFP-positive neurons in this region at 5 different depth levels (I-V). Scale bar, 100 μm.

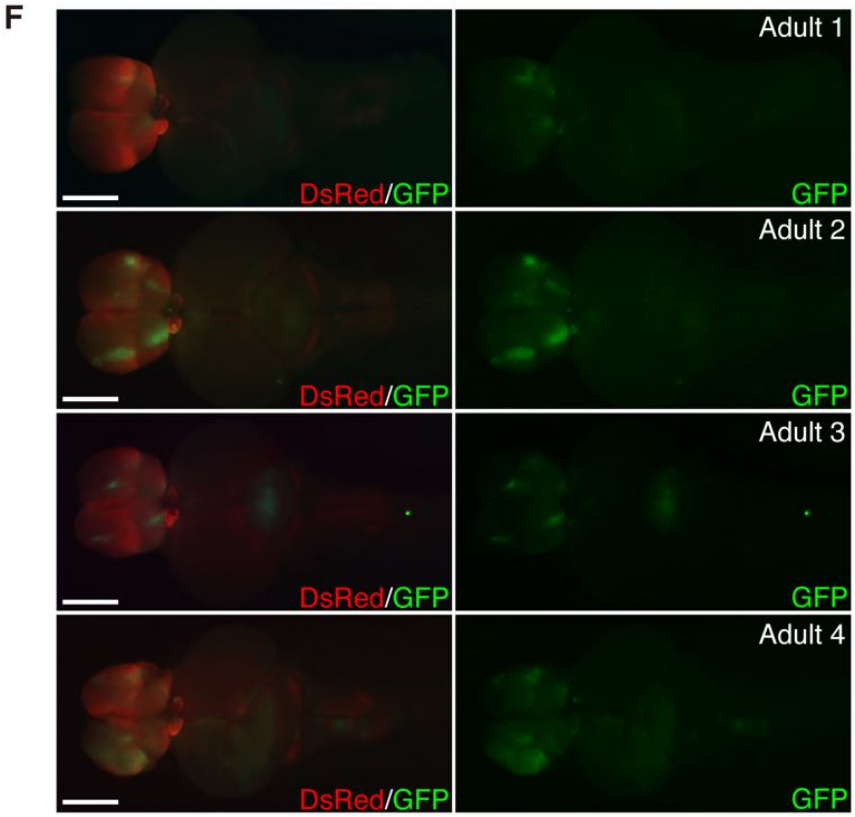

Figure 15. Induction of stochastic Cre/loxP recobination
Mosaic pattern of GFP fluorescence in the Cre mRNA-injected Tg (*HuC*:loxP-*DsRed*-loxP-*GFP*) adult medaka brain. Different GFP patterns were observed in individual brains. Scale bar, 1mm.

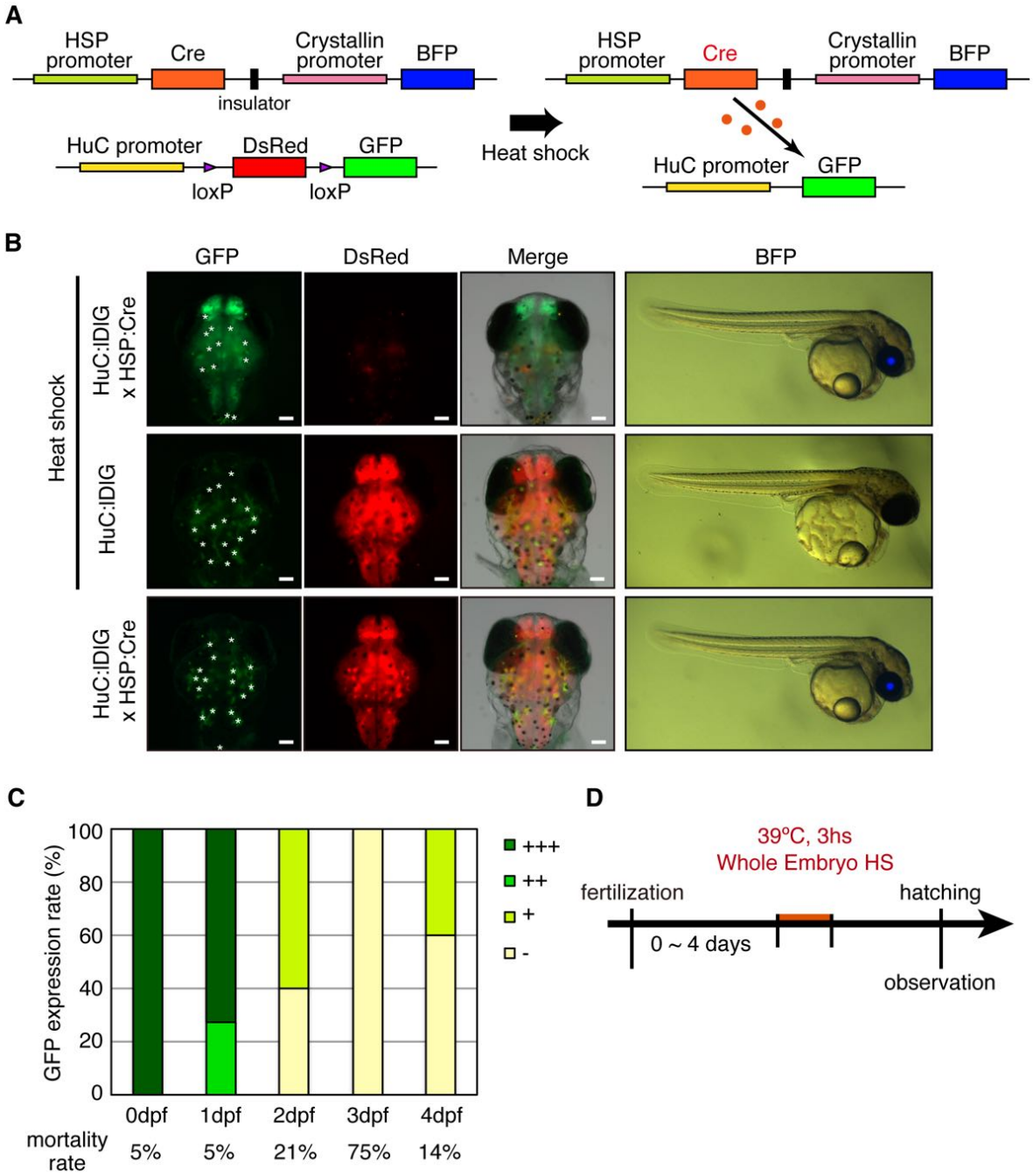

Figure 16. *Heat shock protein* (*HSP*) promoter-induced Cre/mediated recombination. (A) Schematic drawing of *HSP*:*Cre*/*Crs*:*BFP* constructs and mechanism of fluorescence change from DsRed to GFP in *HuC*:loxP-*DsRed*-loxP-*GFP* and *HSP*:*Cre*/*Crs*:*BFP* double Tg embryos. (B) Fluorescence color conversion by heat-induced Cre. *HuC*:loxP-*DsRed*-loxP-*GFP*/*HSP*:*Cre*/*Crs*:*BFP* (HuC:lDlG x HSP:Cre) embryos exposed to heat induction (39 C, 3 h) were observed under a stereoscopic fluorescence microscope just after hatching. DsRed expression was significantly reduced and GFP was induced (upper), compared to control embryos of the *HuC*:loxP-*DsRed*-loxP-*GFP* single Tg (HuC:lDlG, middle) and unheated double-Tg lines (lower). Blue eye (BFP) indicates the *HSP*:*Cre*/*Crs*:*BFP* transgene. Left columns are dorsal view images (top, anterior; right, right) and right columns are lateral view images (top, dorsal; right, anterior). Autofluorescence derived from pigment cells is indicated by asterisks in GFP panels. Scale bar, 100 μm. (C) The efficiency of the heat-induced recombination and (D) Experimental procedure. The prominence of the fluorescence color conversion was categorized into four types (+++; strongest GFP fluorescence in whole brain, ++; not so strong GFP fluorescence in whole brain, +; GFP fluorescence in partial brain regions, -; no change).

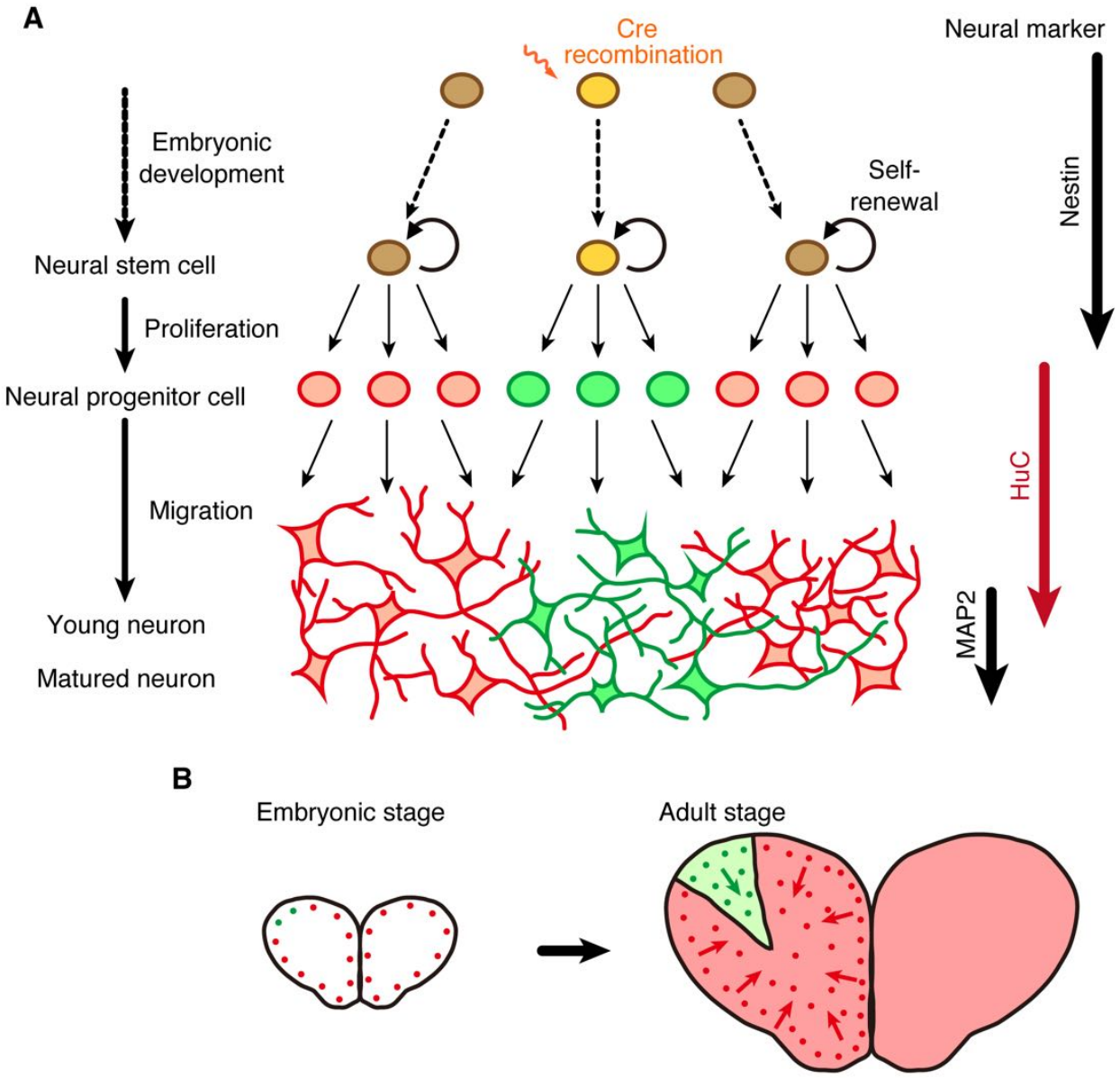

Figure 17. Compartmentalization of clonally-related neurons in the telencephalon.
Site-specific Cre/loxP recombination in a single neural progenitor or small population of neural progenitors during embryonic development led to the formation of compartmentalized blocks comprising clonally-related neurons in the adult telencephalon.

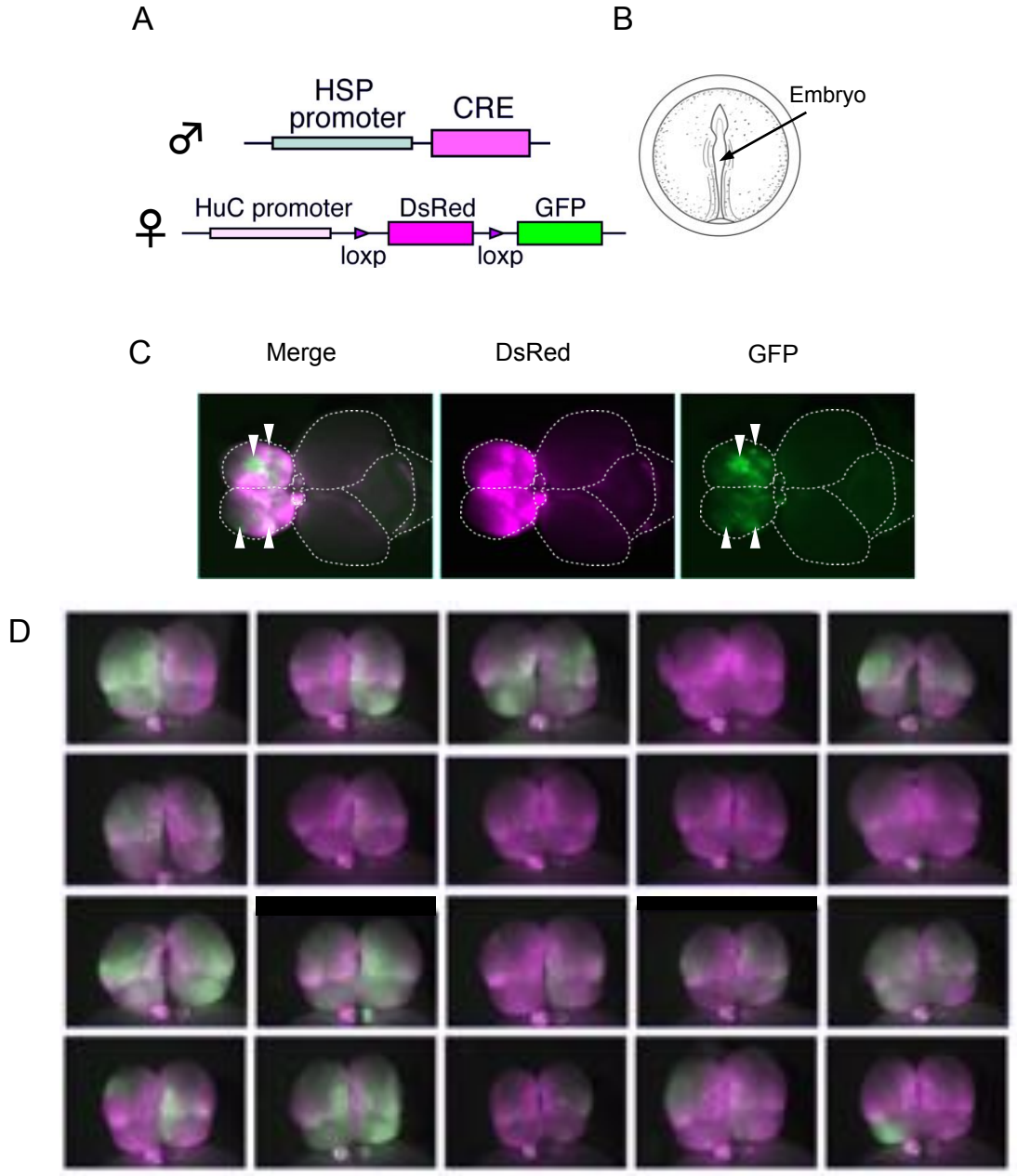

Figure 18. Procedure of induction of Cre/loxP recombination.
(A) Transgenic lines used for this experiment. Male fish of the HSP:Cre line and female fish of the HuC:loxp-DsRed-loxp-GFP line were crossed. (B) Heat shock was performed at the neural tube stage. Two embryos were placed into each PCR tube and mild heat shock was applied to induce stochastic Cre/loxP recombination. (C) An example of whole adult brain with random GFP-positive cells. (D) Examples of telencephalon samples with GFP-positive cells.

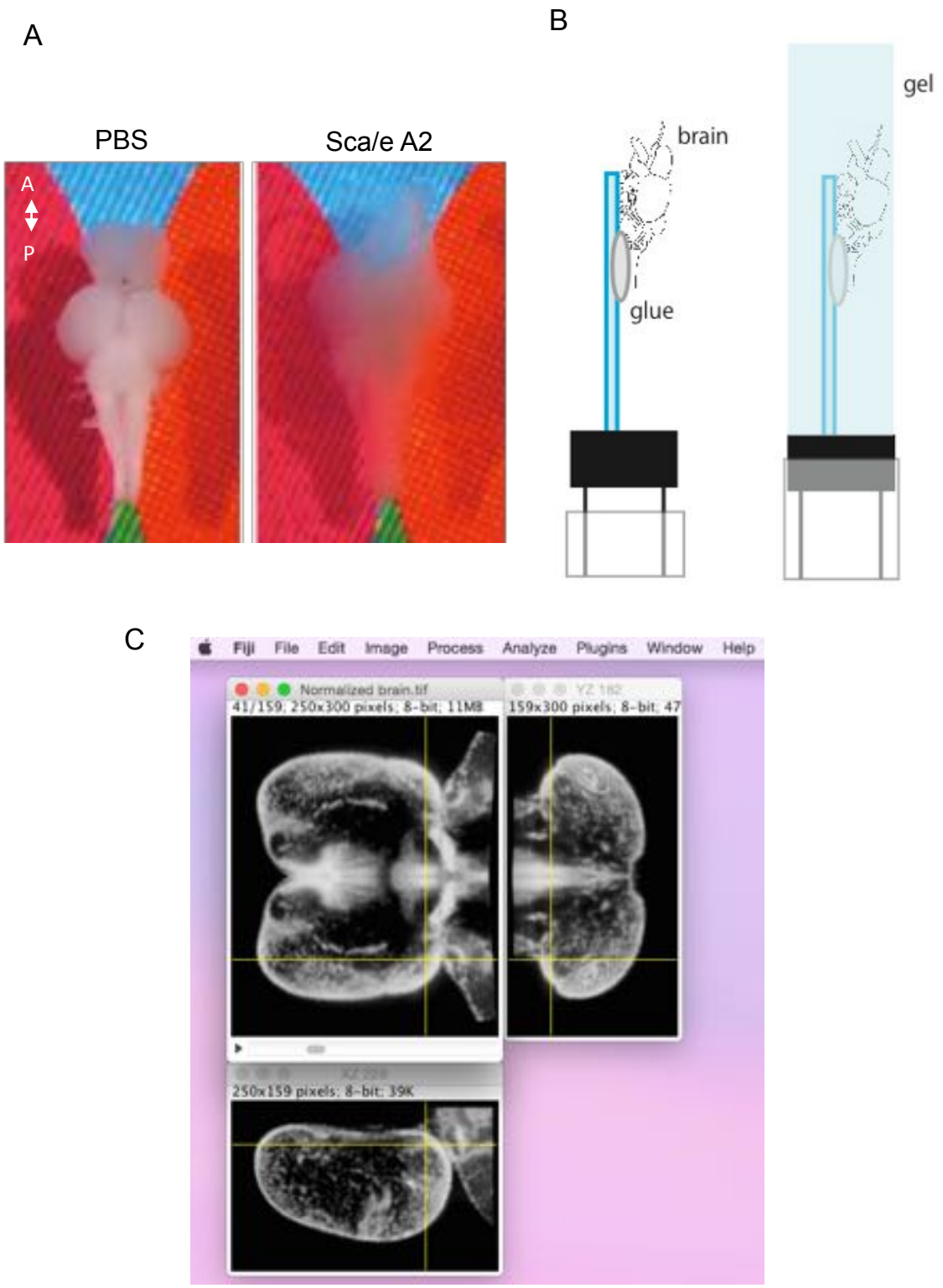

Figure 19. Brain preparation for imaging by DSLM (digital scanned laser light-sheet fluorescence microscopy).
(A) Clearing by Sca/eA2. White brain (left photo) became transparent after being immersed in Sca/e A2 solution. (B) The brain was glued to the glass (left figure). Then the whole brain was embedded in gelatin with Sca/e A2 solution. (C) One example of orthogonal view of the normalized brain. Horizontal section (left upper slice), transverse section (right upper slice), and lateral section (left lower slice) were shown.

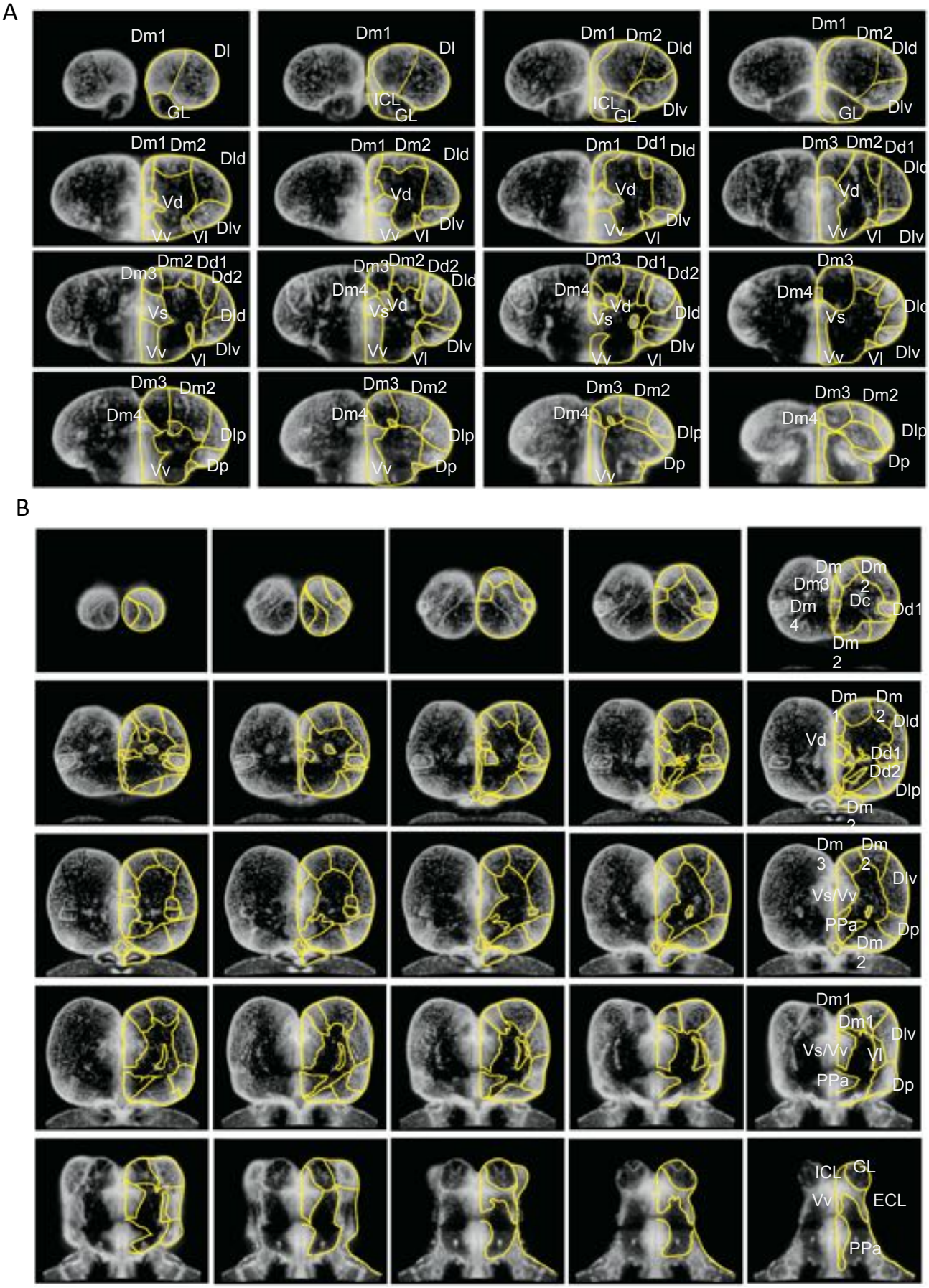

Figure 20. Atlas of the normalized brain.
Transverse sections (A) and horizontal sections (B) of normalized brain. Traditional anatomic regions are indicated by the yellow lines. Slices were arranged from anterior to posterior side in (A) and from dorsal to ventral telencephalon in (B).

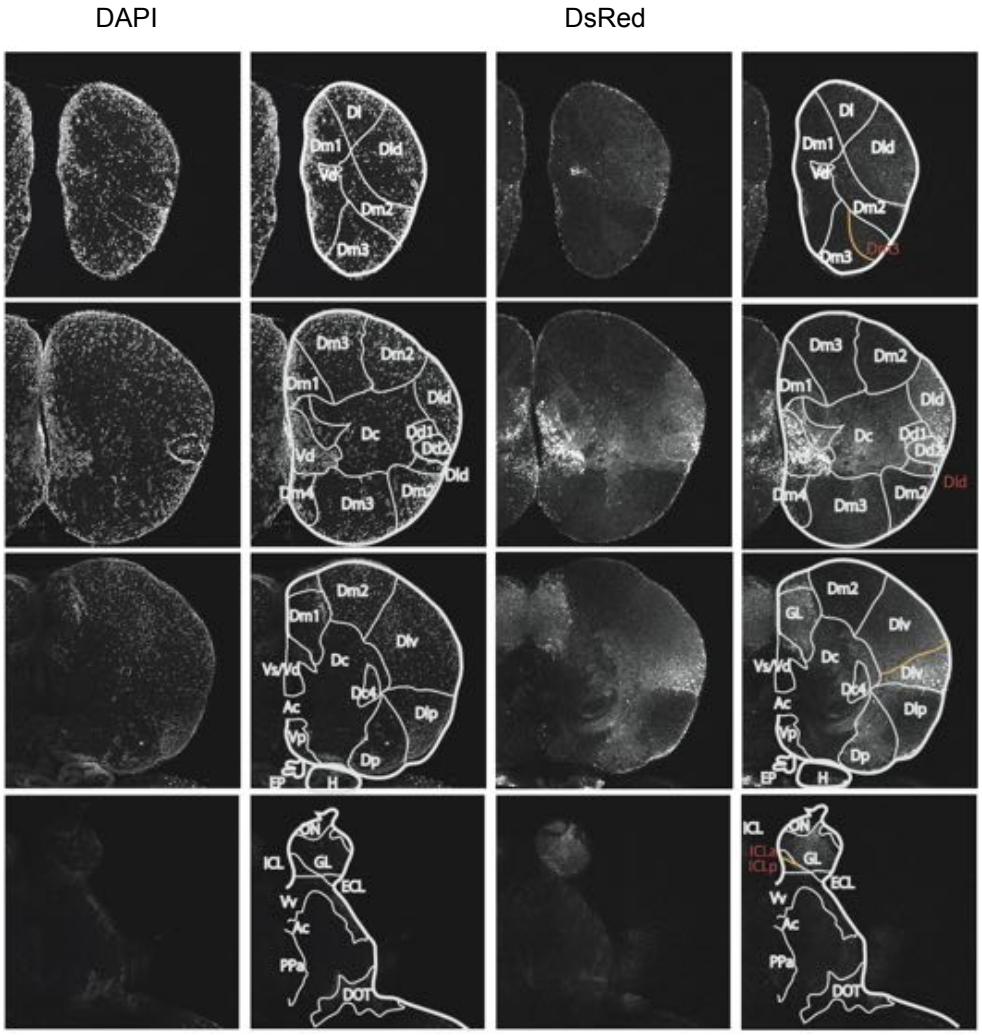

Figure 21. Horizontal section of the adult telencephalon of the Tg line (HuC:loxp- DsRed-loxp-GFP) observed by two-photon microscope.
DAPI signals show the anatomic regions (indicated by white lines and yellow letters). From the DsRed distribution pattern, novel anatomic subdivisions are indicated by orange lines and red letters.

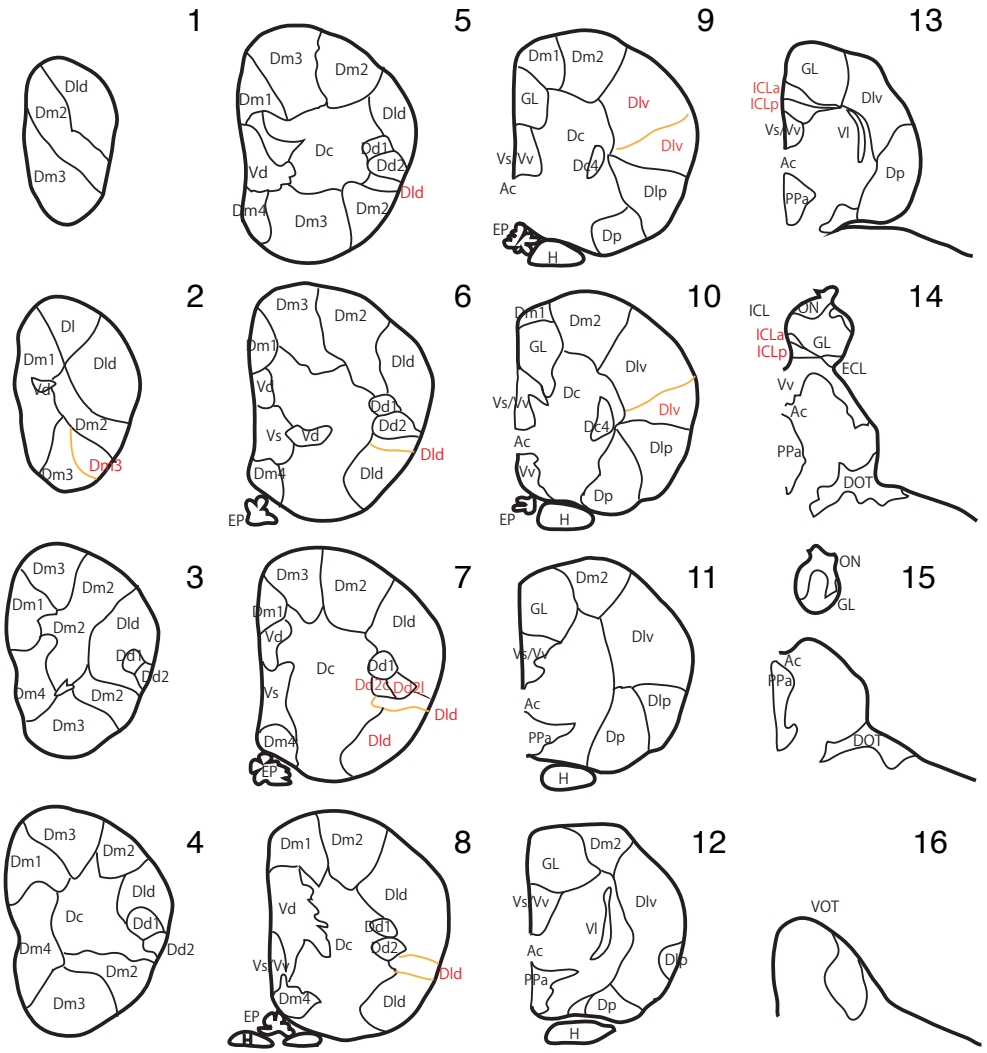

Figure 22. Atlas of horizontal sections of the adult telencephalon.
Black lines show the anatomic regions and subdivisions. Black letters show the names of traditional anatomic regions. Red letters show the names of the novel anatomic subdivisions defined in this study. The numbers show the position of the horizontal section.

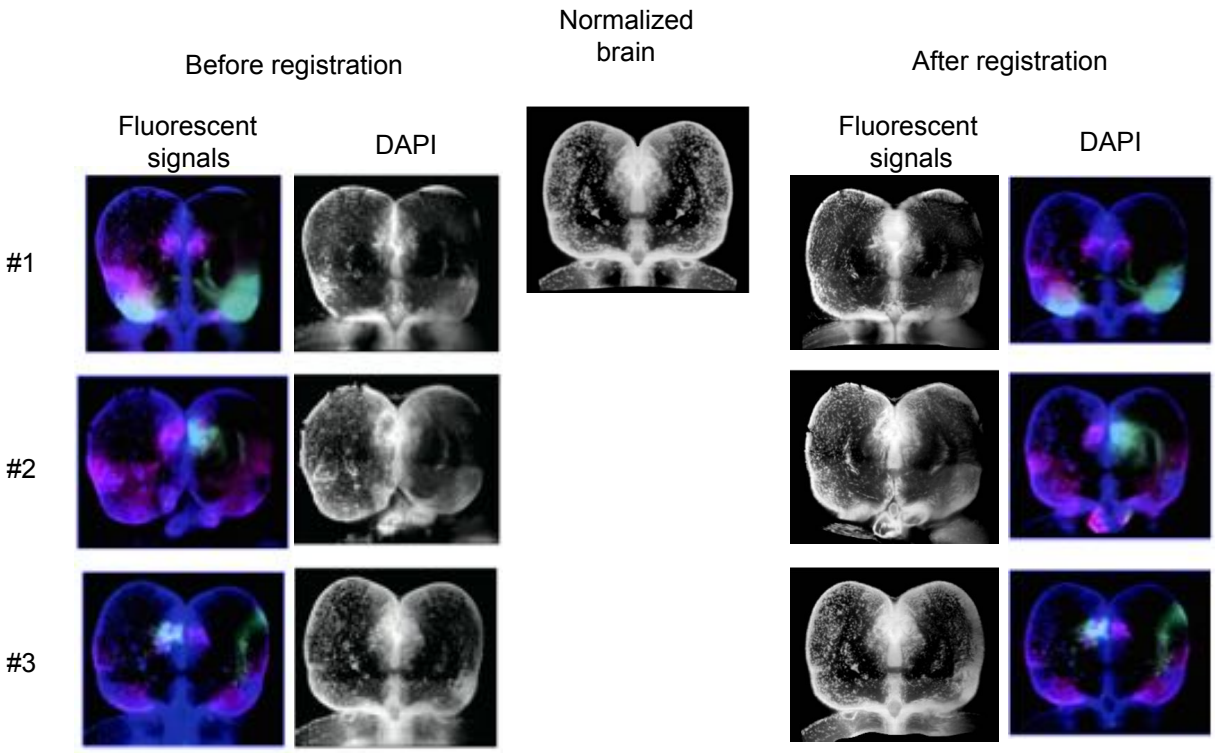

Figure 23. Fluorescent signal registration to the normalized brain.
Three horizontal sections are shown on the left side of the panel. Because of the deviations between samples due to sample preparation, it is difficult to compare the GFP pattern among multiple samples. By using DAPI-signal registration, the DAPI signals of samples were almost the same and the fluorescent signals projected to the DAPI signals could be compared.

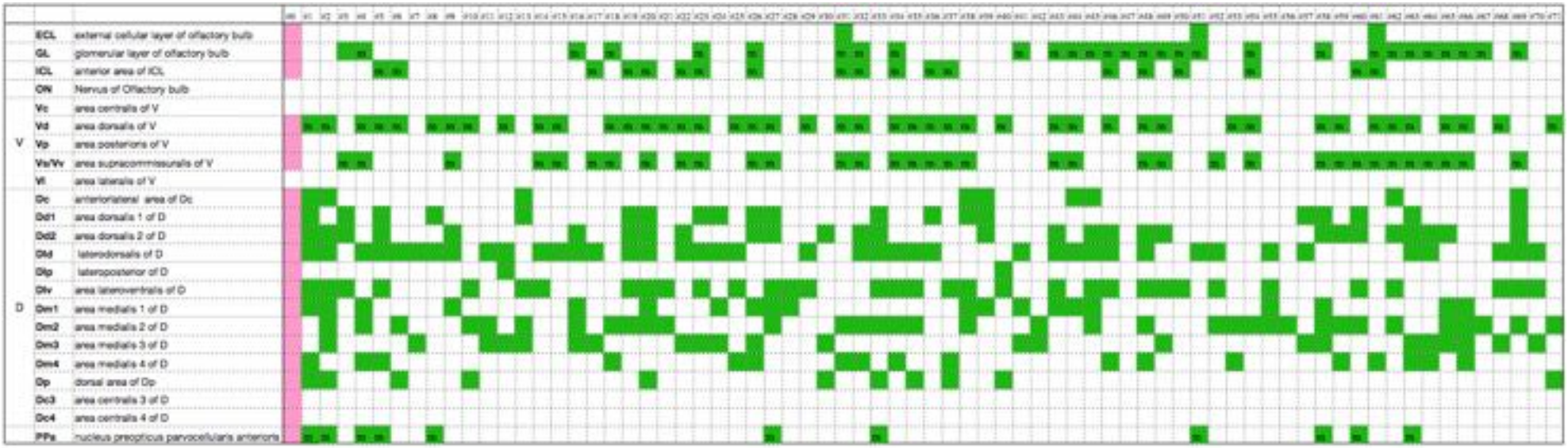
ECL external cellular layer of olfactory bulb
GL glomerular layer of olfactory bulb
ICL anterior area of ICL
ON Nervus of Olfactory bulb
Vc area centralis of V
Vd area dorsalis of V
Vp area posterioris of V
Vs/Vv area supracommissuralis of V
Vl area lateralis of V
Dc anteriorlateral area of Dc
Dd1 area dorsalis 1 of D
Dd2 area dorsalis 2 of D
Dld lateradorsalis of D
Dlp lateroposterior of D
Dlv area lateroventralis of D
Dm1 area medialis 1 of D
Dm2 area medialis 2 of D
Dm3 area medialis 3 of D
Dm4 area medialis 4 of D
Dp dorsal area of Dp
Dc3 area centralis 3 of D
Dc4 area centralis 4 of D
PPa nucleus preopticus parvocellularis anterioris
V
D

Table 1. Clonal mapping analysis

The position of GFP-positive cells was identified based on the DAPI signals. Green boxes indicate the presence of GFP-positive cells. ‘m’ indicates the mosaic pattern.

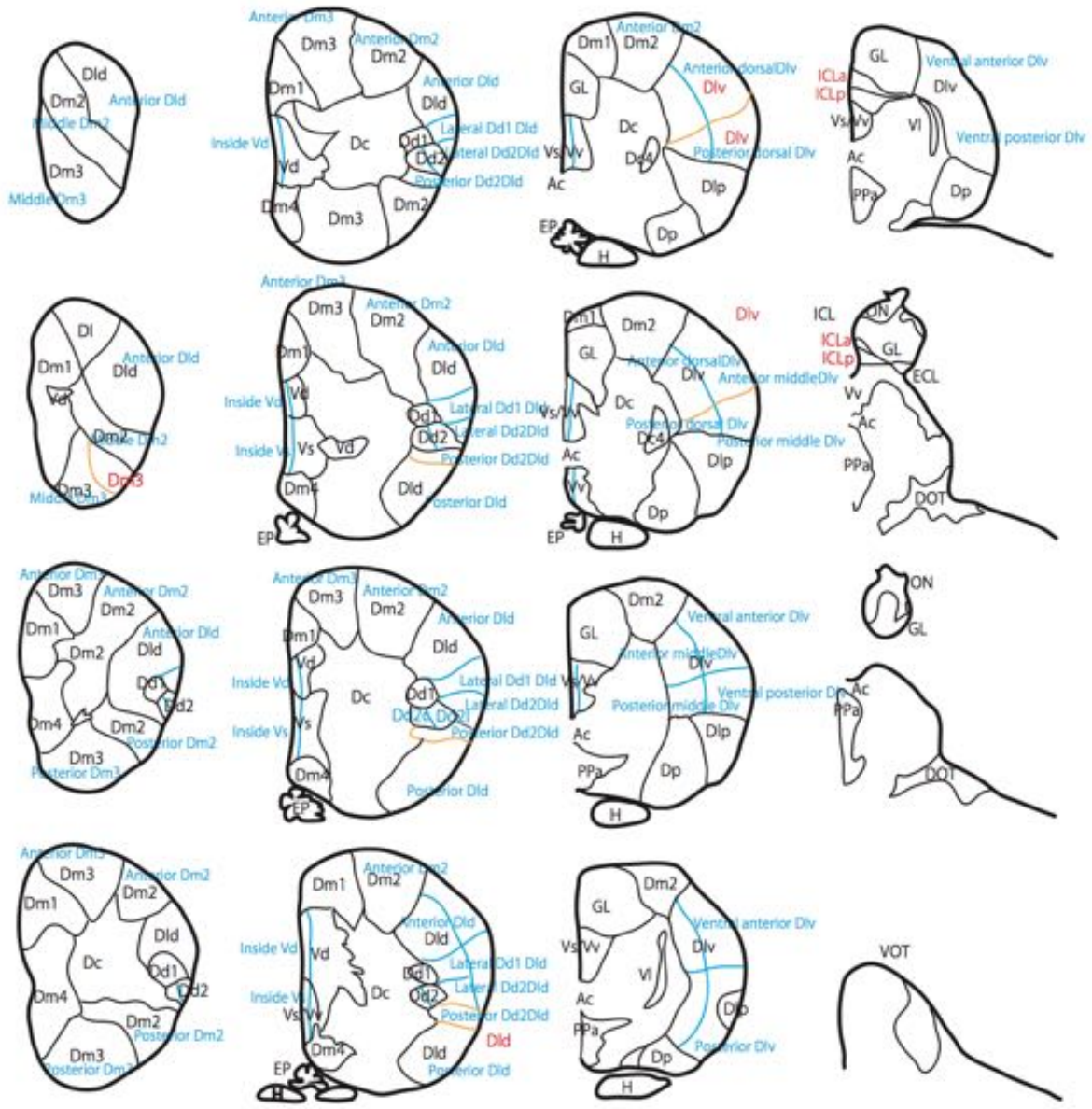

Figure 24. Atlas of horizontal sections of the adult telencephalon.
Black lines show the anatomic regions and subdivisions. Black letters show the names of traditional anatomic regions. Red letters show the names of the novel anatomic subdivisions defined in this study. The numbers show the position of the horizontal section.

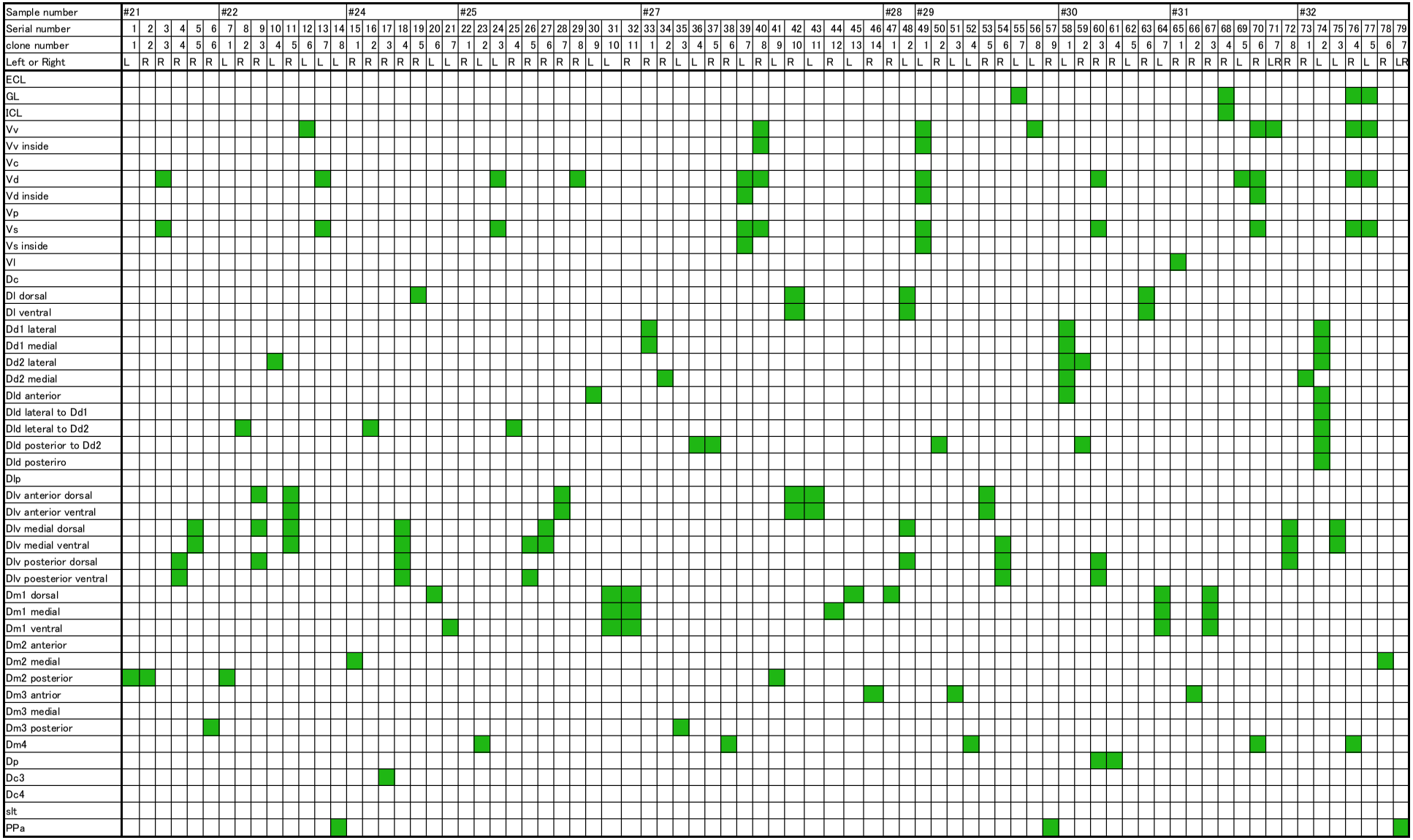
Sample number
#21
#22
#24
#25
#27
#28
#29
#30
#31
#32
Serial number
clone number
Left or Right
ECL
GL
ICL
Vv
Vv inside
Vc
Vd
Vd inside
Vp
Vs
Vs inside
Vl
Dc
Dl dorsal
Dl ventral
Dd1 lateral
Dd1 medial
Dd2 lateral
Dd2 medial
Dld anterior
Dld lateral to Dd1
Dld leteral to Dd2
Dld posterior to Dd2
Dld posteriro
Dlp
Dlv anterior dorsal
Dlv anterior ventral
Dlv medial dorsal
Dlv medial ventral
Dlv posterior dorsal
Dlv poesterior ventral
Dm1 dorsal
Dm1 medial
Dm1 ventral
Dm2 anterior
Dm2 medial
Dm2 posterior
Dm3 antrior
Dm3 medial
Dm3 posterior
Dm4
Dp
Dc3
Dc4
slt
PPa

Table 2. Example of clonal mapping analysis in one clone level.
According to the atlas in Figure 24, the position of GFP-positive cells was identified based on the DAPI signals. Green boxes indicate the presence of GFP-positive cells. L indicates GFP-positive cells detected in the left hemisphere. R indicates GFP-positive cells detected in the right hemisphere.

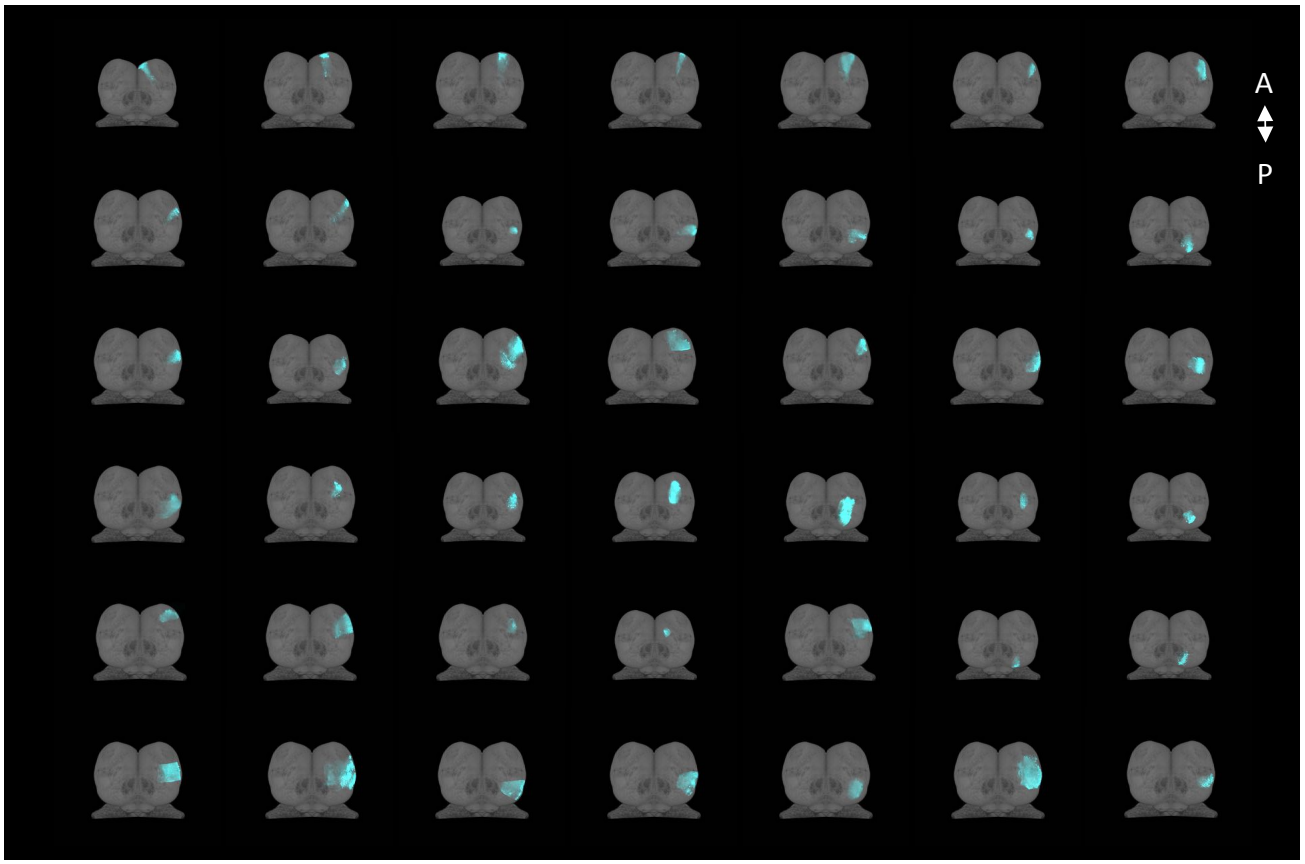

Figure 25. Examples of clonal unit mapping analysis.
Light blue signals indicate the structure of a single clonal unit in the adult telencephalon. Dorsal views of 3D reconstructions are shown.

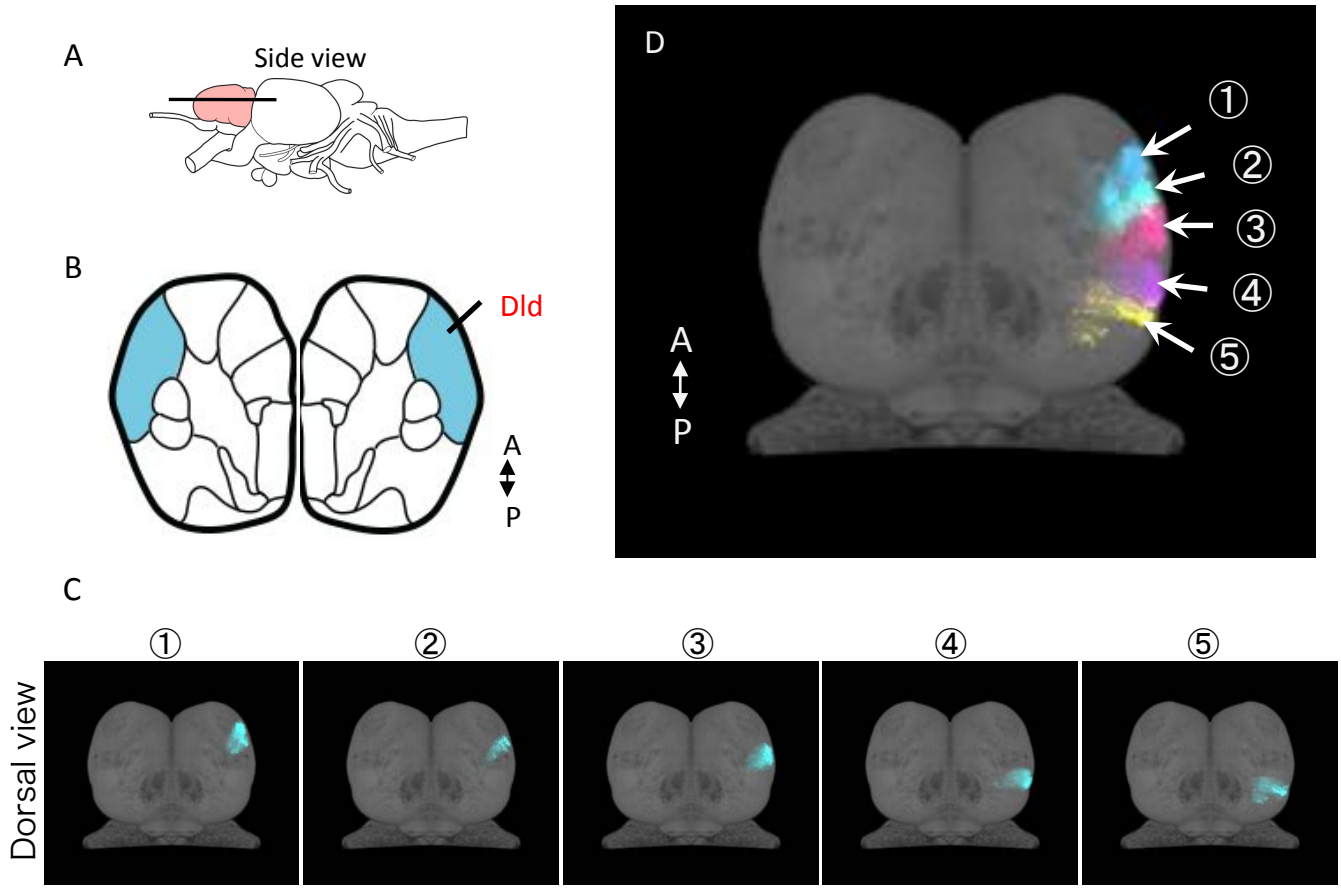

Figure 26-1. Examples of clonal units that constitute the anatomic region in the dorsal telencephalon.
(A) Side view of the whole brain. Pink indicates the telencephalon. The line indicates the position of the horizontal section shown in B. (B) Atlas of horizontal section. Blue indicates the anatomic region Dld. (C) Single clonal unit mapping to the normalized brain. Dorsal view of 3D reconstruction. (D) 5 clonal units (①-⑤) constitute the anatomic region, Dld.

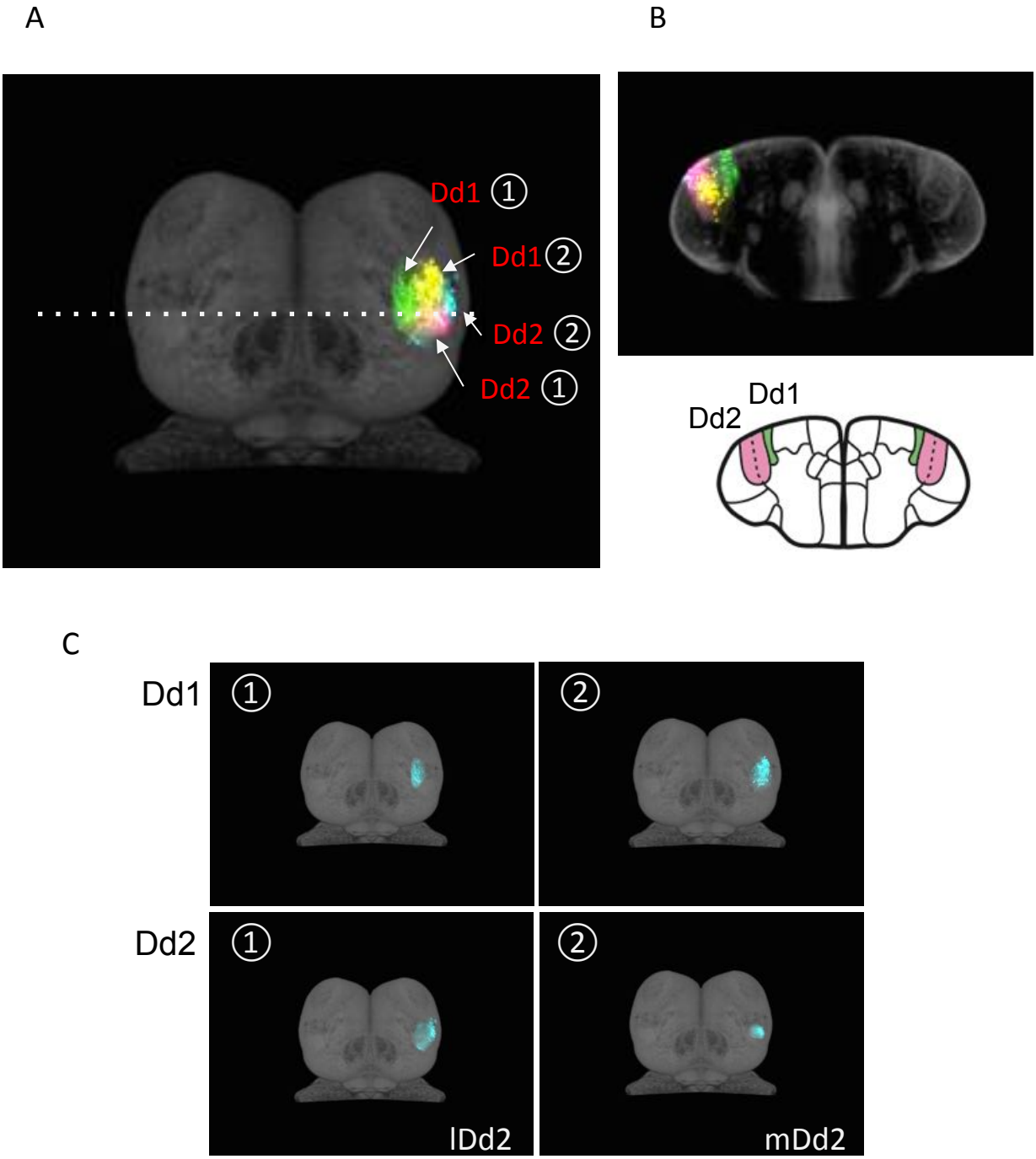

Figure 26-2 Examples of clonal units that constitute the anatomic region in the dorsal telencephalon.
(A) 2 clonal units constitute the anatomical region, Dd1 and Dd2. The line indicates the position of transverse section in (B). (B) Schematic drawing of transverse section. (C) Single clonal units of Dd1 and Dd2 mapping to the normalized brain. Dorsal view of 3D reconstruction.

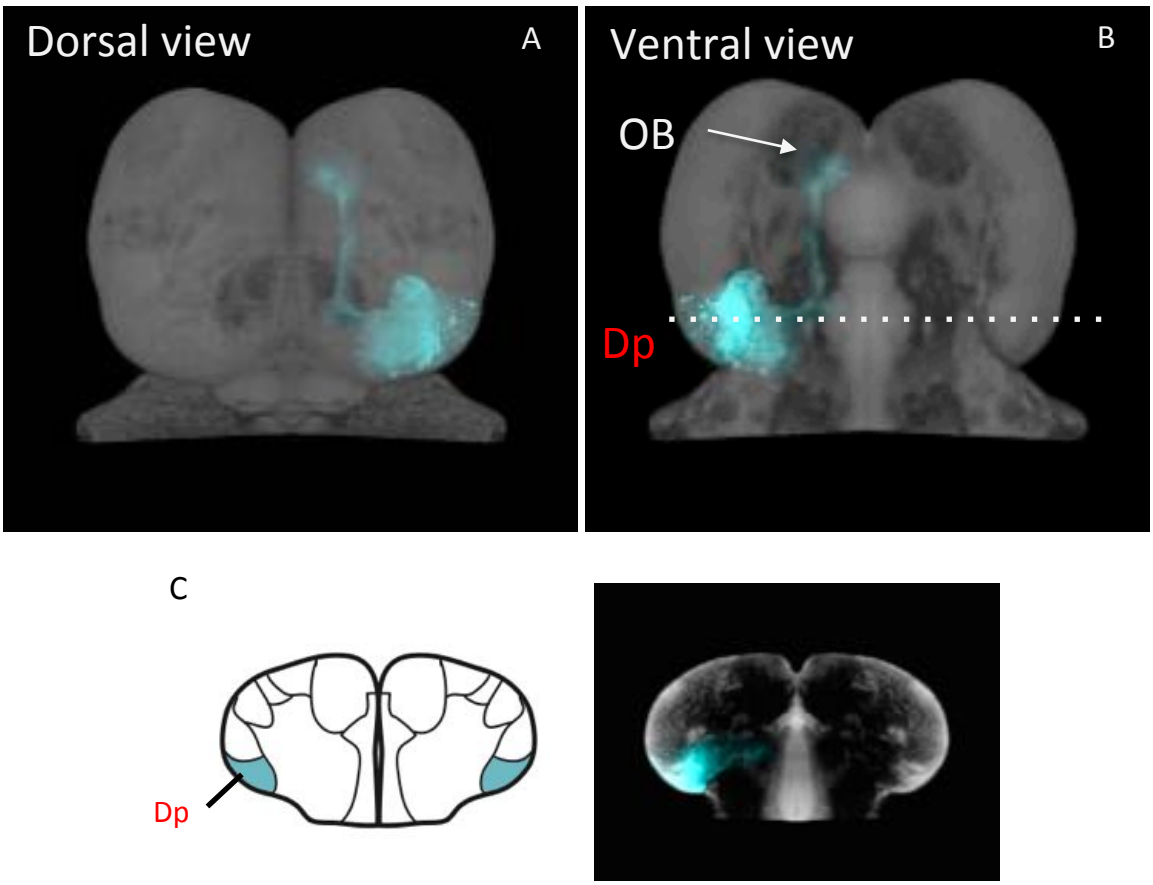

Figure 26-3 Examples of clonal units that constitute the anatomic region in the dorsal telencephalon.
Dorsal view (A) and ventral view (B) of clonal units of Dp. Axons integrated to olfactory bulb (OB) were observed. White line in (B) shows the position of transverse section in (C). (C) shows the position of cell bodies of Dp.

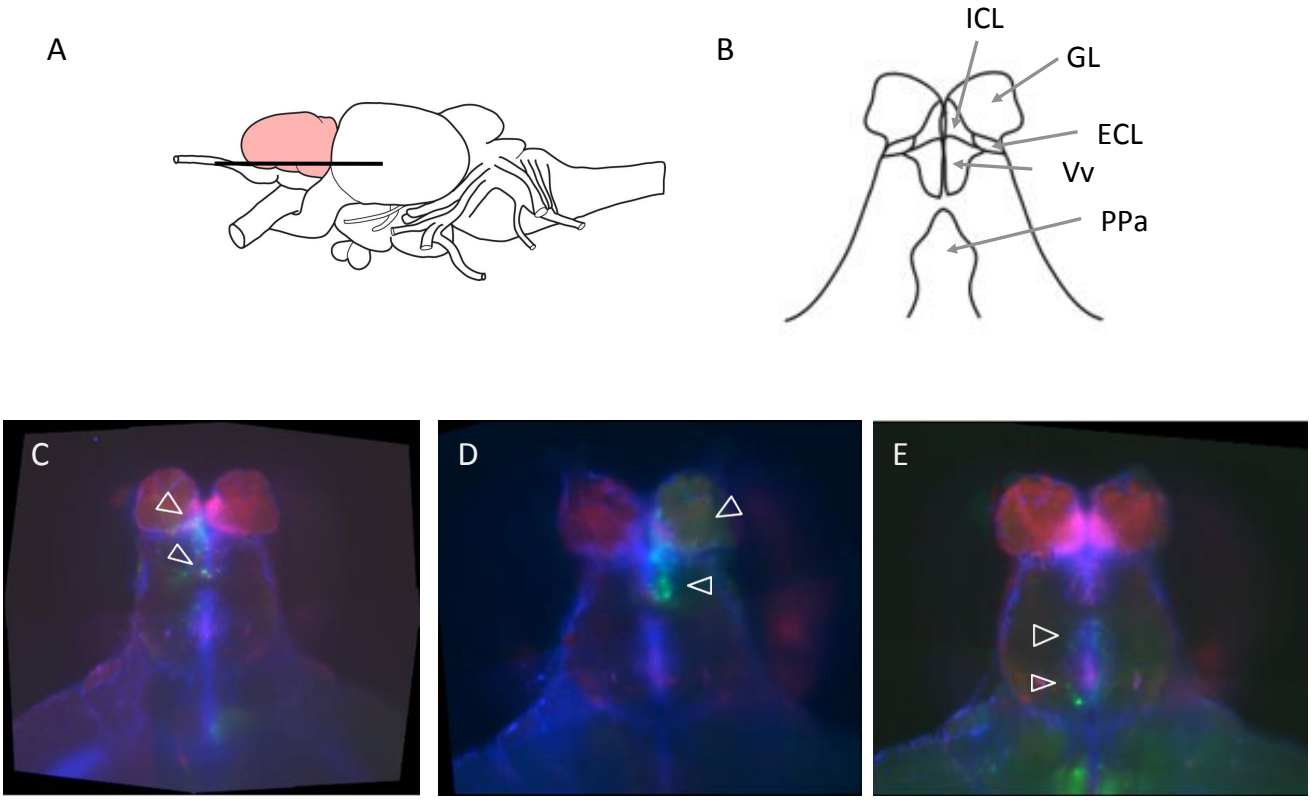

Figure 27. Examples of clonal units that constitute the anatomic region in the dorsal telencephalon.
GFP-positive cells were not observed as compartmentalized blocks in ECL, ICL, GL, Vv and PPa. White triangles show GFP-positive cells in ICL, Vv in (C), GL, ECL,ICL, Vv in (D), PPa in (E) in different samples.

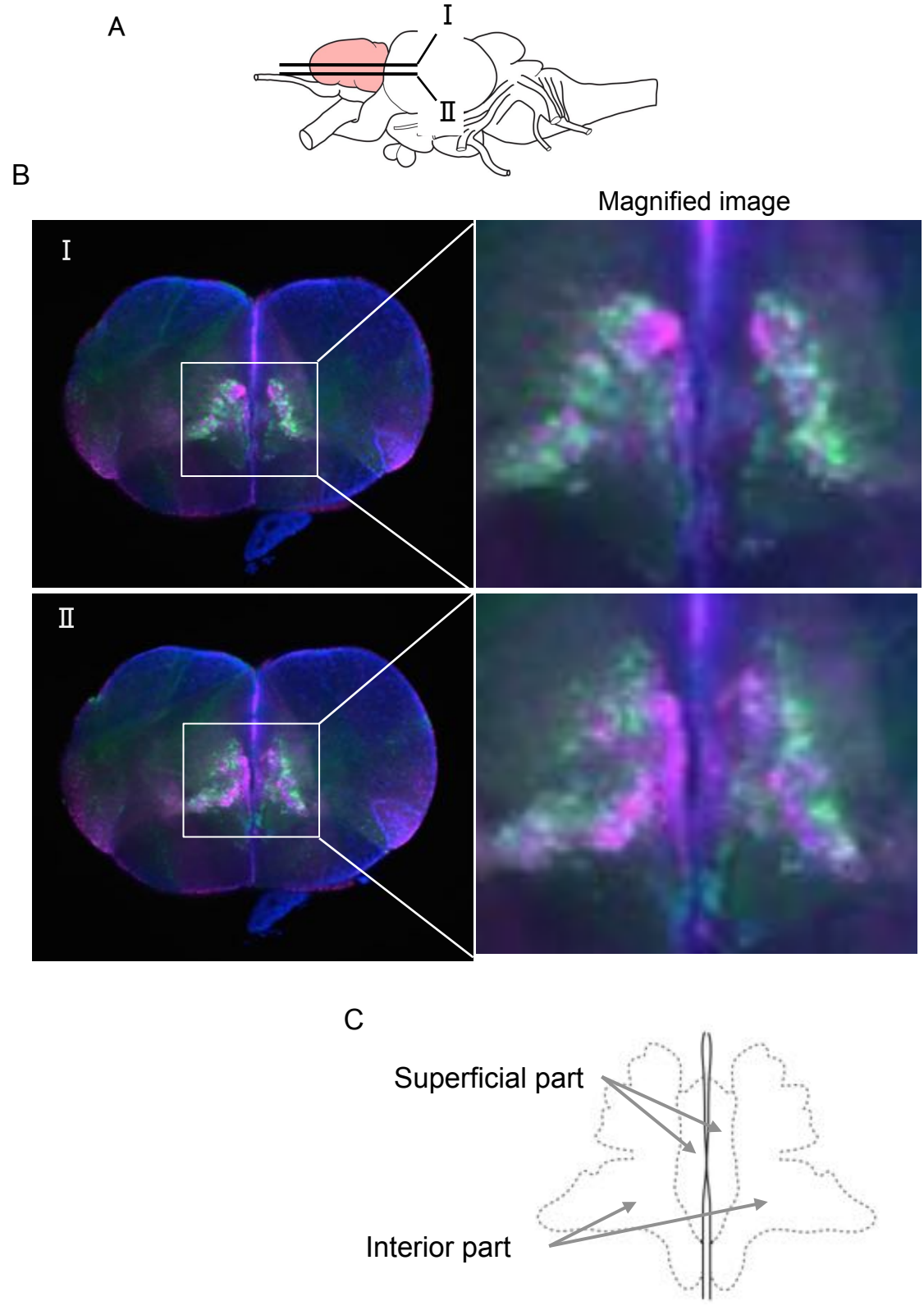

Figure 28. Mosaic pattern in the ventral telencephalon.
(A) Positions of the two horizontal sections shown in B. (B) Left photos show the whole horizontal sections. Right micrograph is a magnification of the region shown by the white rectangle in the left micrograph. DsRed-positive cells (red) and GFP-positive cells (green) were mixed in the ventral telencephalon. (C) Schematic drawing of (B)-Ⅱ. From GFP- an DsRed-distribution, the ventral telencephalon can be devided in to superficial and interior parts.

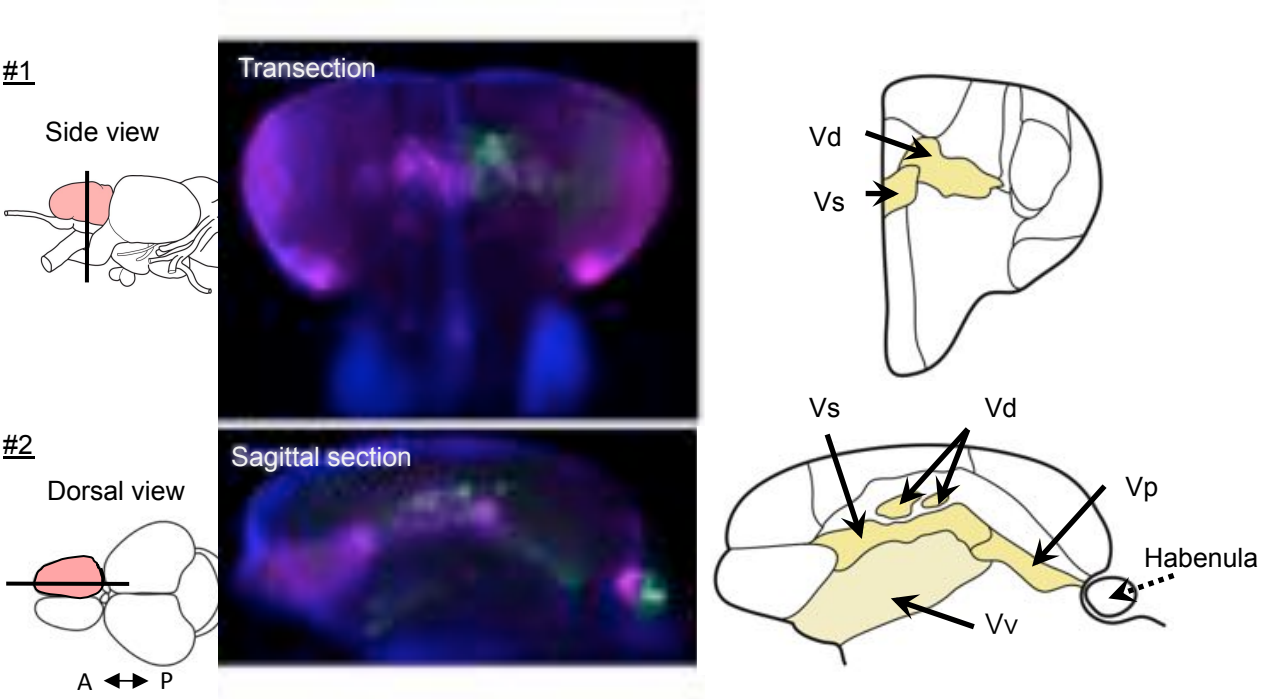

Figure 29. Transection/sagittal section of clonal units in the ventral telencephalon.
Transection/sagittal section of clonal units in the ventral telencephalon. The leftmost image shows the whole telencephalon. The black line indicates the position of the sagittal section. The middle micrograph shows the fluorescent image of the section. The rightmost image show the distribution of GFP-positive cells in yellow. The upper and lower panels show different samples.

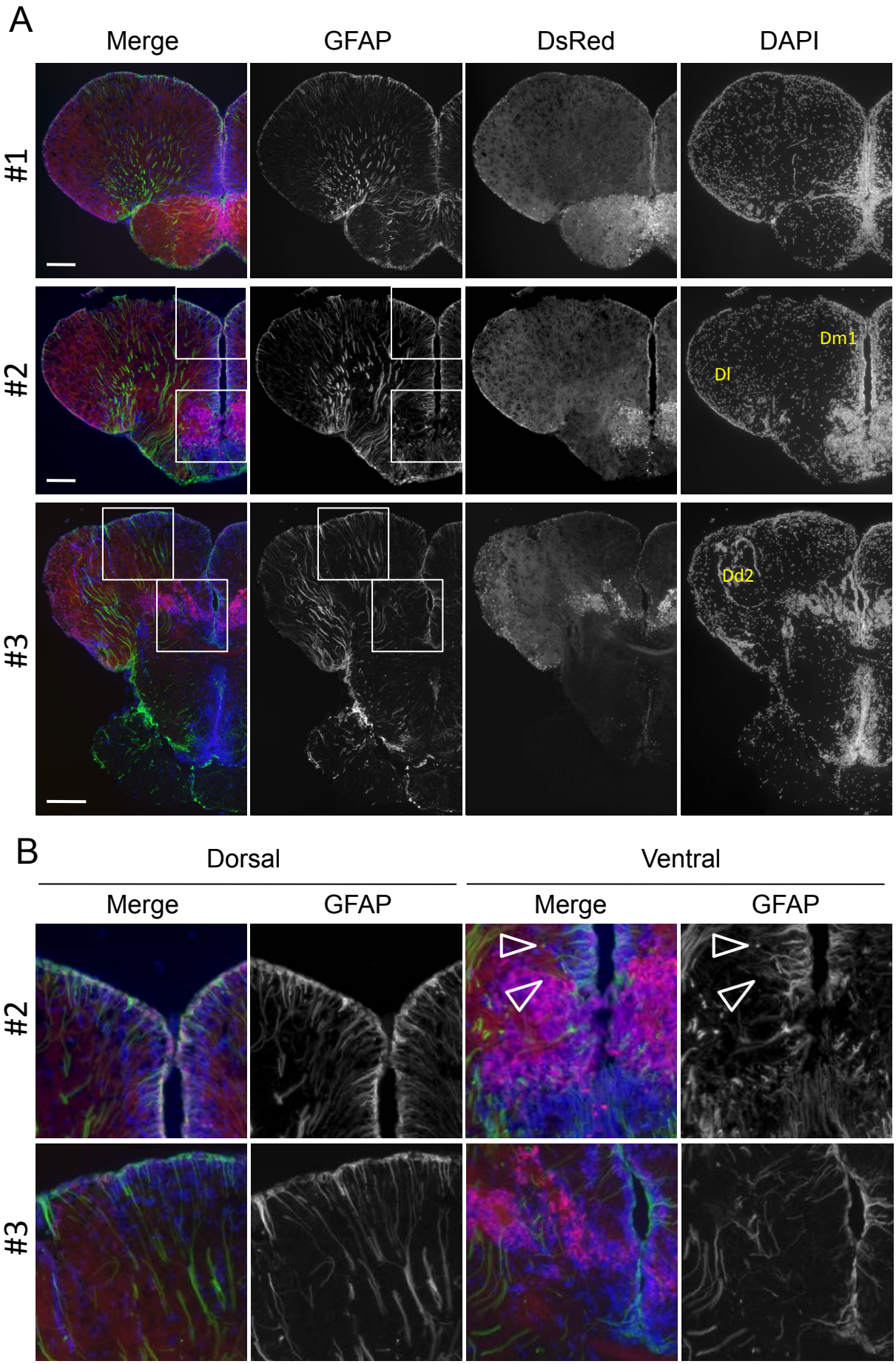
A
Merge
GFAP
DsRed
DAPI
#1
#2
#3
Dm1
Dl
Dd2
B
Dorsal
Ventral
Merge
GFAP
Merge
GFAP
#2
#3

Figure 30. Distribution pattern of radial glial cells by anti-GFAP immunohistochemistry.
(A) Transverse sections of the telencephalon of Tg (HuC:loxP-DsRed-loxP-GFP) line. Green signals indicate GFAP-positive cells. Red signals indicate DsRed expression driven by the HuC promoter. Blue signals indicated DAPI signals. #1~3 are different slices. White line: 100 um. Magnified image of merged image and GFAP-positive cells in white rectangle are shown in (B). The distribution of GFAP-positive signals is different in the dorsal (left) and ventral (right) telencephalon.

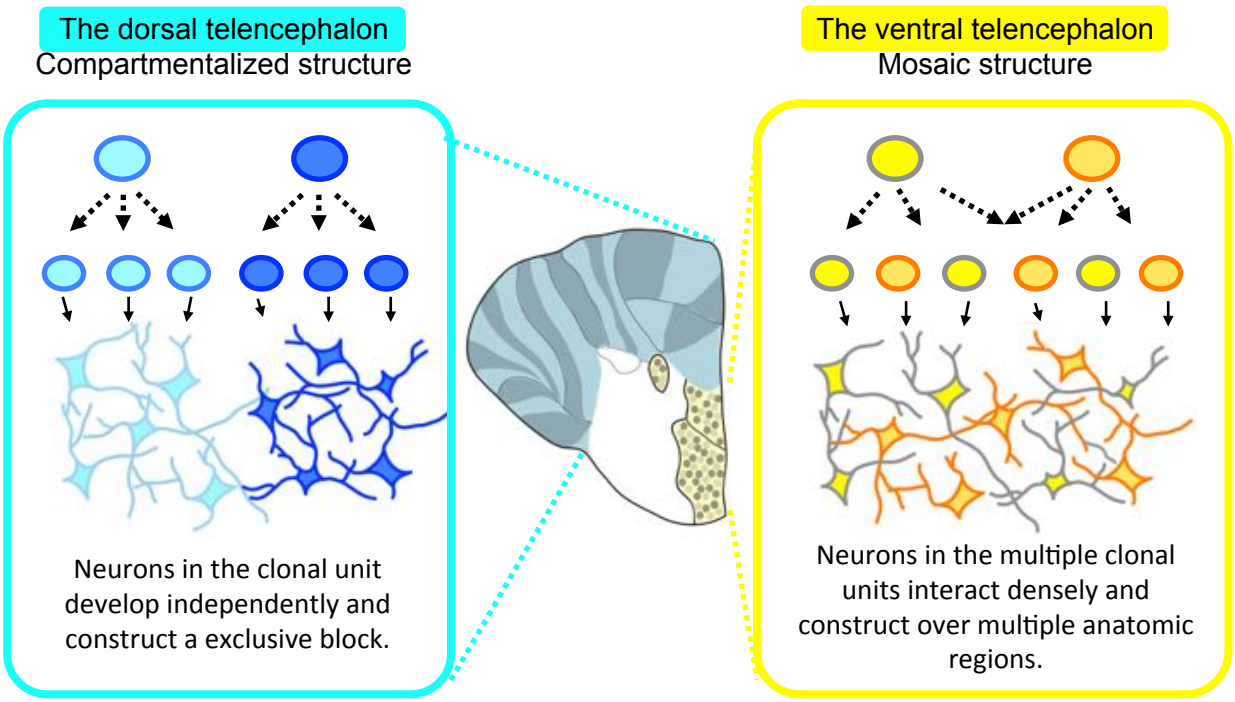

Figure 31 Summary of the findings in Chapter 3
The structures of the clonal units in the anatomic regions were different between the dorsal telencephalon (pallium; left) and the ventral telencephalon (subpallium; right).

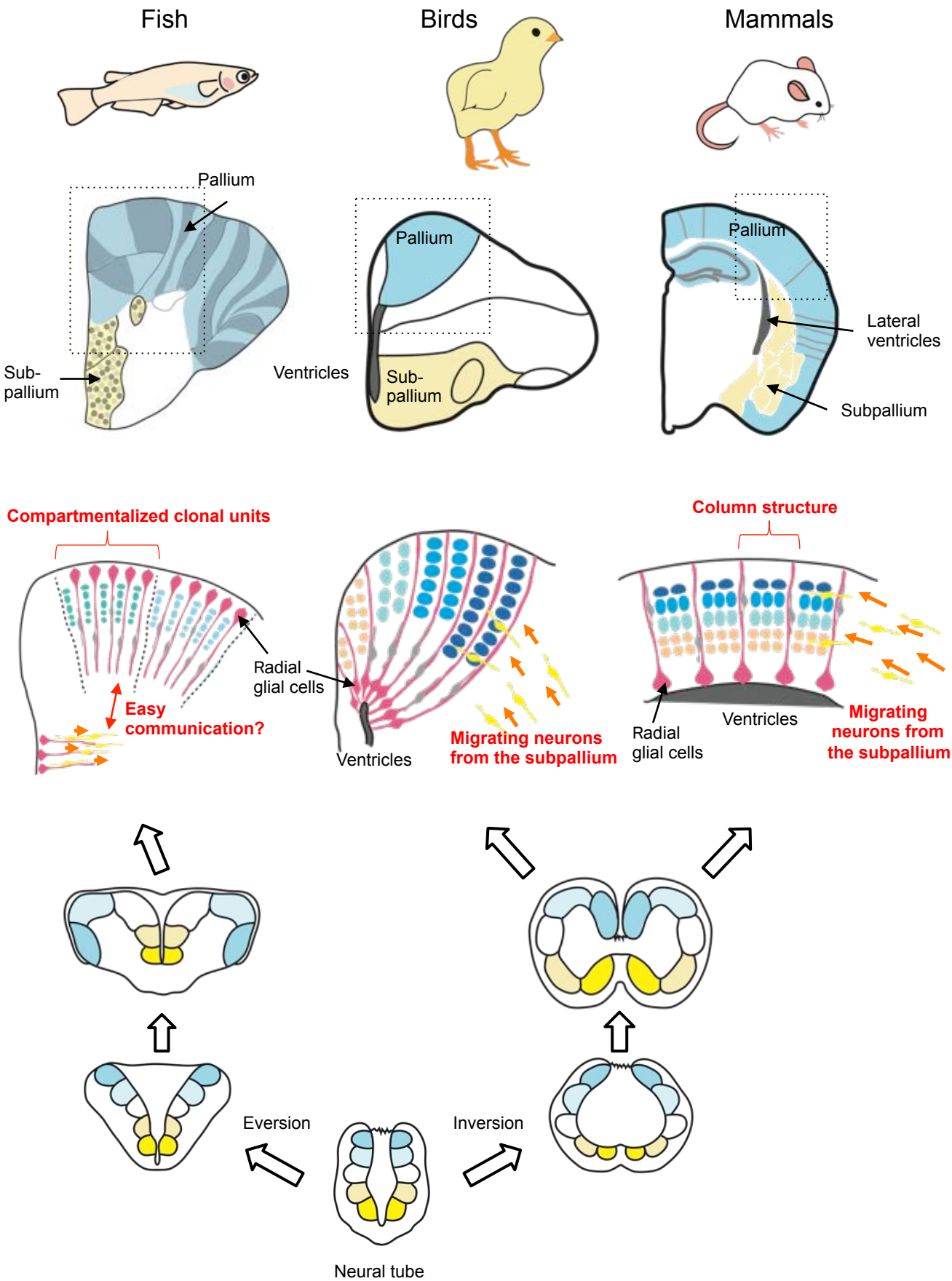

Figure 32 Comparison of structure of the telencephalon among vertebrates. Schematic drawings of the development process of the telencephalon of the earlier stages (bottom), post-hatch/natal stage (middle), and adult stage (top) of fish (left), birds (middle), and mammals (right).

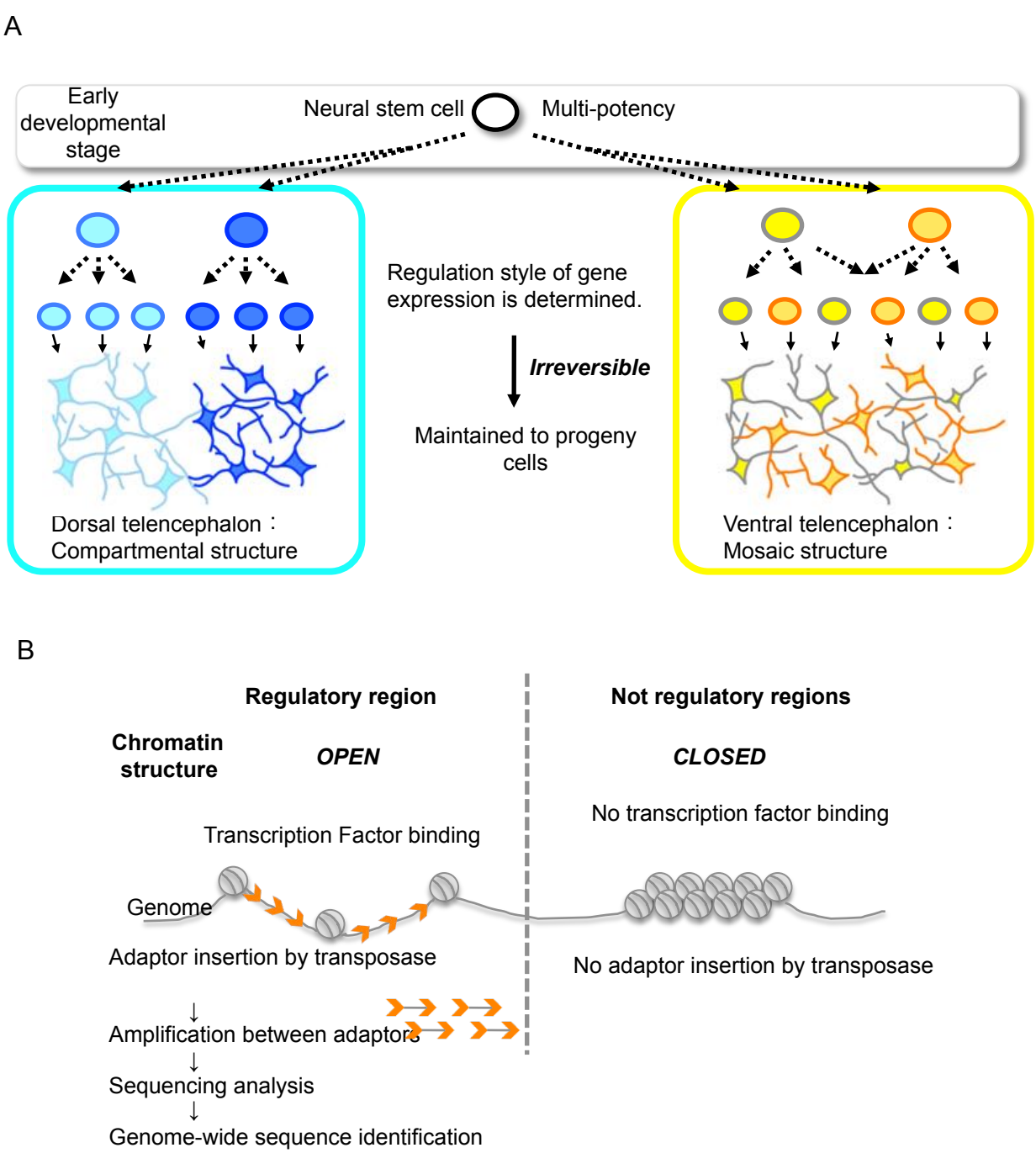

Figure 33. Analysis of regulation of gene expression in the dorsal and ventral telencephalon.

(A) Schematic diagrams of how the destiny of neurons in clonal units is determined by epigenetic modification. At early developmental stages, neural stem cells have multipotency. At later developmental stages, differential regulation of gene expression is determined in each clonal unit, and irreversibly maintained in progeny cells. (B) Schematic diagrams of ATAC-seq. Transcription factors bind to regulatory regions in the genome, so the chromatin is kept open and accessible by transposase. Genome-wide sequencing is available using adaptor insertion with transposase. On the other hand, transposase cannot access closed chromatin, which is assumed not to be a regulatory region in the genome.

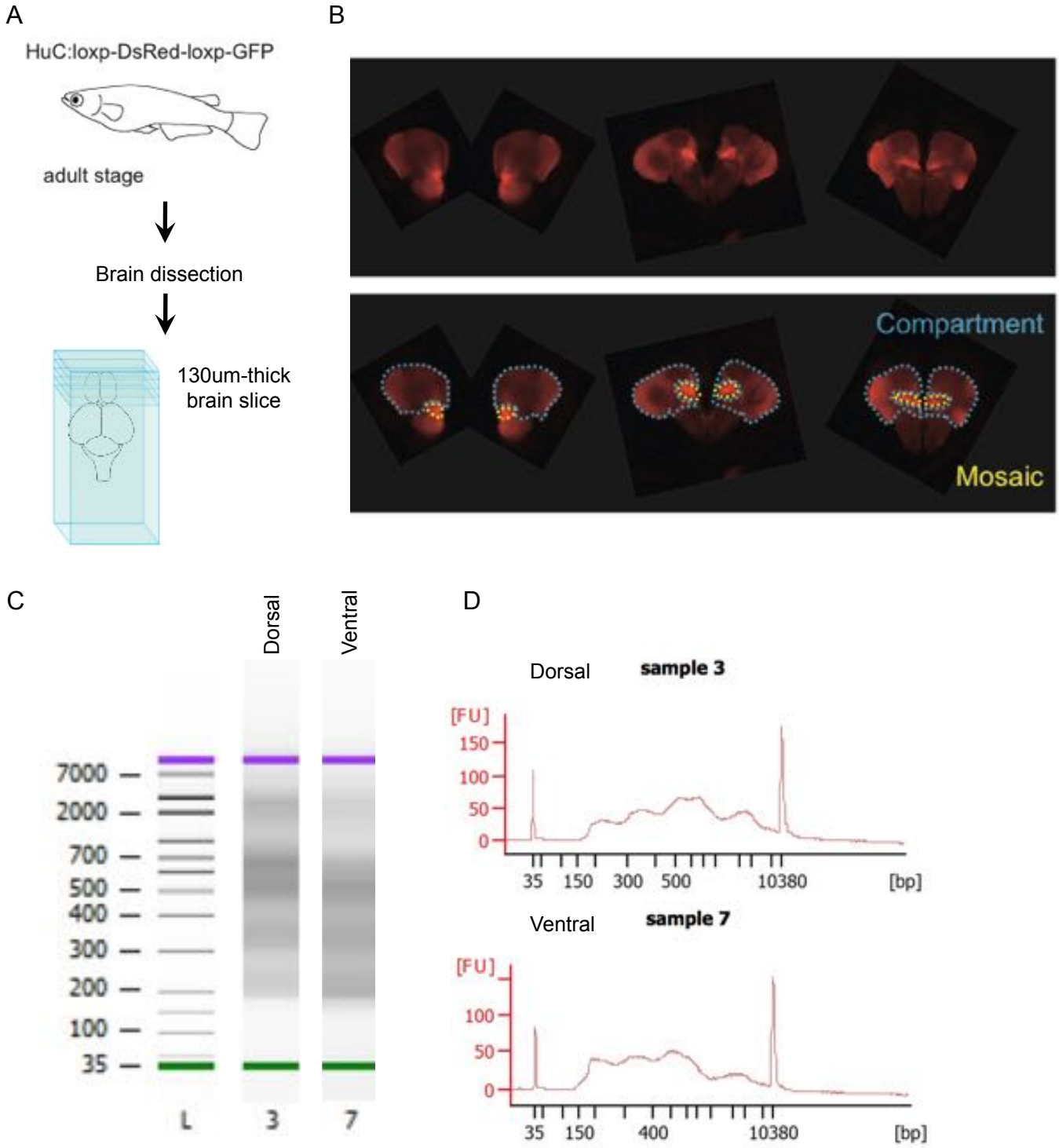

Figure 34. Procedure of sample preparation for ATAC-seq
(A) Schematic diagram of the slice dissection preparation. (B) Examples of brain slices from one adult brain of the Tg line (upper photo). Based on the distribution of DsRed-positive cells in the slice, I dissected the brain and collected slices as ‘dorsal’ and ‘ventral’ samples. (C,D) Fragment sizes of amplified ATAC-seq libraries from the dorsal and ventral telencephalon, determined by the Bioanalyzer. The signal intensity is quantified in (D). Stepwise curves were detected in both samples.

A

	Total reads	Mapped (map Q > 20)
Dorsal	74.2M	51.4M
Ventral	32.4M	21.2M

B

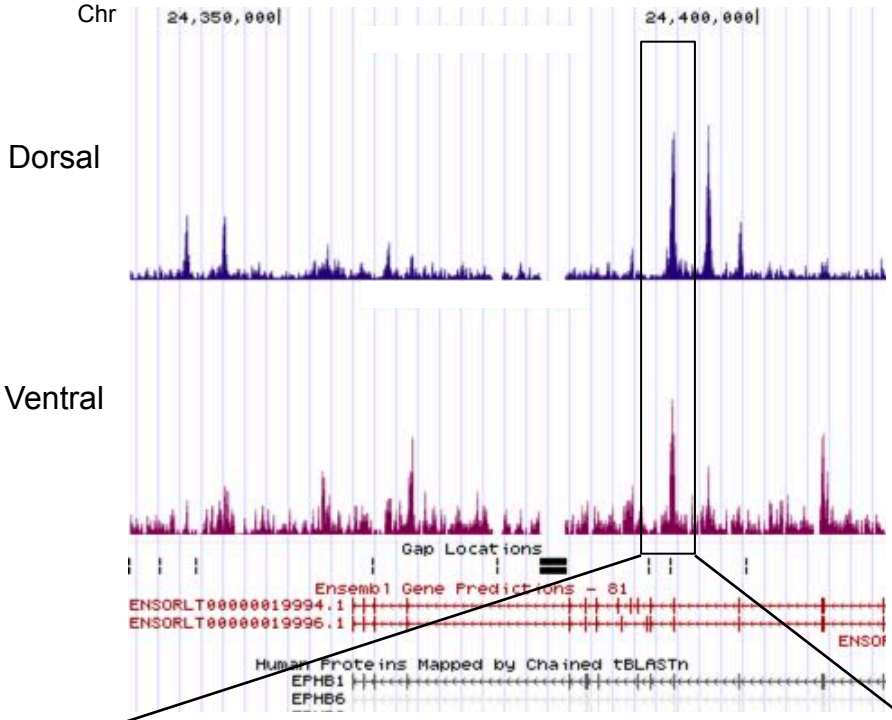

C

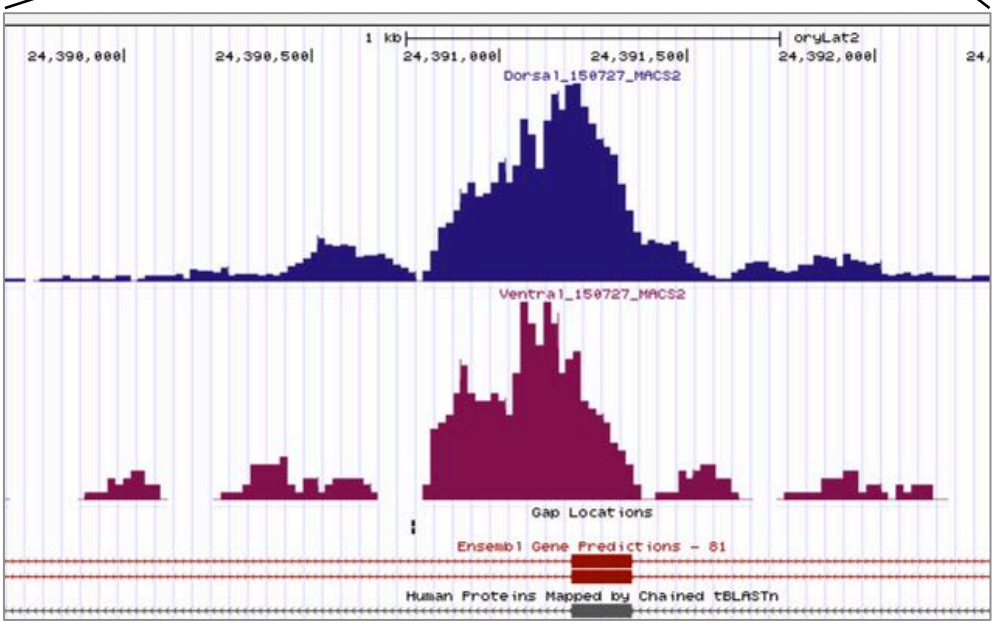

Figure 35. ATAC-seq of the dorsal and ventral telencephalon.
(A) Table of the ATAC-seq results. (B,C) Genome browser representation of open chromatin at the EPHB1 locus. One of the exon loci is shown in (C).

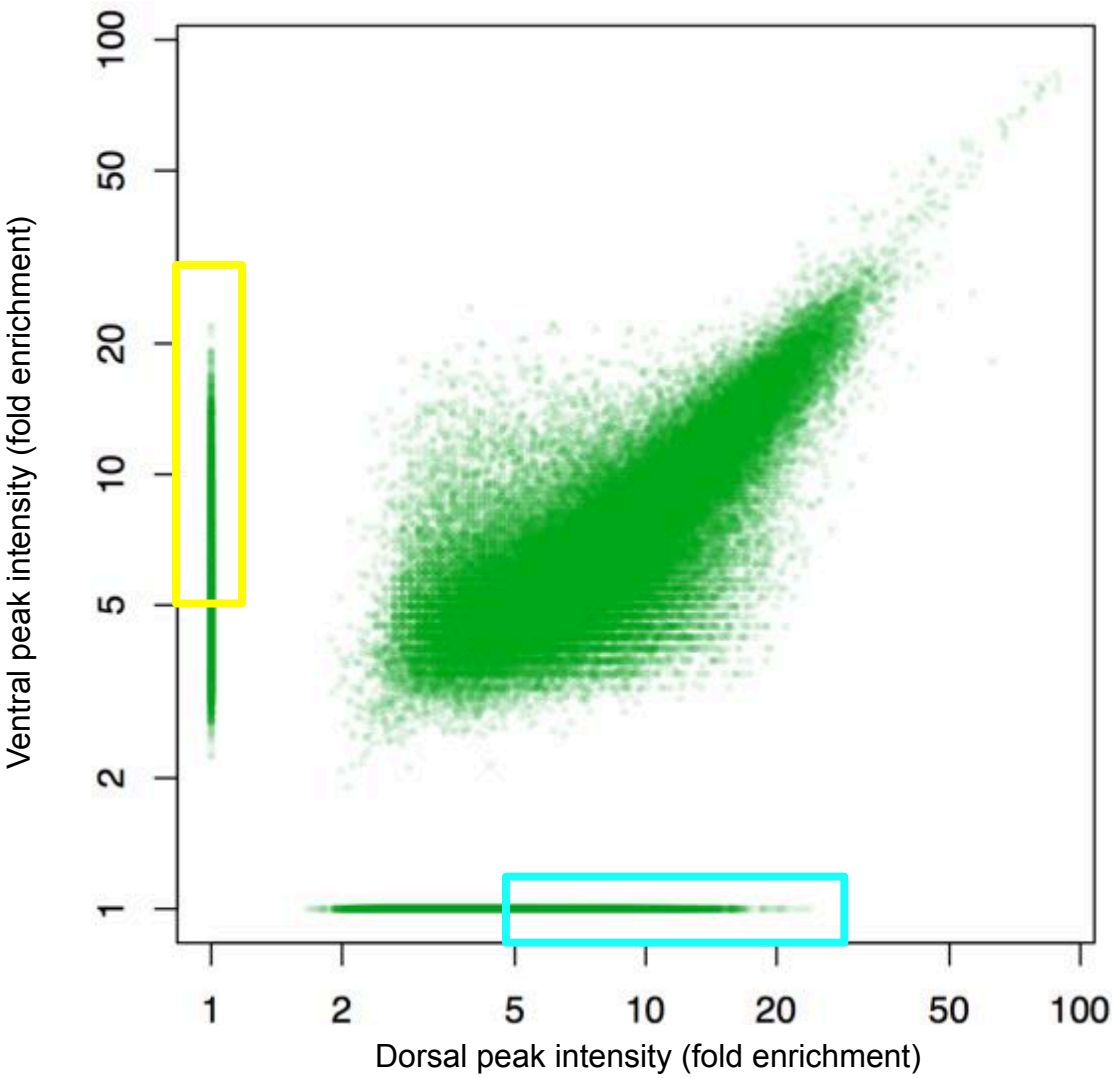

Figure 36. Genome-wide peak call by MACS2
(A) Scatter plot of peaks identified in the dorsal and ventral samples. Green dots indicate each peak. “Fold enrichment of the dorsal sample” was assigned to the horizontal axis and “Fold enrichment of the ventral sample” was assigned to the vertical axis. Green dots near the axis suggest specific peaks. Dots inside the blue rectangle were defined as “dorsal specific peaks” and dots inside the yellow rectangle were defined as “ventral specific peaks”.

Term	Count	%	P-value	FDR
Axon guidance	18	2.7	1.1E-4	1.3E-1
Cell adhesion molecules	12	1.8	3.7E-3	4.3E0
Focal adhesion	19	2.9	5.8E-3	6.6E0
Leukocyte transendothelian migration	12	1.8	1.8E-2	2.0E1
ECM-receptor interaction	9	1.4	2.4E-2	2.4E1
B cell receptor signalling pathway	7	1.1	6.5E-2	5.5E1
Arrhythmogenic right ventricular cardiomyopathy	8	1.2	7.1E-2	5.8E1
Dilated cardiomyopathy	9	1.4	7.3E-2	5.9E1
Regulation of actin cytoskeleton	15	2.3	8.3E-2	6.4E1
Neuroactive ligand-receptor interaction	17	2.6	8.5E-2	6.5E1

Term	Count	%	P-value	FDR
Axon guidance	18	4.6	3.0E-7	3.6E-5
Neuroactive ligand-receptor interaction	15	3.8	1.2E-2	5.1E-1
Calcium signaling pathway	11	2.8	3.9E-2	8.0W-1
Progensterone-mediated oocyte maturation	7	1.8	5.1E-2	8.0E-1
Oocyte meiosis	7	1.8	9.9E-2	9.2E-1

Table 3 Result of KEGG pathway enrichment analysis of the dorsal (upper) and ventral (lower) telencephalon.

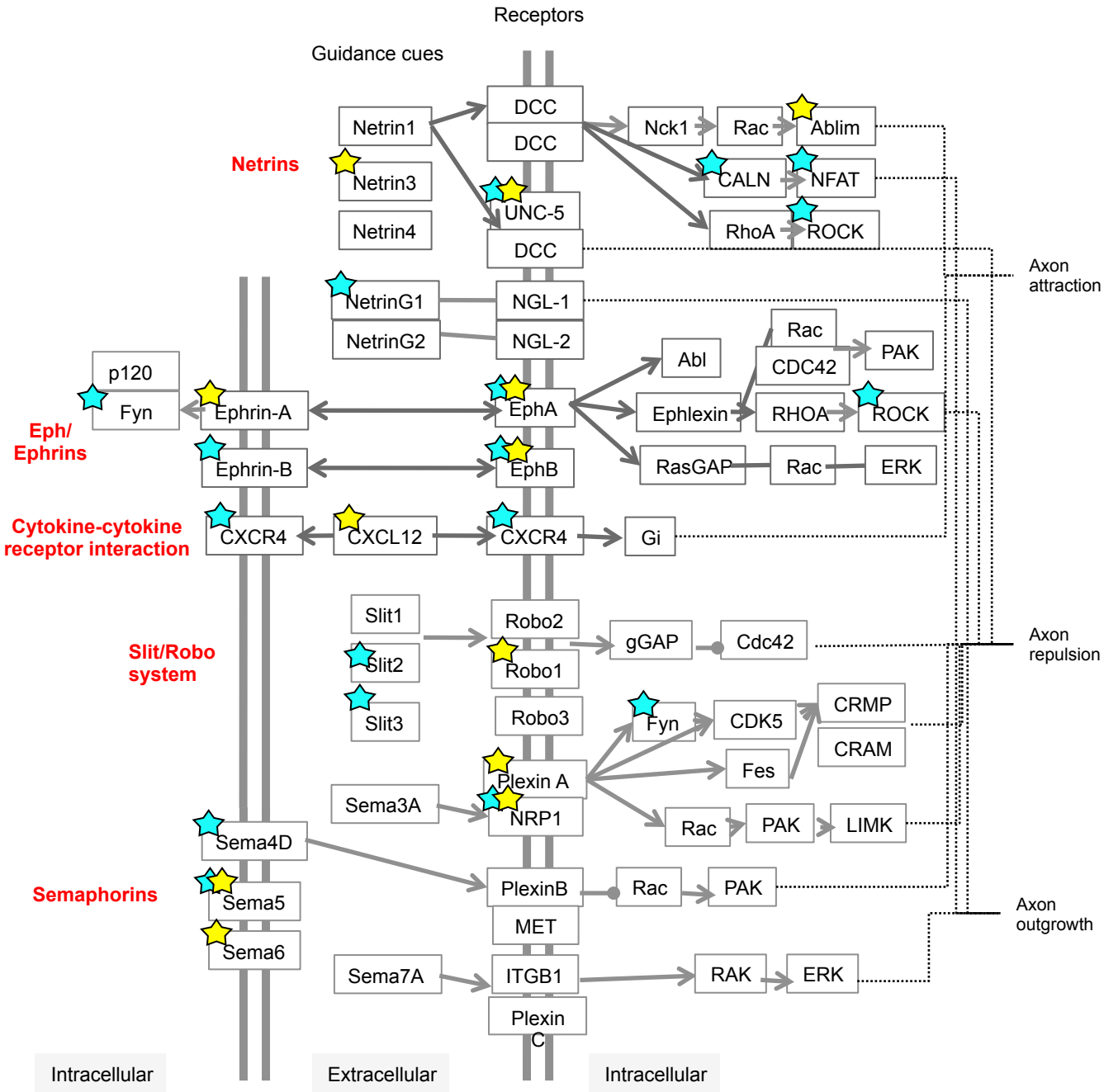

Figure 37. Axon guidance pathway map
The blue stars indicate the associations between “dorsal specific peaks” and pathway genes. The yellow stars indicate the associations between “ventral specific peaks” and pathway genes.

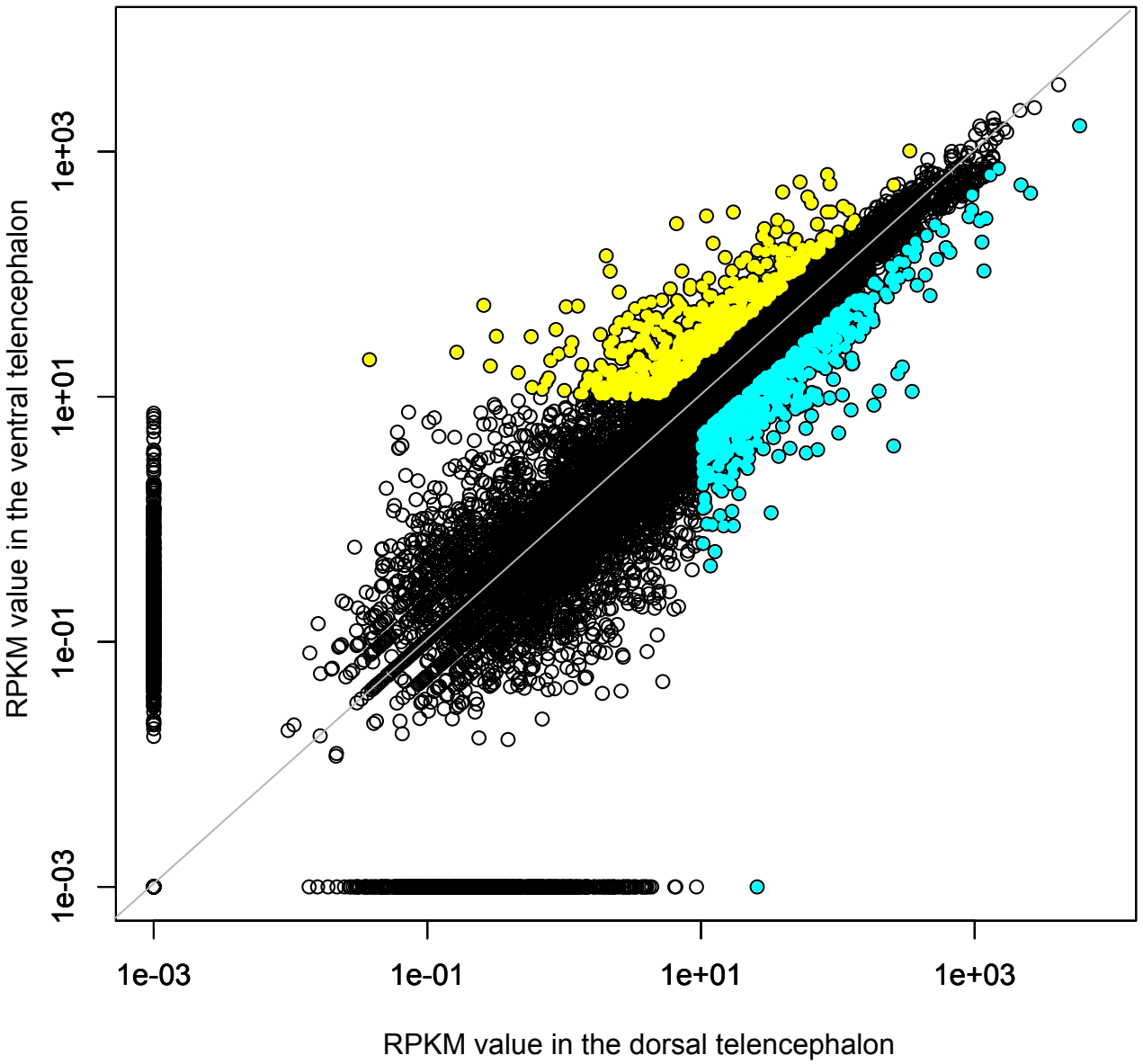

Figure 38. Comparison of all genes expression level
A scatter plot of the levels of all genes expressed in the dorsal telencephalon (horizontal axis) versus the ventral telencephalon (vertical axis). Blue dots indicate the genes that the RPKM value in the dorsal telencephalon is twice as high as that in the ventral telencephalon and RPKM value is larger than 10. Yellow dots indicate the genes that the RPKM value in the ventral telencephalon is twice as high as that in the dorsal telencephalon and RPKM value is larger than 10. The gray line represents the 1:1 diagonal.

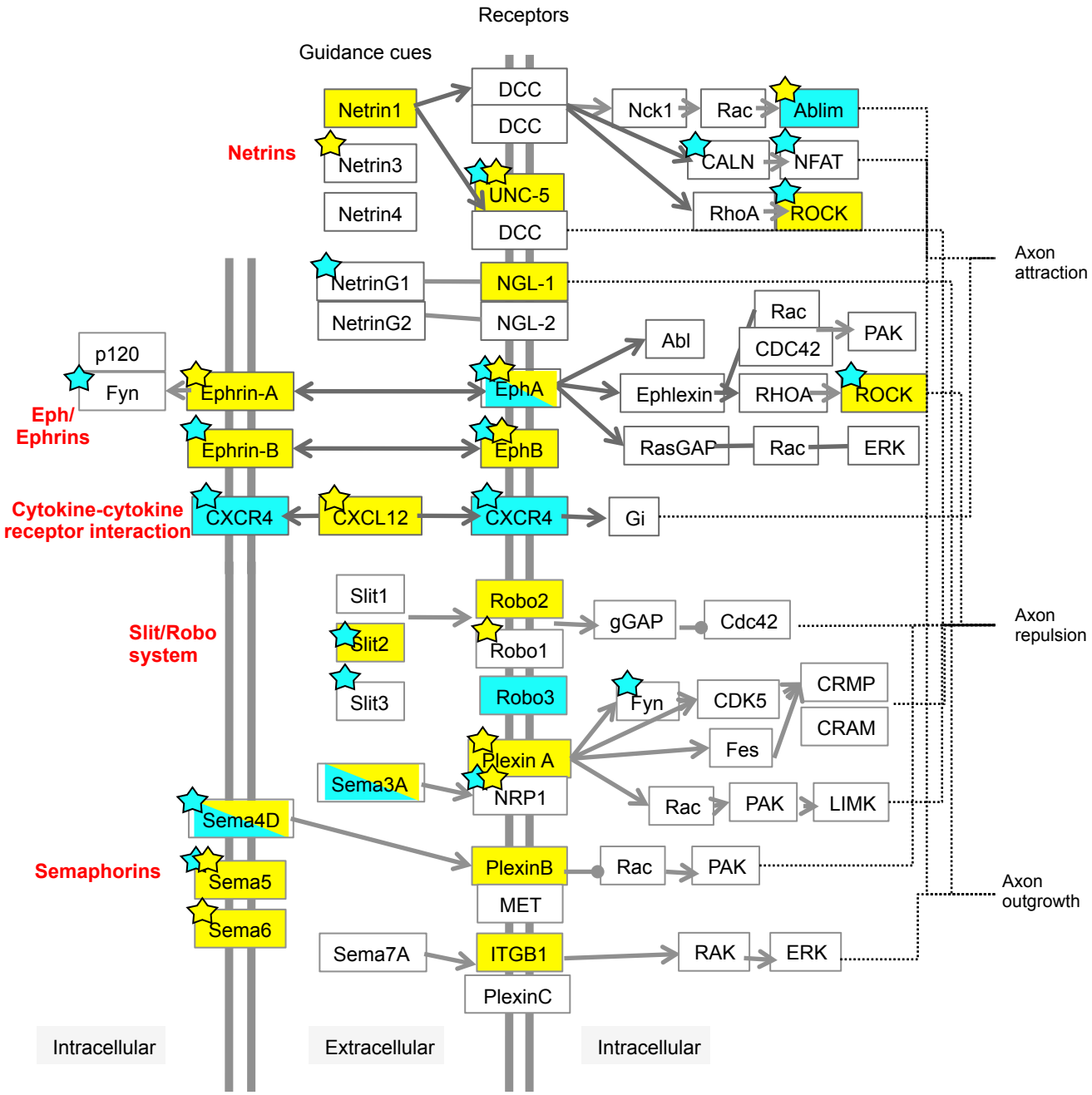

Figure 39. Axon guidance pathway map

The blue stars indicate the associations between “dorsal specific peaks” and pathway genes. The yellow stars indicate the associations between “ventral specific peaks” and pathway genes. In addition, blue- or yellow-colored rectangular indicate the genes strongly expressed in the dorsal or ventral telencephalon. The rectangular with both color indicate the genes differentially expressed among the gene family.

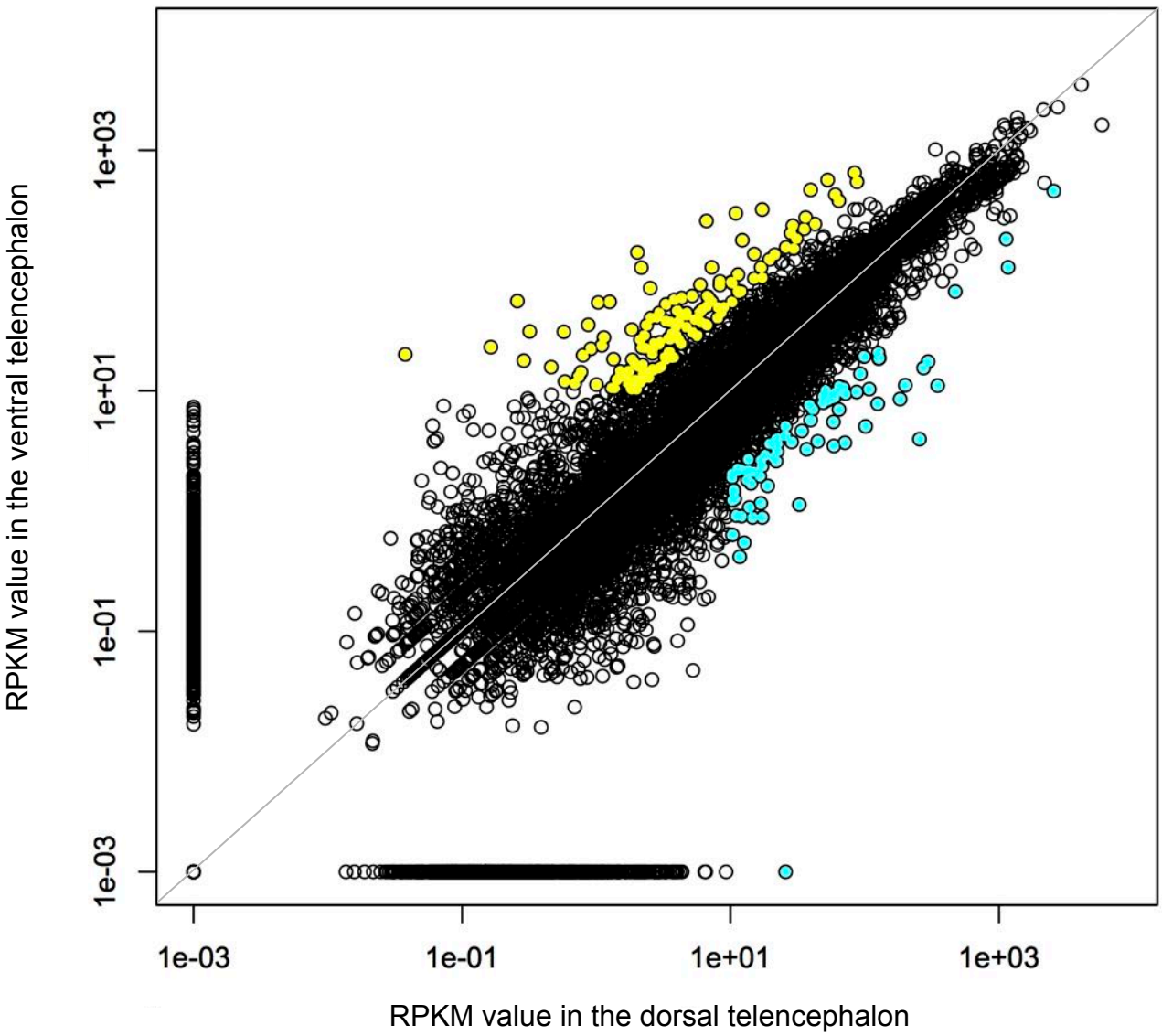

Figure 40. Comparison of all genes expression level
A scatter plot of the levels of all genes expressed in the dorsal telencephalon (horizontal axis) versus the ventral telencephalon (vertical axis). Blue dots indicate the genes that the RPKM value in the dorsal telencephalon is five times as high as that in the ventral telencephalon and RPKM value is larger than 10. Yellow dots indicate the genes that the RPKM value in the ventral telencephalon is five times as high as that in the dorsal telencephalon and RPKM value is larger than 10. The gray line represents the 1:1 diagonal.

Gene symbol		RPKM_dorsal	RPKM_ventral
Netrins			
UNC5CL	ENSORLG00000005278	28.27	45.64
UNC5A	ENSORLG00000006750	14.97	28.54
∗unc5da	ENSORLG00000002892	6.05	37.10
unc5c	ENSORLG00000007815	10.84	22.91
ntn4 (1 of 2)	ENSORLG00000016622	14.65	18.85
NTNG1	ENSORLG00000005716	22.27	11.18
unc5db	ENSORLG00000016270	5.71	14.06
NTN1	ENSORLG00000015276	3.08	14.08
UNC5B	ENSORLG00000011553	9.75	3.80
DCC	ENSORLG00000015328	1.39	5.02
NTN3	ENSORLG00000007171	0.89	1.27
NTN5	ENSORLG00000006869	0.04	0.14
ntn4 (2 of 2)	ENSORLG00000004087	0.00	0.08
ntng2a	ENSORLG00000016605	0.05	0.00
Eph/Ephrins pathway			
epha4b	ENSORLG00000014565	104.93	87.51
ephb3a	ENSORLG00000009010	68.17	110.60
epha4a	ENSORLG00000008991	35.02	93.92
epha4l	ENSORLG00000014683	52.70	46.65
EPHB6	ENSORLG00000011883	41.36	55.34
∗EPHA5	ENSORLG00000011769	68.30	9.79
EPHA7	ENSORLG00000017959	43.96	30.85
EPHA10	ENSORLG00000009982	31.72	30.16
EPHB1 (1 of 2)	ENSORLG00000015972	26.65	28.54
EPHA6 (2 of 2)	ENSORLG00000015611	24.53	10.25
ephb2a	ENSORLG00000019878	11.02	13.70
EPHB4	ENSORLG00000006909	11.13	9.23
ephb2b	ENSORLG00000017097	9.90	10.47
EPHA3	ENSORLG00000015835	13.37	4.18
EPHA8	ENSORLG00000012405	4.37	10.56
∗EPHB1 (2 of 2)	ENSORLG00000011003	1.59	13.22
EPHB3 (1 of 2)	ENSORLG00000007219	3.99	9.88
EPHA2 (1 of 2)	ENSORLG00000020136	6.50	5.67
epha2	ENSORLG00000003543	1.54	1.24
epha6	ENSORLG00000005357	0.31	1.64
Cytokine-cytokine receptor interaction			
∗CXCL14	ENSORLG00000000201	52.96	565.20
cxcr4b	ENSORLG00000020496	14.01	4.55
CXCR5	ENSORLG00000002476	2.92	3.04
CXCR7	ENSORLG00000017874	2.62	3.73
cxcr3.2	ENSORLG00000013459	1.42	1.76
cxcr3.1 (1 of 2)	ENSORLG00000013488	1.93	0.64
cxcr4a	ENSORLG00000011337	1.18	0.87
cxcr3.1 (2 of 2)	ENSORLG00000013468	0.51	0.15
CXCR1	ENSORLG00000018075	0.00	0.00

Table 4 Lists of reads per kilobase of exon per million mapped reads (RPKM) of the axon guidance pathway genes.

The transcripts of axon guidance pathways are categorized into five groups listed from high to low, based on quantitative transcript level (RPKM). The Ensembl accession number is also listed. Asterisks represent genes in which the RPKM of either the dorsal or ventral telencephalon was more than 5 times larger than that of the other, and also larger than 10.

Gene symbol		RPKM_dorsal	RPKM_ventral
Slit/Robo system			
SLITRK1	ENSORLG00000004606	77.20	146.78
SLITRK5	ENSORLG00000004630	80.68	60.39
SLITRK4	ENSORLG00000008548	57.83	78.74
SLITRK3 (2 of 2)	ENSORLG00000012102	65.63	58.40
robo2	ENSORLG00000004097	34.96	52.33
ROBO3	ENSORLG00000005288	60.62	25.77
robo1	ENSORLG00000004126	43.99	23.85
SLITRK2	ENSORLG00000008527	33.05	24.01
SLITRK6	ENSORLG00000004618	11.54	33.80
slitrk3b	ENSORLG00000014064	31.08	24.70
slit1b	ENSORLG00000000055	13.33	17.58
slit1a	ENSORLG00000007918	9.61	12.23
SLIT2	ENSORLG00000005750	4.70	16.17
ROBO1 (2 of 2)	ENSORLG00000010043	6.00	6.42
SLIT3	ENSORLG00000000335	0.52	2.40
Semaphorins			
SEMA6B (1 of 2)	ENSORLG00000014868	75.52	82.64
sema7a	ENSORLG00000007240	75.29	55.74
sema3aa	ENSORLG00000015034	42.04	71.78
SEMA4B (2 of 2)	ENSORLG00000012629	28.43	71.57
SEMA6A	ENSORLG00000003447	35.14	46.06
SEMA4C	ENSORLG00000015302	36.43	29.90
sema3h	ENSORLG00000002802	23.81	49.97
SEMA4D	ENSORLG00000005743	26.29	31.30
SEMA5A	ENSORLG00000007742	16.83	41.69
SEMA6D	ENSORLG00000002823	20.21	29.80
SEMA6B (2 of 2)	ENSORLG00000016416	21.98	24.28
sema6e	ENSORLG00000015839	14.93	33.32
sema6d	ENSORLG00000001218	14.08	15.35
sema4ga	ENSORLG00000007299	21.12	9.47
SEMA3E	ENSORLG00000009509	20.10	6.41
SEMA4F	ENSORLG00000005915	12.05	7.43
SEMA5B (1 of 2)	ENSORLG00000006593	10.72	9.37
sema4ba	ENSORLG00000008247	8.14	11.47
sema3ab	ENSORLG00000009475	11.23	4.95
SEMA3G	ENSORLG00000003333	3.68	11.38
sema5b	ENSORLG00000009896	5.62	8.25
sema4e	ENSORLG00000014954	6.76	4.62
SEMA3F	ENSORLG00000014370	3.21	8.49
sema3ga	ENSORLG00000014173	4.64	5.71
SEMA4G (1 of 2)	ENSORLG00000011518	4.08	5.29
SEMA3C	ENSORLG00000016082	3.06	4.98
SEMA4A	ENSORLG00000016896	2.58	5.02
SEMA3D	ENSORLG00000009459	1.41	0.38

Table 4 (Continued)

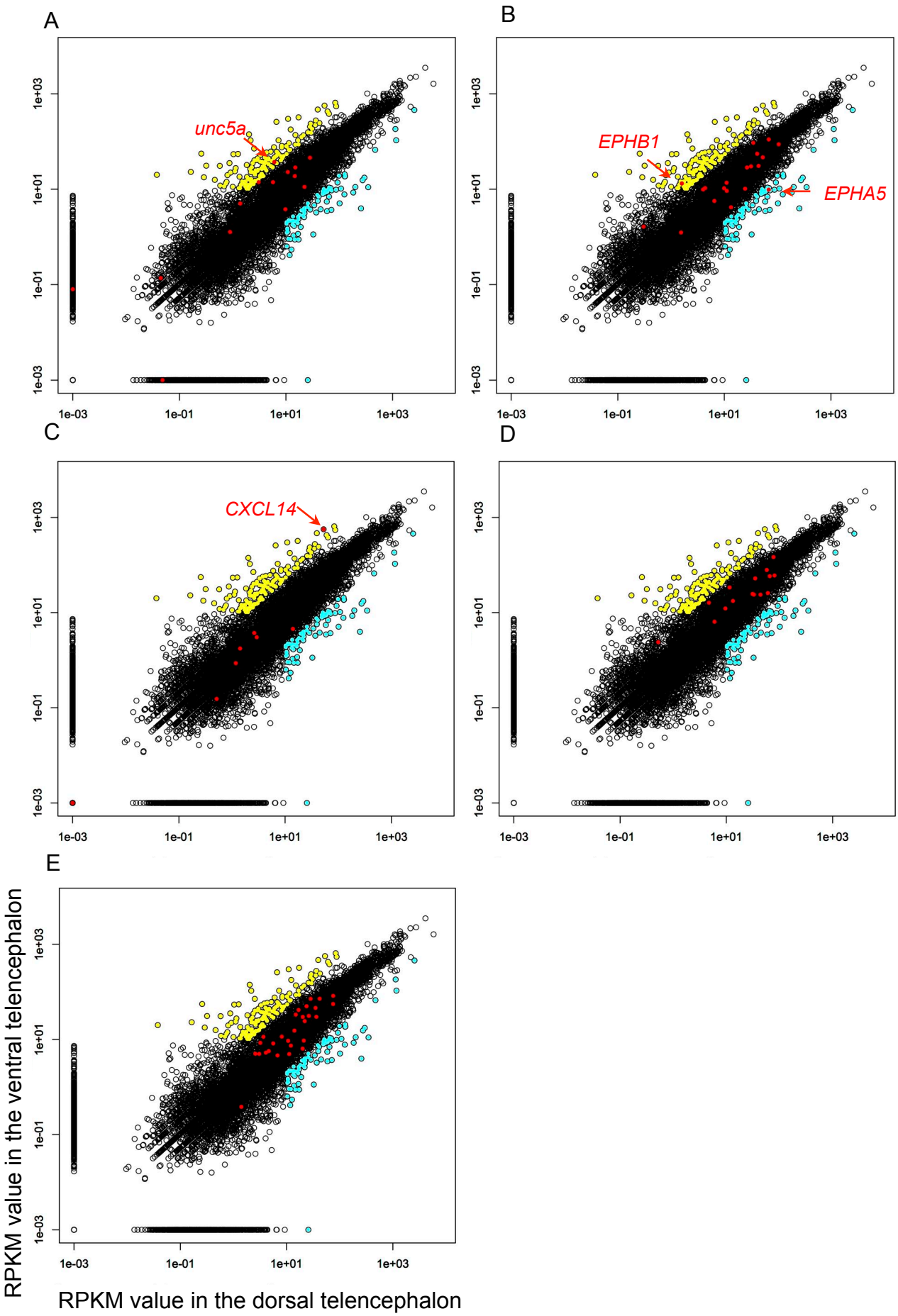
A
unc5a
B
EPHB1
EPHA5
C
CXCL14
D
E
1e-03
1e-01
1e+01
1e+03
RPKM value in the ventral telencephalon
RPKM value in the dorsal telencephalon

Figure 41. Comparison of levels of axon guidance pathway gene expression.
Scatter plots of axon guidance pathway genes (red) (netrin family (A), Eph/ephrins (B), cytokine-cytokine receptor interaction (C), Slit/Robo system (D), semaphorins (E) expression levels in the dorsal and ventral telencephalon Blue dots indicate genes strongly expressed in the pallium, and yellow dots indicate genes strongly expressed in the subpallium. Axon guidance pathway genes strongly expressed in dorsal/ventral are represented in red.

A

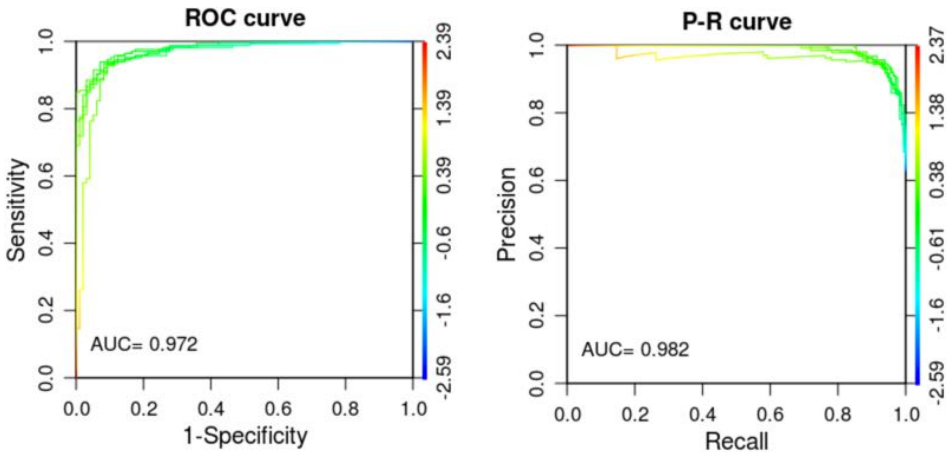

B

Dorsal specific 6-mers	
6−mer	Motif
AGATGG	Atoh1
CTTGGC	NFIA
TGCCAA	NFIA
AGCCAA	NFIC
ATGCTG	Mafb

Ventral specific 6-mers	
6−mer	Motif
CTGTCA	Meis1
ACAATG	Sox15
AACAAT	Sox5
TGTCAA	Meis2
TGACAA	Irx3

C

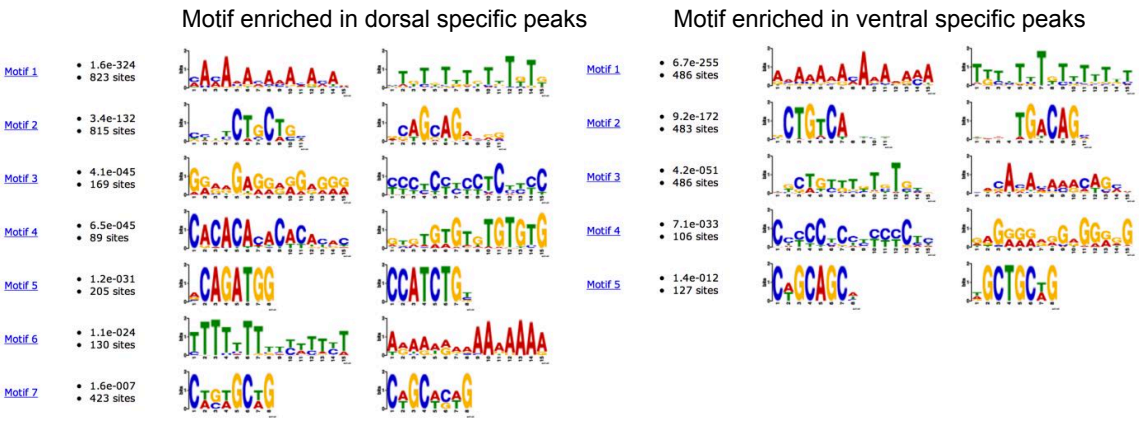

Figure 42. Identification of predictive regulatory sequences
Regulatory sequences of the open chromatin in the dorsal and ventral telencephalon are predicted by kmer-SVM (A,B) and MEME (C). (A) Receiver operating characteristic (ROC) curve (left) and Precision-Recall curve (right). The area under the ROC curve (AUROC, AUC) (left) and the area under the PR curve (AUPRC, AUC) (right) are represented at the bottom of the graphs. (B) The top five 6-mers are identified in the table. (C) Motifs enriched in the dorsal or ventral specific peaks identified by MEME.

Gene symbol		RPKM_dorsal	RPKM_ventral
Dorsal			
neurod2	ENSORLG00000008303	435.50	98.55
nfixb (1 of 2)	ENSORLG00000016601	224.26	70.01
NEUROD2 (2 of 2)	ENSORLG00000003441	229.78	65.36
nfixa	ENSORLG00000003734	150.57	37.75
NEUROD6	ENSORLG00000017789	99.86	87.60
nfixb (2 of 2)	ENSORLG00000016602	120.32	45.08
NFIB	ENSORLG00000005185	29.86	12.62
MAFG (2 of 2)	ENSORLG00000007850	15.26	26.62
MAFG (1 of 2)	ENSORLG00000012170	12.28	24.62
NFIC	ENSORLG00000002516	17.26	16.70
NFIA	ENSORLG00000003529	20.51	6.72
mafbb	ENSORLG00000013930	12.55	3.61
maf (1 of 2)	ENSORLG00000009643	1.50	13.17
mafba	ENSORLG00000009479	5.57	5.47
BHLHA15	ENSORLG00000003401	4.03	5.79
MAFK	ENSORLG00000004687	4.95	1.03
NRL	ENSORLG00000002003	1.72	3.06
neurod4 (1 of 2)	ENSORLG00000007467	3.46	1.25
neurod	ENSORLG00000010563	3.99	0.00
NEUROG1	ENSORLG00000020531	0.86	0.13
MAFA	ENSORLG00000013090	0.14	0.43
Mafb	ENSORLG00000010298	0.25	1.11
neurod4 (2 of 2)	ENSORLG00000019867	0.00	0.11
ATOH1	ENSORLG00000004876	0.00	0.09
ATOH7	ENSORLG00000013722	0.00	0.00
Ventral			
∗Meis2a	ENSORLG00000013127	10.96	298.54
Sox5	ENSORLG00000008803	61.64	31.79
PKNOX1	ENSORLG00000020833	29.48	27.08
TGIF1	ENSORLG00000010346	17.44	19.99
MEIS3	ENSORLG00000008534	13.20	14.18
SOX6B	ENSORLG00000006705	8.28	16.23
SOX6A	ENSORLG00000001260	6.28	12.18
Meis1	ENSORLG00000002411	5.39	10.79
TGIF2	ENSORLG00000016614	6.62	5.67
SOX13	ENSORLG00000012066	0.67	9.81
irx1b	ENSORLG00000014300	1.80	1.08
irx7	ENSORLG00000019207	0.31	0.96
IRX5	ENSORLG00000013711	0.22	0.14
IRX4	ENSORLG00000014288	0.19	0.14
IRX2	ENSORLG00000005150	0.00	0.50
IRX4	ENSORLG00000005134	0.00	0.00
MKX	ENSORLG00000009614	0.00	0.00
IRX6	ENSORLG00000013697	0.00	0.00

Table 5 Lists of reads per kilobase of exon per million mapped reads (RPKM) of the transcription factors.

The transcripts of candidate transcription factors that bind to regulatory regions estimated by the SVM and those paralogs are listed from high to low based on quantitative transcript levels (RPKM). The Ensembl accession number is also listed. Asterisk represents a gene in which the RPKM of either the dorsal or ventral telencephalon was more than 5 times larger than that of the other, and also larger than 10.

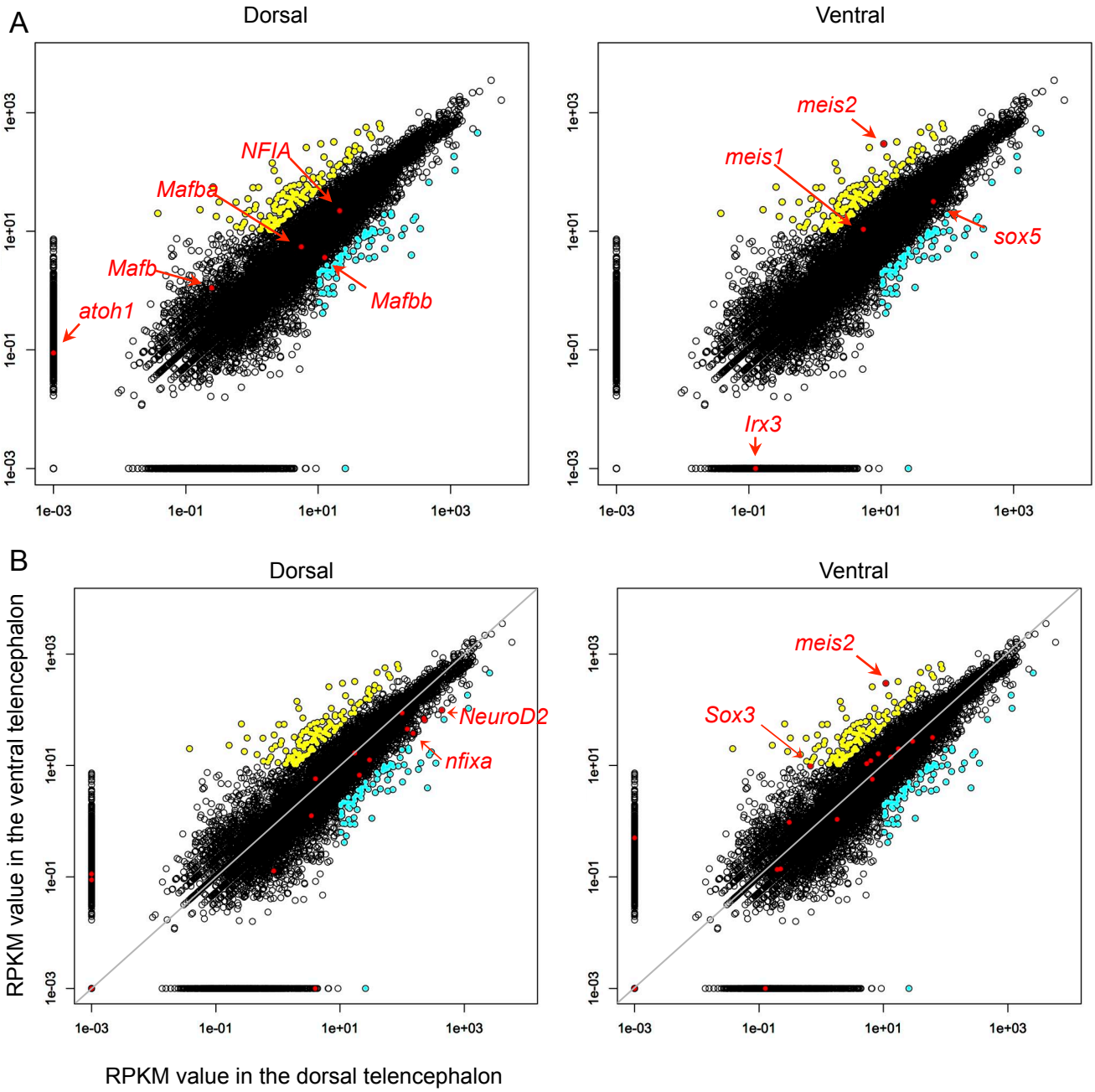

Figure 43. Comparison of transcription factor gene expression levels
Scatter plots of transcription factors that are estimated to bind predictive regulatory sequences by SVM (red) (A). Expression level of transcription factors and their paralogs are also compared in (B). Transcription factors expressed preferentially in the pallium or subpallium are represented in red (B). Blue dots indicate genes strongly expressed in the pallium, and yellow dots indicate genes strongly expressed in the subpallium.

A

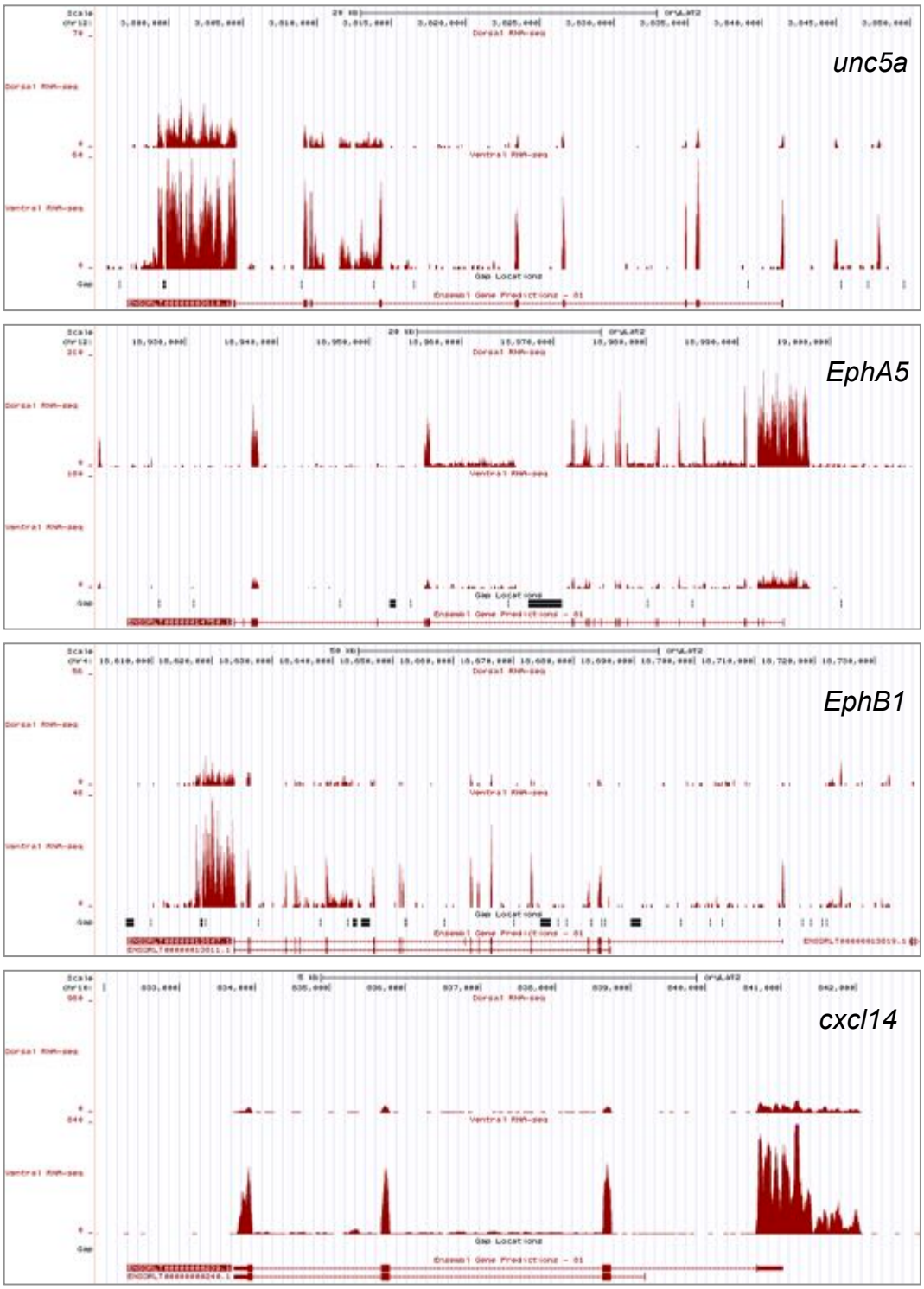

Figure 44. Coverage plots showing the distribution of RNA-seq reads across the genes.

Coverage plots of genes of axon guidance pathway (A) and genes of transcription factors (B) identified as preferentially expressed in the dorsal or ventral tenecephalon. Vertical axis is adjusted to the total reads of the dorsal (35,166,176) and ventral (31,488,710) telencephalon.

B

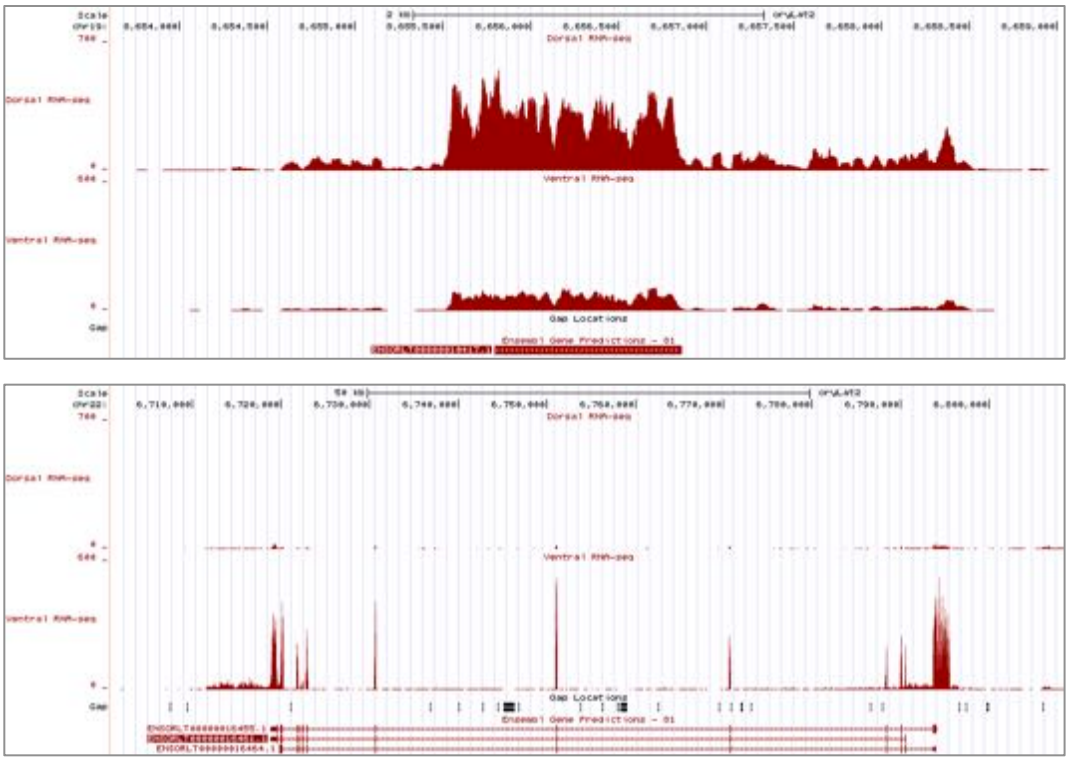

Figure 44. (Continued.)

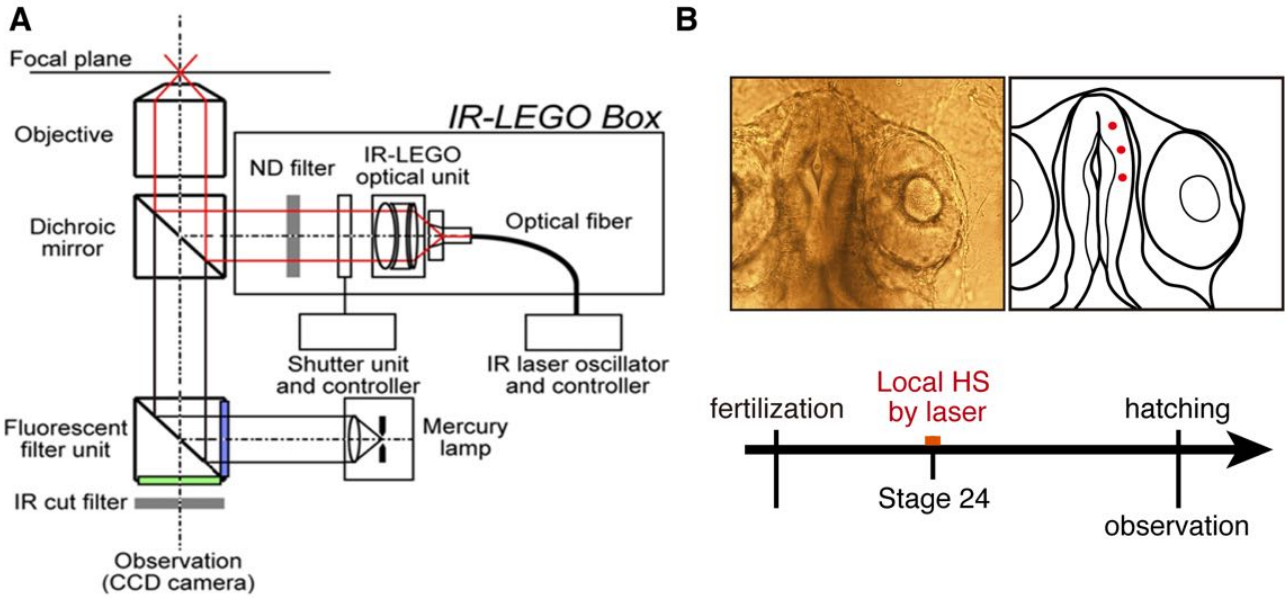

Figure 45. Spatial distribution of neural progenitor cell linage originating from a few neural stem cells in the telencephalon.
(A) Schematic diagram of infrared laser-evoked gene operator (IR-LEGO) microscope system. An IR laser beam (1480 nm) was introduced into the IR-LEGO optical unit through an optical fiber. Irradiation duration was controlled by a shutter unit. CCD, charge-coupled device; ND, neutral density. (B) Red dots indicate the point of infrared-laser irradiation (21.6 mW, 1 sec) at embryonic stage. Local heat shock by laser was performed at Stage 24 and the treated embryos were observed under a stereoscopic fluorescence microscope just after hatching (5 days after irradiation).

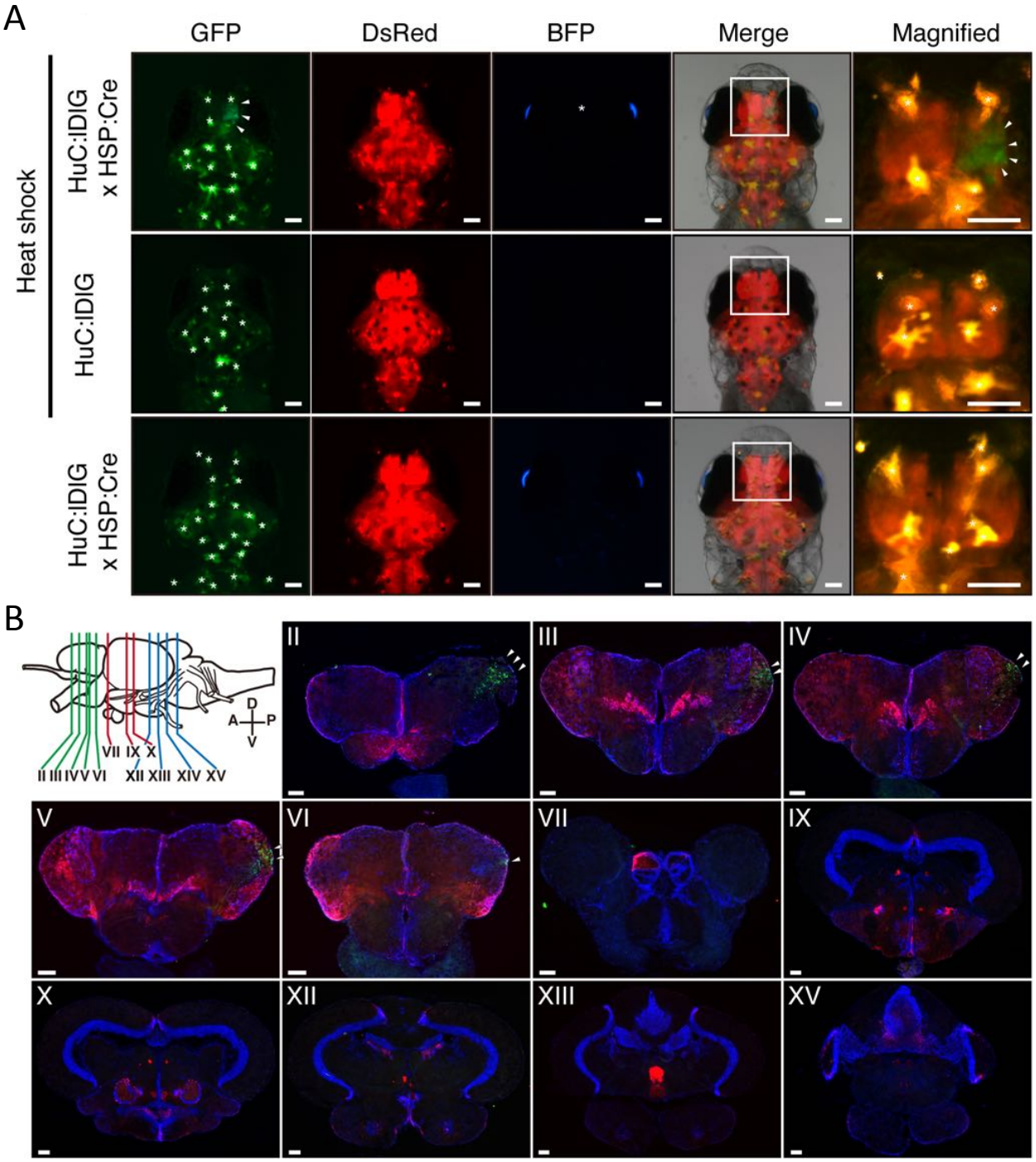

Figure 46 Visualized clonally-related cells by spatially-controlled heat induction. (A) Fluorescence conversion from DsRed to GFP by IR-LEGO induced Cre in juvenile brain. The images show heat-treated *HuC*-loxP-*DsRed*-loxP-*GFP*/*HSP:Cre*/*Crs:BFP* (upper arrowheads), heat-treated *HuC*:loxP-*DsRed*-loxP-*GFP* (middle), and non-treated *HuC*-loxP-*DsRed*-loxP-*GFP*/*HSP:Cre*/*Crs:BFP* (lower). A magnified view of the telencephalon (white box) shows the spatial compartmentalization of GFP-positive neurons originating from Cre/induced neural stem cells. Autofluorescence derived from pigment cells is indicated by asterisks in GFP panels. (B) Cross sectional analysis of GFP expression in the infrared-laser irradiated adult brain. GFP expression was seen only in right side. Scale bars 100 μm.

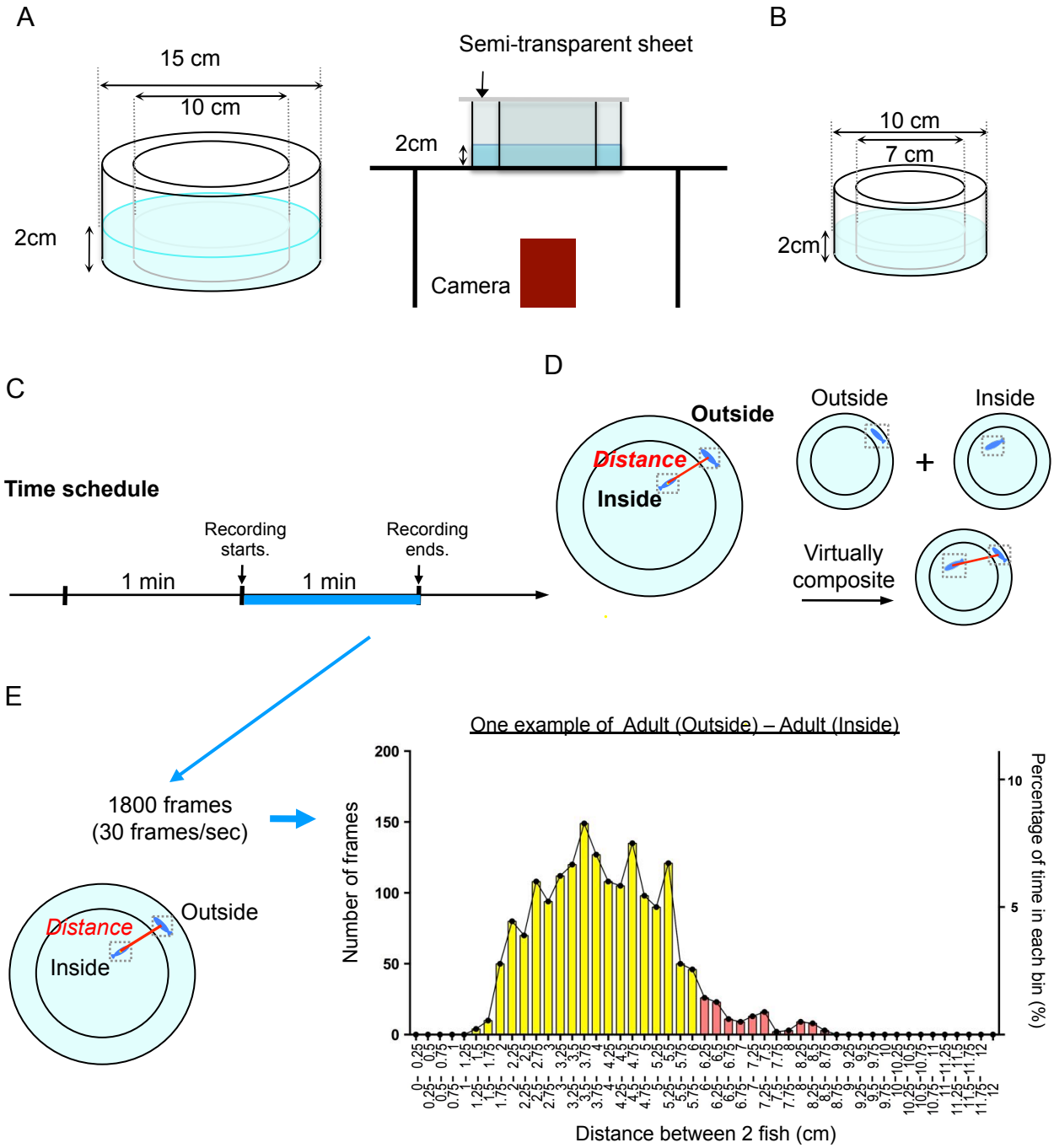

Figure 47. Behavioral system to assess the proximity between two fish.
(A) Behavior recording system. Round water tanks of two different sizes were used depending on fish size. This figure shows tanks for juvenile and adult fish (B) Schematic drawing of the behavioral assay system used for larval medaka fish. (C) Two fish were placed into the water tank, separated into "Outside" and "Inside" parts. The distance between the gravity center of two fish was calculated. For negative controls, a video of only one fish in each part was recorded, and a virtual composite was created from the two videos, each containing only one fish (1 Outside or 1 Inside). (D) Time schedule of the behavioral assay. (E) Calculation method for proximity frequency. A 1-min movie was transformed into 1800 frames of images (30 frames/s). The distance between the centers of the two fish was calculated and histograms of the number of frames with a distance within each bin (2.5-cm width) were made. The right panel shows a representative example of an experiment using two adult female fish. Yellow bars indicate frames in which the distance between two fish was ≤6 cm. Proximity frequency was calculated based on the total number of frames in the yellow bars divided by 1800 multiplied by 100.

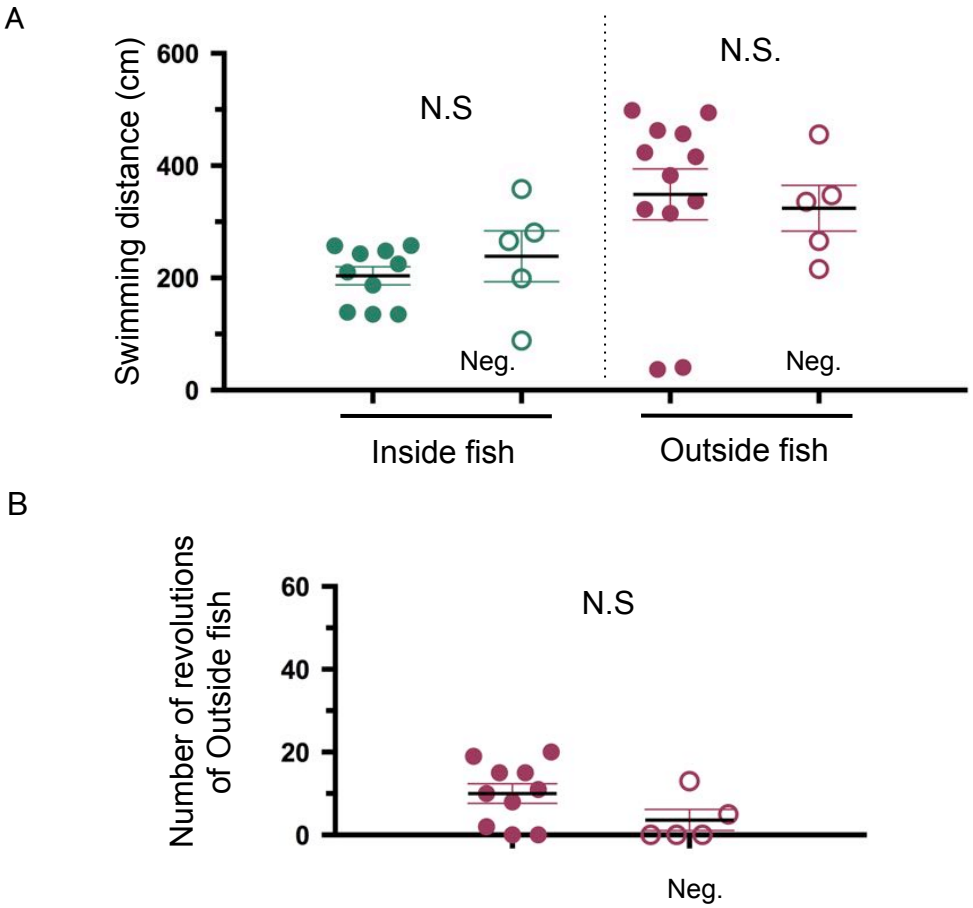

Figure 48. Comparison of the swimming distance and number of direction changes of two adult medaka fish with the negative control.
(A) The swimming distance did not differ significantly between experimental fish and negative control fish for both the Inside fish and Outside fish. Mann-Whitney U test. (B) The number of direction changes of Outside fish did not differ significantly between experimental fish and negative control fish. Mann-Whitney U test.

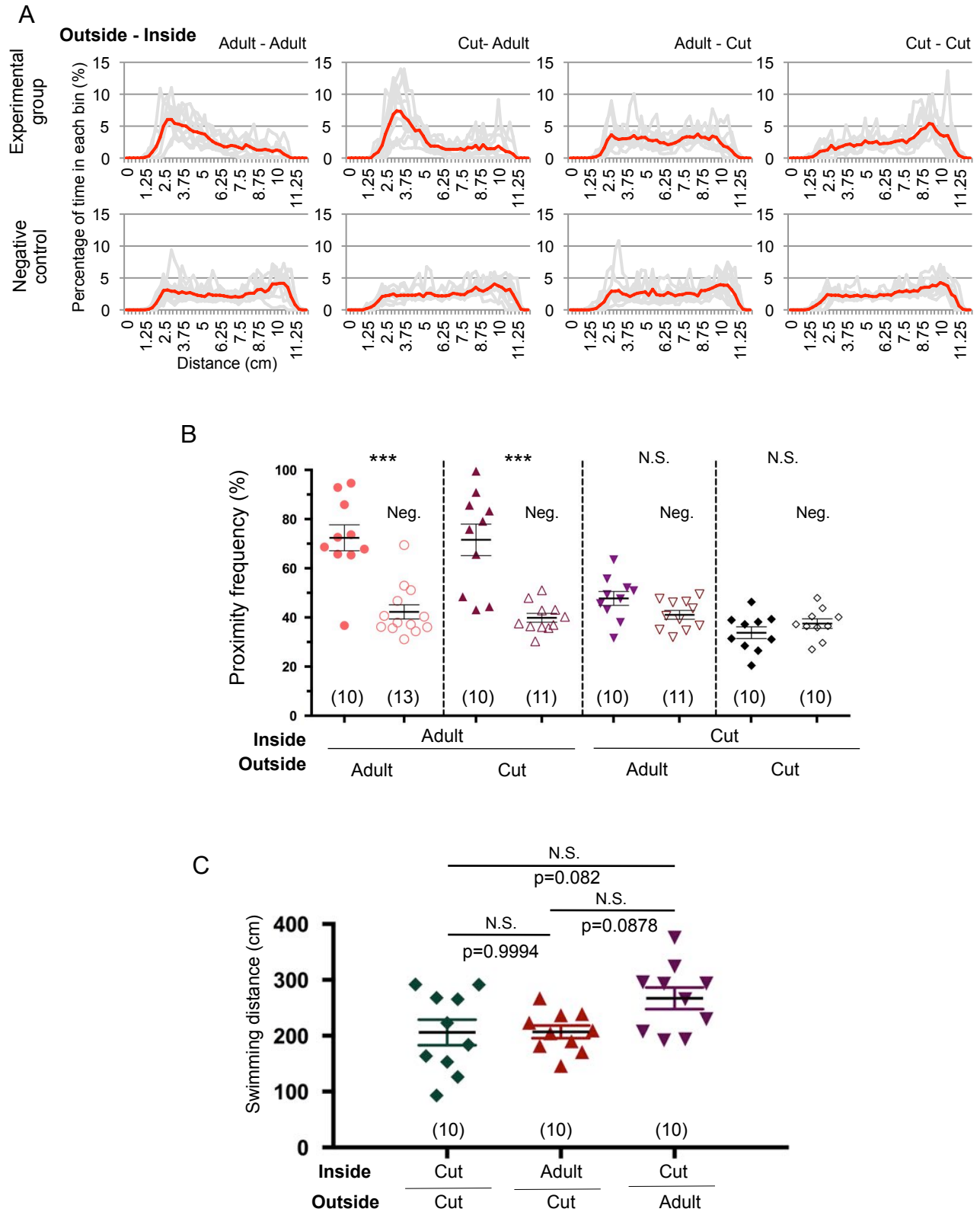

Figure 49. Quantification of proximity in this behavioral paradigm.
(A) Histograms of the percentage of time in each bin between two fish. “Cut” indicates fish with its optic nerves cut. Gray line indicates the value of the percentage of time in each bin in the individual test. Red line indicates the mean value of the percentage of time in each bin. (B) Proximity frequency was calculated in tests using two normal female fish (Mann-Whitney U=12, p=0.0005, sig≤0.05, 2-tailed), one Inside and a “Cut” fish on the Outside (Mann-Whitney U=5.5, p=0.0001, sig≤0.05, 2-tailed), a normal fish on the Outside and a “Cut” fish Inside (Mann-Whitney U=30, p=0.0841, sig≤0.05, 2-tailed), and two “Cut fish”, one Inside and one Outside (Mann-Whitney U=37.50, p=0.3630, sig≤0.05, 2-tailed). Closed symbols indicate data of the experimental group and open symbols indicate data of the negative control. Numbers at the bottom of the graph indicate the trial number. Mann-Whitney U test: ***P<0.001. Mean ± SEM. (C) The swimming distance of Outside fish was calculated in tests using same conditions as (B). Numbers at the bottom of the graph indicate the trial number. No significant difference in the swimming distance was detected. One-way ANOVA: Scheffé’s post-hoc. Mean ± SEM.

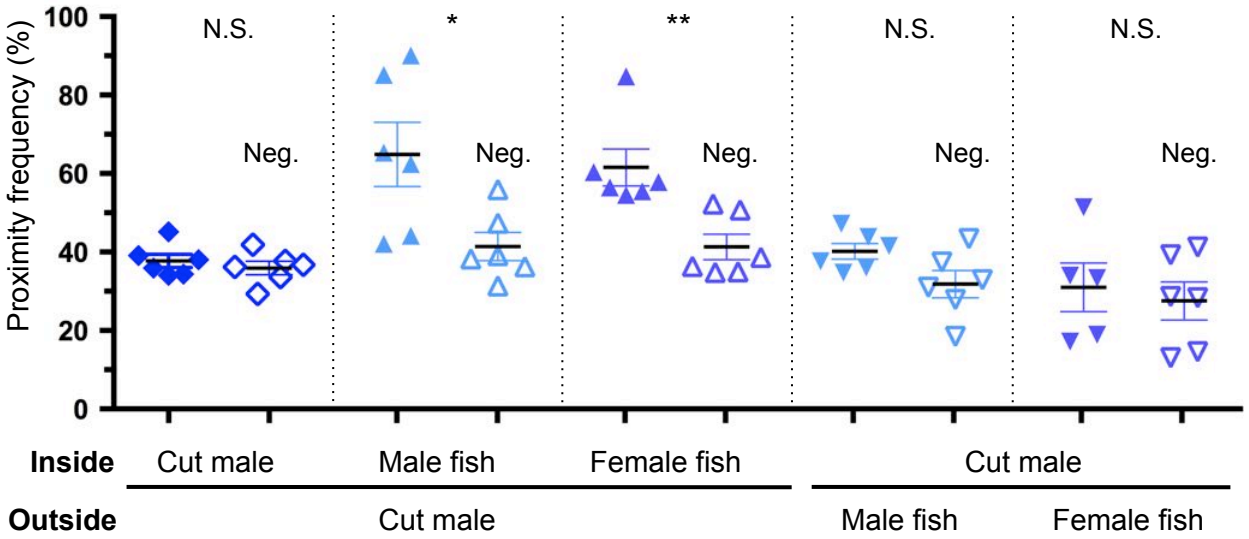

Figure 50. Comparison of the proximity frequency using male Cut fish.
Proximity frequency was calculated in tests using two male "Cut fish" (Mann-Whitney U=14, p=0.5714, 2-tailed), one normal male fish on the Inside and a male "Cut fish" on the Outside (Mann-Whitney U=4, p=0.026, sig≤0.05, 2-tailed), a normal female fish on the Inside and a male "Cut fish" on the Outside (Mann-Whitney U=0, p=0.0022, sig≤0.05, 2-tailed), one normal male fish on the Outside and a male "Cut fish" on the Inside (Mann-Whitney U=6, p=0.0649, 2-tailed), and one normal female fish on the Outside and a male "Cut fish" on the Inside (Mann-Whitney U=12, p=0.6494, 2-tailed). Closed symbols indicate data of the experimental group and open symbols indicate data of the negative control. Mann-Whitney U test: *P<0.05, **P<0.01. Mean ± SEM.

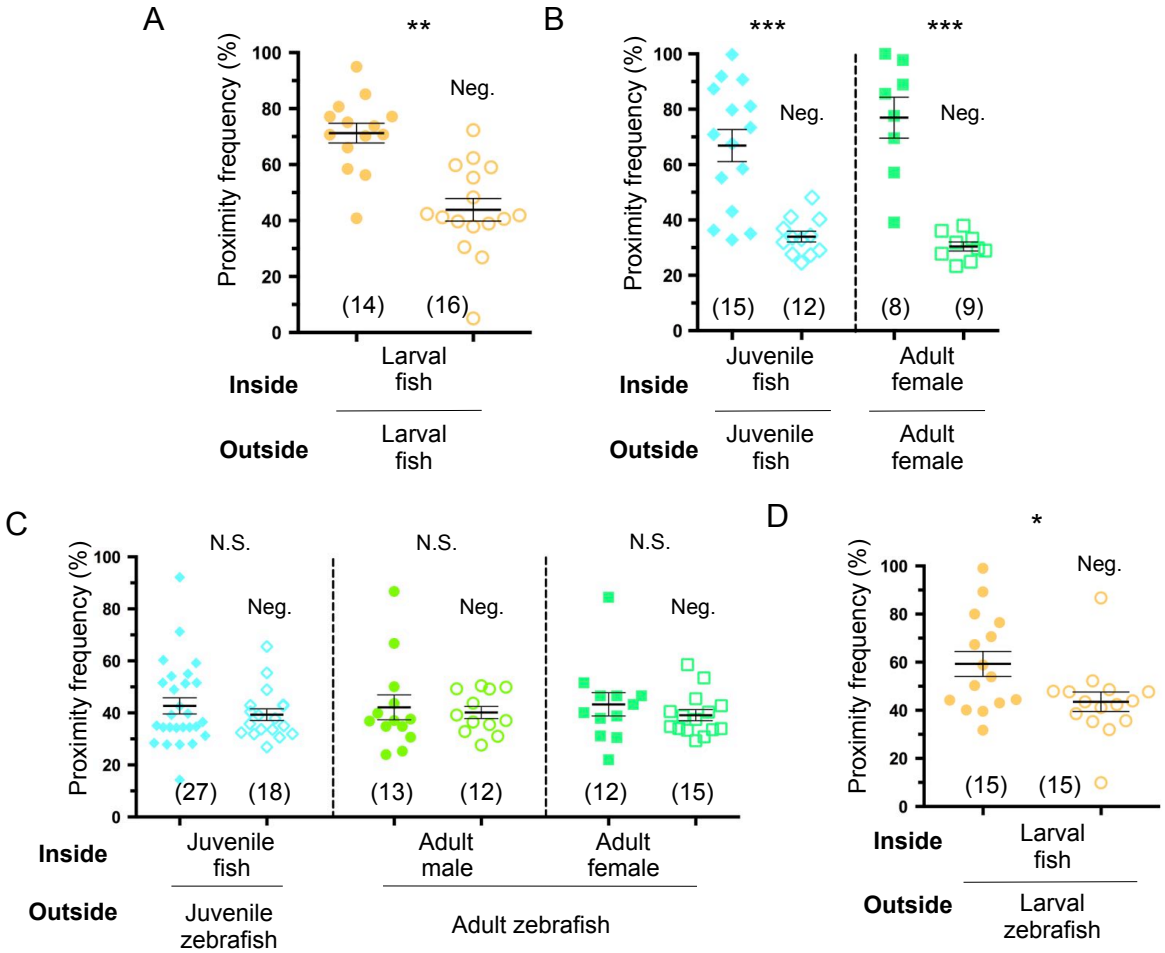

Figure 51. Change in the proximity to conspecifics/heterospecifics during growth.
(A) Procedure of behavioral experiments with familiar/unfamiliar fish. The left panel shows the procedure of the “before mating test” and the right panel shows the procedure of the “after mating test”. (B) The upper panels show the proximity frequencies of focal female fish with the familiar or unfamiliar males. The lower panels show focal male fish. The left and right panels show the proximity frequencies before and after mating, respectively. Wilcoxon signed-rank test: *P<0.05. Mean ± SEM.

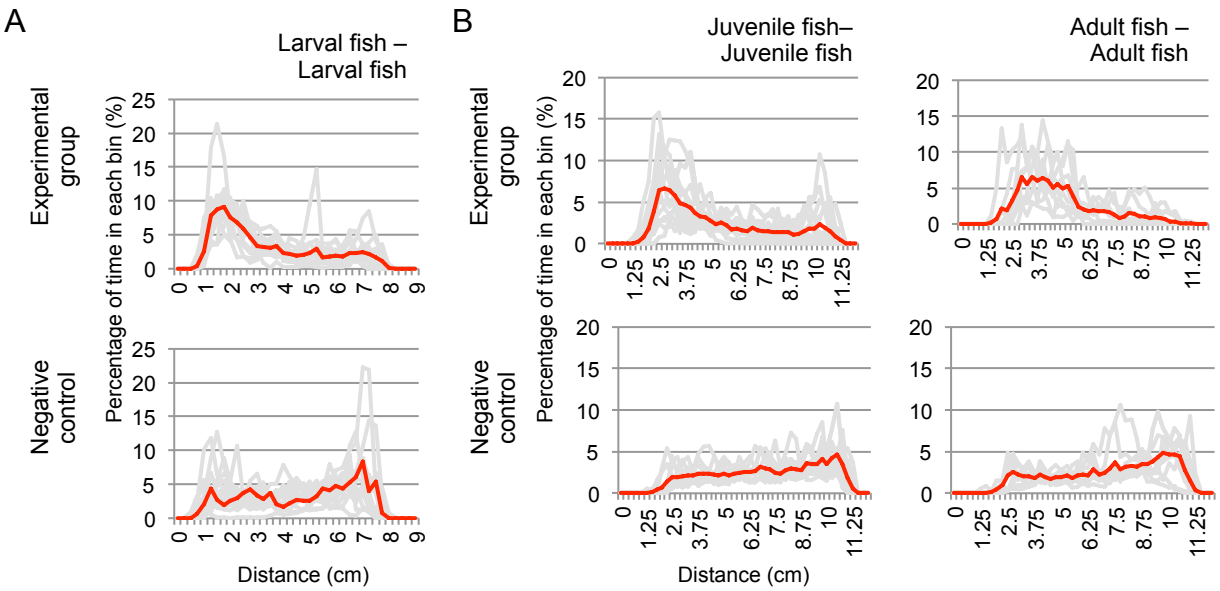

Outside		Inside	U	p
medaka fish	larval	larval	21	<0.0001
	juvenile	juvenile	16	<0.0001
	adult	adult	0	<0.0001

Figure 52. Histograms of the percentage of time in each bin between two medaka fish.
(A) Histograms of the percentage of time in each bin between two larval medaka fish. Assays were performed using smaller tanks (Figure. 3A). (B) Histograms of the percentage of time in each bin between two juvenile medaka fish and adult medaka fish. Only female fish were used in these experiments. Red lines indicate the mean value of the percentage of time in each bin. The table at the bottom of the figure shows the statistical results of experiments in Figure. 3. Mann-Whitney U test: *P<0.05, **P<0.01, ***P<0.001. Mean ± SEM.

A

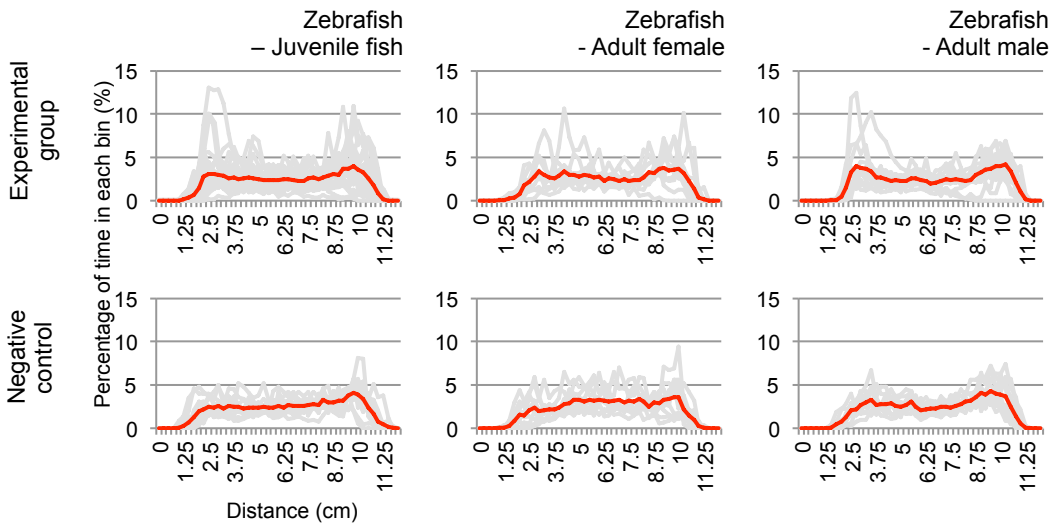

B

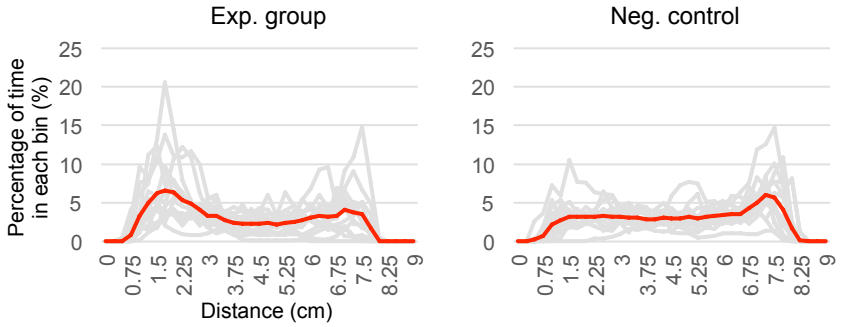

Outside		Inside	U	p
zebrafish	larval	larval	62	0.0357
	juvenile	juvenile	221	0.6177
	adult	adult male	72.5	0.779
		adult female	73	0.4198

Figure 53. Histograms of the percentage of time in each bin between medaka fish and zebrafish. (A) Histograms of the percentage of time in each bin between larval medaka fish and same-size zebrafish. Assays were performed using smaller tanks (Figure. 3A). (B) Histograms of the percentage of time in each bin between two juvenile medaka fish and adult medaka fish. Red lines indicate the mean value of the distance frequency. The table at the bottom of the figure shows the statistical results of experiments in Figure. 3. Mann-Whitney U test: *P<0.05, **P<0.01, ***P<0.001. Mean ± SEM.

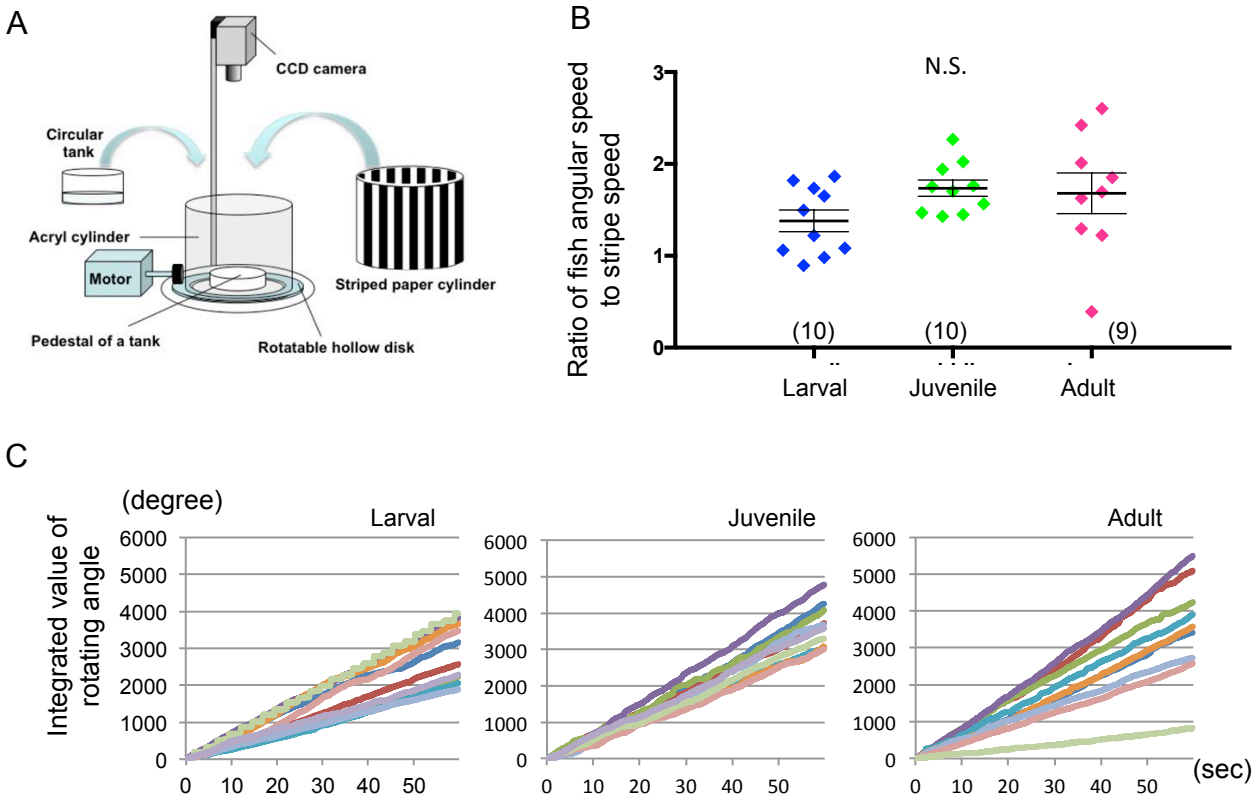

Figure 54. Optomotor response of larval, juvenile, and adult medaka fish.
(A) Behavioral equipment for optomotor response [16]. (B) Integrated angular velocity during 60 s of medaka fish in 3 different growth stages. (C) Ratio of the mean fish angular speed to the stripe speed. The optomotor response did not differ significantly among the three growth stages (one-way ANOVA: Scheffe's post hoc test; F=0.3499, p=0.70663). Numbers at the bottom of the graph indicate the trial number.

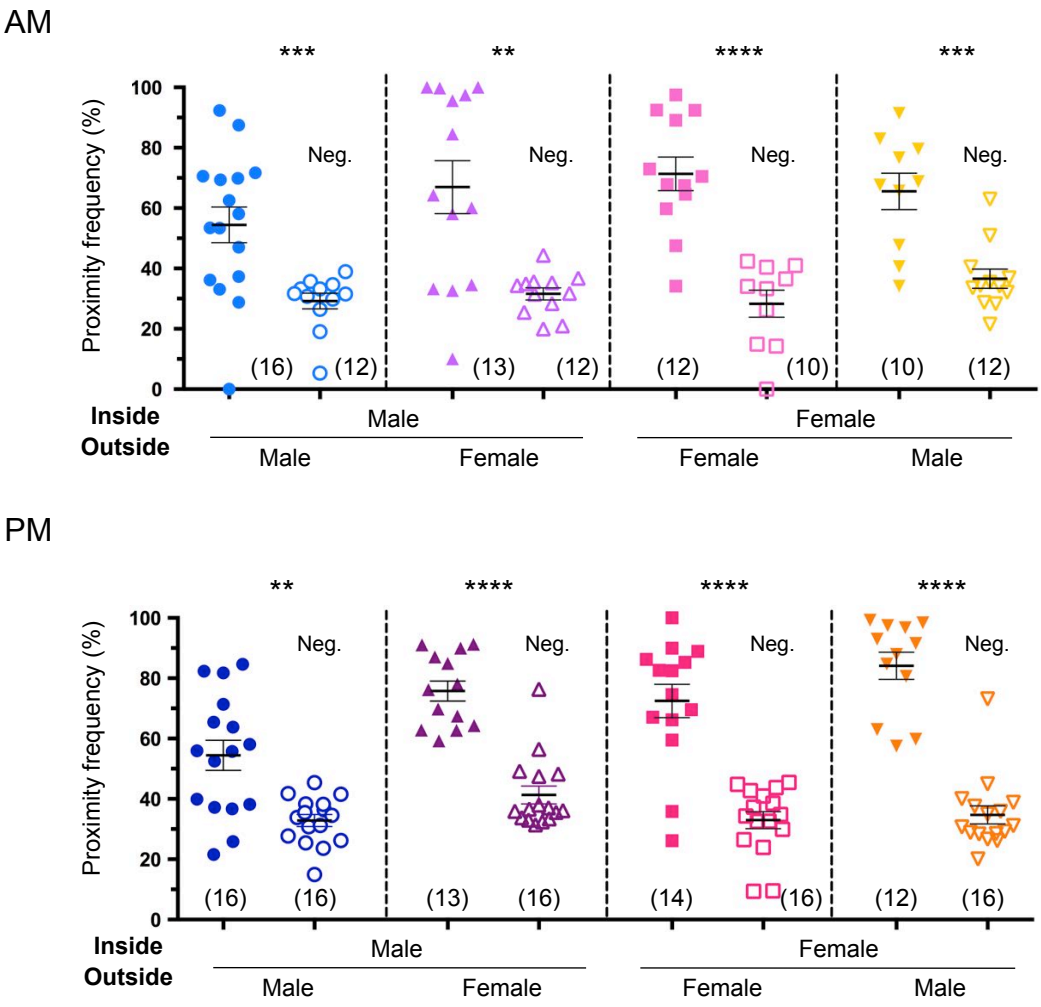

Figure 55. Sexual differences in proximity to conspecifics.
A significant increase in the proximity frequency was detected for all combinations of interactions in the morning. Also, a significant increase in the proximity frequency was detected for all combinations of interactions in the afternoon. The statistical results are shown in the table at the bottom of Sup. fig. 5. In the afternoon, proximity frequency in the test using two male fish tended to be lower. Numbers at the bottom of the graph indicate the trial number. Mann-Whitney U test: **P<0.01, ***P<0.001, ****P<0.0001. Mean ± SEM.

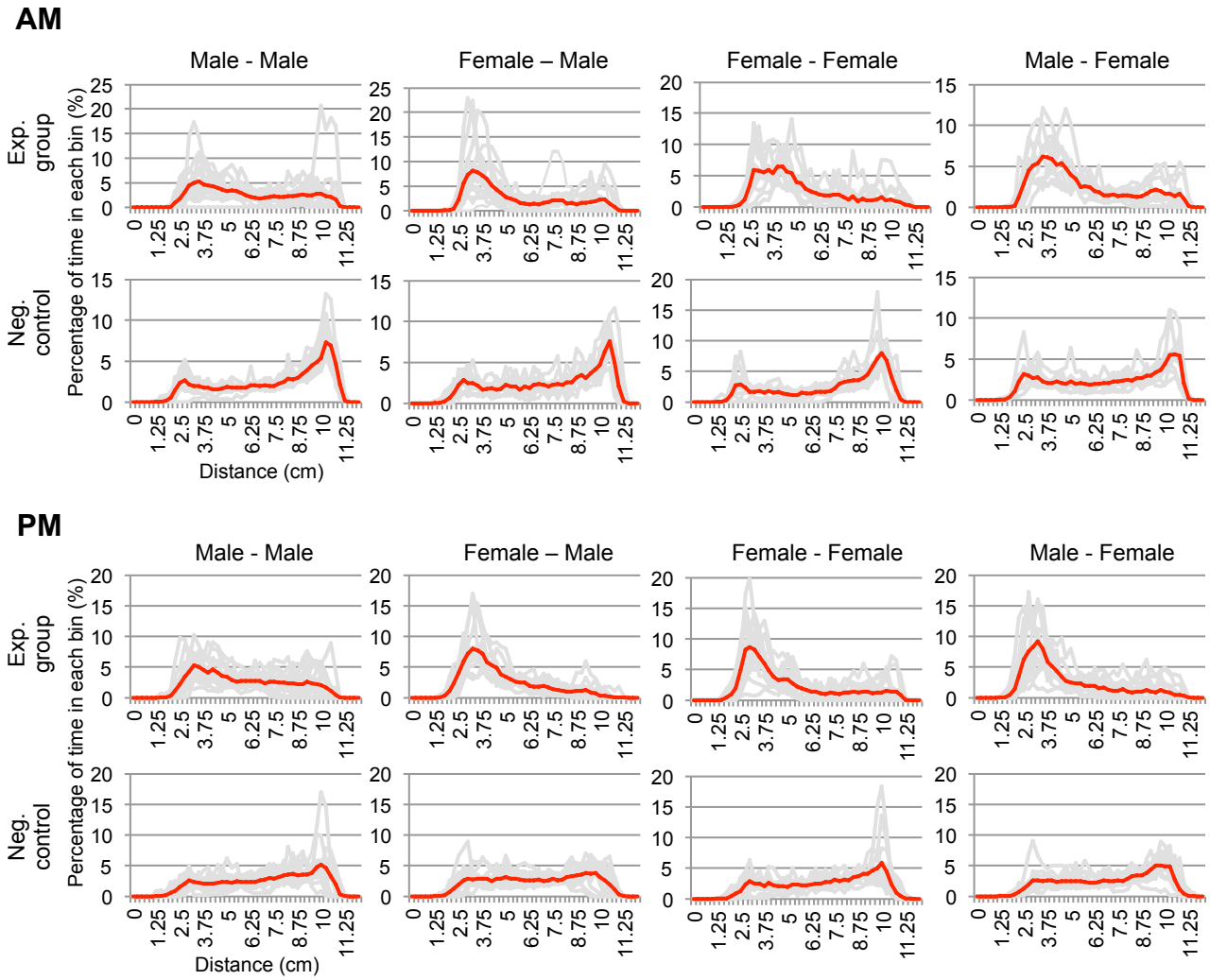

	Outside	Inside	U	p
AM	Male	Male	28	0.001
	Female		29	0.0065
	Female	Female	4	<0.0001
	Male		10.5	0.0005
PM	Male	Male	46	0.0014
	Female		7	<0.0001
	Female	Female	20	<0.0001
	Male		3.5	<0.0001

Figure 56. Histograms of the percentage of time in each bin between two adult medaka fish (intrasexual and intersexual relationship).
The upper panel shows the histograms of the percentage of time in each bin between two medaka fish evaluated in the morning (AM10~12). The lower panel shows the histograms of the percentage of time in each bin between two medaka fish evaluated in the afternoon (PM17~19). Red lines indicate the mean percentage of time in each bin. The table at the bottom of the figure shows the statistical results of experiments in Figure. 4. Mann-Whitney U test: *P<0.05, **P<0.01, ***P<0.001.

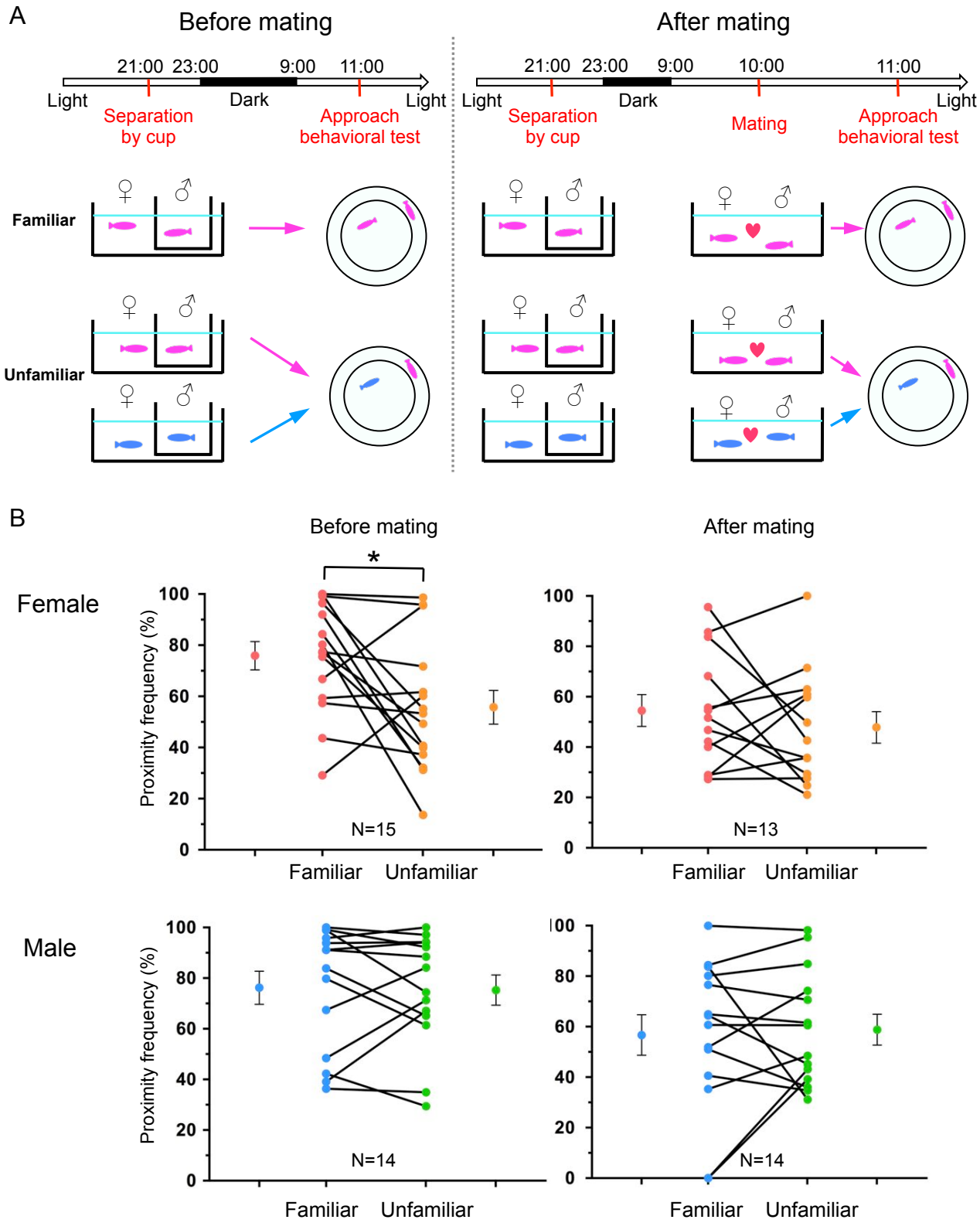

Figure 57. Effects of spawning and social familiarity on proximity to the opposite sex.
(A) Procedure of behavioral experiments with familiar/unfamiliar fish. The left panel shows the procedure of the "before mating test" and the right panel shows the procedure of the "after mating test". (B) The upper panels show the proximity frequencies of focal female fish with the familiar or unfamiliar males. The lower panels show focal male fish. The left and right panels show the proximity frequencies before and after mating, respectively. The proximity frequency with familiar males from females was significantly higher than that with unfamiliar males before mating (Wilcoxon matched-pairs signed rank test, p=0.0181, sig≤0.05, 2-tailed), but not after mating (Wilcoxon matched-pairs signed rank test, p=0.4548, 2-tailed). The proximity frequency of males with familiar females did not differ significantly from that of males with unfamiliar females before mating (Wilcoxon matched-pairs signed rank test, p=0.7609, 2-tailed) and after mating (Wilcoxon matched-pairs signed rank test, p=0.9032, 2-tailed). Therefore, mating and familiarization conditions did not affect the proximity of males to females. Wilcoxon signed-rank test: *P<0.05. Mean ± SEM.

Before mating

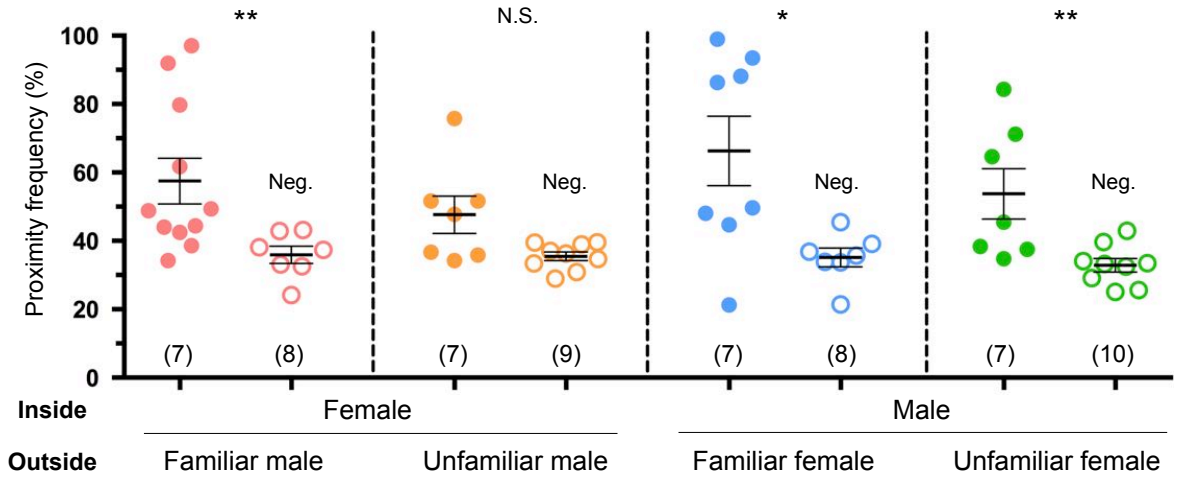

After mating

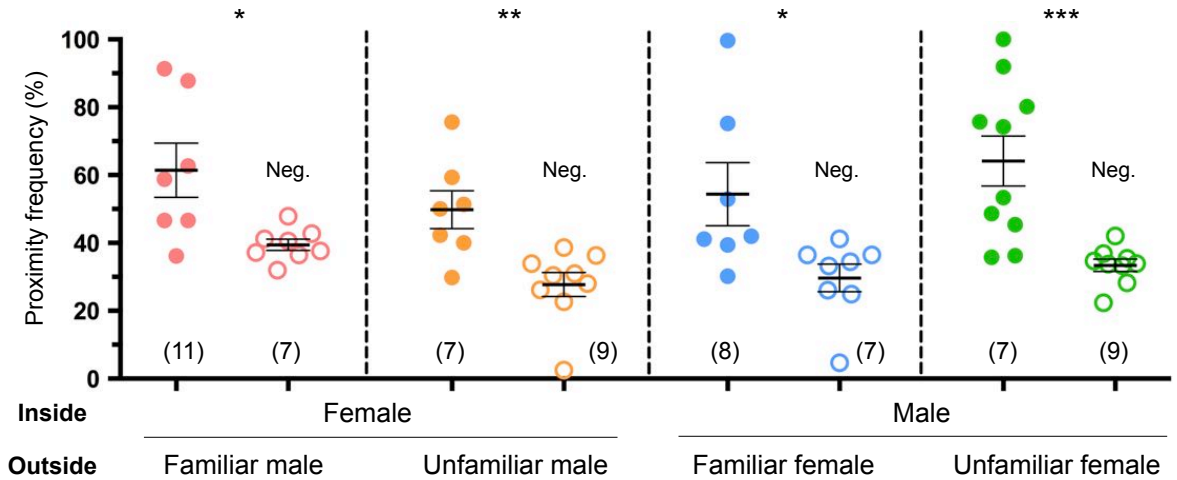

	Outside	Inside		U	p
Before mating	male	female	familiar	8	0.0041
			unfamiliar	15	0.0865
	female	male	familiar	8	0.0205
			unfamiliar	6	0.0052
After mating	male	female	familiar	9	0.0264
			unfamiliar	5	0.0033
	female	male	familiar	7	0.014
			unfamiliar	4	0.0003

Figure 58. Comparison of the proximity frequency toward the opposite sex before/after mating.
The proximity frequency of all of the groups, except that of females toward unfamiliar males, differed significantly from that of the negative control. Numbers at the bottom of the graph indicate the trial number. The table at the bottom of the figure shows the statistical results of this experiment. Mann-Whitney U test: *P<0.05, **P<0.01, ***P<0.001. Mean ± SEM.

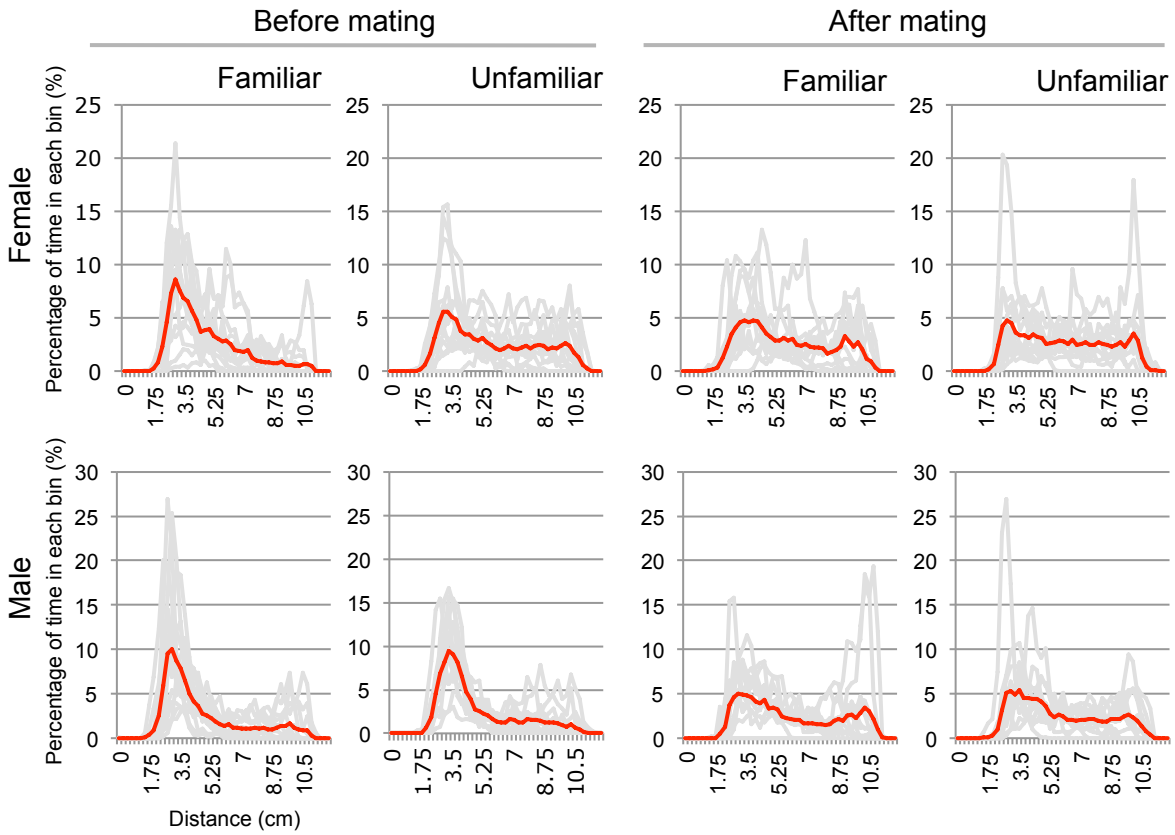

Figure 59. Histograms of the percentage of time in each bin between two adult medaka fish in the morning toward familiar/unfamiliar individuals.
The histogram of the percentage of time in each bin between male and female medaka fish before mating (the left panels) and after mating (the right panels). Red lines indicate the mean value of the percentage of time in each bin.

Contribution

Chapter 1

I conceived and designed the experiments. The *p53* mutant was generated by Dr. Taniguchi. I performed all experiments and analyzed the data.

Chapter 2

The Tg (HuC:loxP-DsRed-loxP-GFP) line was generated by Dr. Okuyama and Mr. Hoki. The Tg (HSP:Cre) line was generated by Dr. Shimizu. The Cre mRNA microinjection was performed by Mr. Yamagishi. I performed the brain dissection and identified the compartmentalized GFP-positive structures. I characterized the Tg (HuC:loxP-DsRed-loxP-GFP) line, and performed the immunohistochemistry, heat-shock experiments, and analysis of the Cre/loxP recombination samples.

Chapter 3

I conceived and designed the experiments. I performed all the experiments, sample preparation, signal detection, signal registration, and clonal analysis.

Chapter 4

Dr. Nakamura and I conceived and designed the experiments. I performed the sample preparation for the ATAC-seq and RNA-seq, the DAVID analysis of ATAC-seq, the library preparation for RNA-seq, and the analysis of the RNA-seq data. Dr. Nakamura performed the library preparation for ATAC-seq and sequencing data mapping.

Chapter 5

Dr. Kamei generated the infrared laser system. Dr. Okuyama and I performed the laser treatment to activate the heat shock. I performed the brain dissection and signal analysis.

Chapter 6

Ms. Konagaya, Ms. Yokoi, and I conceived and designed the experiments. I performed all of the experiments and analyzed all of the data.

References

Adhikari A, Lerner TN, Finkelstein J, Pak S, Jennings JH, Davidson TJ, Ferenczi E, Gunaydin LA, Mirzabekov JJ, Ye L, Kim SY, Lei A, Deisseroth K. Basomedial amygdala mediates top-down control of anxiety and fear. *Nature*. 2015 Nov 12;527(7577):179-85.

Agetsuma M, Aizawa H, Aoki T, Nakayama R, Takahoko M, et al. (2010) The habenula is crucial for experience-dependent modification of fear responses in zebrafish. *Nat Neurosci* 13: 1354-1356.

Anken R, Bourrat F. Brain atlas of the medakafish, *Oryzias latipes*, INRA, Paris, 1998.

Asakawa K, Suster ML, Mizusawa K, Nagayoshi S, Kotani T, et al. (2008) Genetic dissection of neural circuits by Tol2 transposon-mediated Gal4 gene and enhancer trapping in zebrafish. *Proc Natl Acad Sci U S A* 105: 1255-1260.

Asakawa K, Suster ML, Mizusawa K, Nagayoshi S, Kotani T, Urasaki A, Kishimoto Y, Hibi M, Kawakami K. Genetic dissection of neural circuits by Tol2 transposon-mediated Gal4 gene and enhancer trapping in zebrafish. *Proc Natl Acad Sci U S A*. 2008 Jan 29;105(4):1255-60.

Avale ME, Chabout J, Pons S, Serreau P, De Chaumont F, Olivo-Marin JC, Bourgeois JP, Maskos U, Changeux JP, Granon S. Prefrontal nicotinic receptors control novel social interaction between mice. *FASEB J*. 2011;25:2145–55.

Bachy I, Berthon J, Rétaux S. Defining pallial and subpallial divisions in the developing Xenopus forebrain. *Mech Dev*. 2002 Sep;117(1-2):163-72.

Bajoghli B, Aghaallaei N, Heimbucher T, Czerny T (2004) An artificial promoter construct for heat-inducible misexpression during fish embryogenesis. *Dev Biol* 271: 416-430.

Ball GF, Balthazart J, McCarthy MM. Is it useful to view the brain as a secondary sexual characteristic? *Neurosci Biobehav Rev*. 2014;46:628-38.

Barba-Escobedo PA, Gould GG. Visual social preferences of lone zebrafish in a novel environment: strain and anxiolytic effects. *Genes Brain Behav.* 2012;11:366-73.

Ben-Hur A, Ong CS, Sonnenburg S, Schölkopf B, Rätsch G. Support vector machines and kernels for computational biology. *PLoS Comput Biol.* 2008 Oct;4(10):e1000173.

Bonaguidi MA, Wheeler MA, Shapiro JS, Stadel RP, Sun GJ, Ming GL, Song H. In vivo clonal analysis reveals self-renewing and multipotent adult neural stem cell characteristics. *Cell.* 2011 Jun 24;145(7):1142-55.

Bottjer WS, Arnold AP. The Ontogeny of Vocal Learning in Songbirds. In: Blass E, editor. Developmental Psychobiology and Developmental Neurobiology. Handbook of Behavioral Neurobiology. Volume 8: New York: Springer US; 1986. pp 129-61.

Boyle AP, Davis S, Shulha HP, Meltzer P, Margulies EH, Weng Z, Furey TS, Crawford GE. High-resolution mapping and characterization of open chromatin across the genome. *Cell.* 2008 Jan 25;132(2):311-22.

Branchi I. The mouse communal nest: investigating the epigenetic influences of the early social environment on brain and behavior development. *Neurosci Biobehav Rev.* 2009;33:551-9.

Bridges RS. Neuroendocrine regulation of maternal behavior. *Front Neuroendocrinol.* 2015;36:178-96.

Buenrostro JD, Giresi PG, Zaba LC, Chang HY, Greenleaf WJ. Transposition of native chromatin for fast and sensitive epigenomic profiling of open chromatin, DNA-binding proteins and nucleosome position. *Nat Methods.* 2013 Dec;10(12):1213-8.

Buenrostro JD, Wu B, Chang HY, Greenleaf WJ. ATAC-seq: A Method for Assaying Chromatin Accessibility Genome-Wide. *Curr Protoc Mol Biol.* 2015 Jan 5;109:21.29.1-9.

Burmeister SS, Munshi RG, Fernald RD. Cytoarchitecture of a cichlid fish telencephalon. *Brain Behav Evol*. 2009;74(2):110-20.

Campagne MV, Gill R. Tumor-suppressor p53 is expressed in proliferating and newly formed neurons of the embryonic and postnatal rat brain: Comparison with expression of the cell cycle regulators p21(Waf1/Cip1), p27(Kip1), p57(Kip2), p16(Ink4a), cyclin G1, and the proto-oncogene Bax. *J. Comp. Neurol.* 397 (1998) 181-198.

Campbell P, Pasch B, Warren AL, Phelps SM. Vocal ontogeny in neotropical singing mice (*Scotinomys*). *PLoS One.* 2014;9:e113628.

Carvalho PSM, Noltie DB, Tillitt DE. Ontogenetic improvement of visual function in the medaka *Oryzias latipes* based on an optomotor testing system for larval and adult fish. *Anim Behav.* 2002;64:1–10.

Cerri S, Piccolini VM, Bernocchi G. Postnatal development of the central nervous system: anomalies in the formation of cerebellum fissures. *Anat Rec (Hoboken)*. 2010 Mar;293(3):492-501.

Chapouton P, Jagasia R, Bally-Cuif L (2007) Adult neurogenesis in non-mammalian vertebrates. *Bioessays* 29: 745-757.

Cheal M. Social olfaction: a review of the ontogeny of olfactory influences on vertebrate behavior. *Behav Biol.* 1975;15:1-25.

Clark PJ, Bhattacharya TK, Miller DS, Kohman RA, DeYoung EK, Rhodes JS. New neurons generated from running are broadly recruited into neuronal activation

associated with three different hippocampus-involved tasks. *Hippocampus*. 2012 Sep;22(9):1860-7.

Cobos I, Puelles L, Martínez S. The avian telencephalic subpallium originates inhibitory neurons that invade tangentially the pallium (dorsal ventricular ridge and cortical areas). *Dev Biol*. 2001 Nov 1;239(1):30-45.

Cohen DH, Duff TA, Ebbesson SO. Electrophysiological identification of a visual area in shark telencephalon. *Science*. 1973 Nov 2;182(4111):492-4.

Croft DP, Hamilton PB, Darden SK, Jacoby DM, James R, Bettaney EM et al.. The role of relatedness in structuring the social network of a wild guppy population. *Oecologia*. 2012;170:955-63.

Cummings DM, Snyder JS, Brewer M, Cameron HA, Belluscio L. (2014) Adult neurogenesis is necessary to refine and maintain circuit specificity. *J Neurosci*. 2014 Oct 8;34(41):13801-10.

Danilova N, Sakamoto KM, Lin S. p53 family in development. *Mech. Dev.* 125 (2008) 919-931.

Davie K, Jacobs J, Atkins M, Potier D, Christiaens V, Halder G, Aerts S. Discovery of transcription factors and regulatory regions driving in vivo tumor development by ATAC-seq and FAIRE-seq open chromatin profiling. *PLoS Genet.* 2015 Feb 13;11(2):e1004994.

de Kort SR, Eldermire ER, Cramer ER, Vehrencamp SL. The deterrent effect of bird song in territory defense. *Behav Ecol.* 2009;20:200-6.

Deguchi T, Itoh M, Urawa H, Matsumoto T, Nakayama S, et al. (2009) Infrared laser-mediated local gene induction in medaka, zebrafish and Arabidopsis thaliana. *Dev Growth Differ* 51: 769-775.

Dirian L, Galant S, Coolen M, Chen W, Bedu S, Houart C, Bally-Cuif L, Foucher I. Spatial regionalization and heterochrony in the formation of adult pallial neural stem cells. *Dev Cell*. 2014 Jul 28;30(2):123-36.

Dobbing J, Sands J. Quantitative growth and development of human brain. *Arch Dis Child*. 1973 Oct;48(10):757-67.

Ekstrom P, Johnsson CM, Ohlin LM. Ventricular proliferation zones in the brain of an adult teleost fish and their relation to neuromeres and migration (secondary matrix) zones. *J. Comp. Neurol.* 436 (2001) 92-110.

Engeszer RE, Barbiano LA, Ryan MJ, Parichy DM. Timing and plasticity of shoaling behaviour in the zebrafish, *Danio rerio*. *Anim Behav*. 2007;74:1269-75.

Enter D, Colzato LS, Roelofs K. Dopamine transporter polymorphisms affect social approach-avoidance tendencies. *Genes Brain Behav*. 2012;11:671–76.

Fantz RL. Pattern Vision in Newborn Infants. *Science.* 1963;140:296-7.

Farronia T, Johnson MH, Brockbank M, Simiona F. Infants' use of gaze direction to cue attention: The importance of perceived motion. *Visual Cog.* 2000;doi: 10.1080/13506280050144399.

Fletcher RB, Prasol MS, Estrada J, Baudhuin A, Vranizan K, Choi YG, Ngai J. p63 regulates olfactory stem cell self-renewal and differentiation. *Neuron* 72 (2011) 748-759.

Fletez-Brant C, Lee D, McCallion AS, Beer MA. kmer-SVM: a web server for identifying predictive regulatory sequence features in genomic data sets. *Nucleic Acids Res.* 2013 Jul;41(Web Server issue):W544-56.

Fowler CD, Liu Y, Ouimet C, Wang Z. The effects of social environment on adult

neurogenesis in the female prairie vole. *J Neurobiol.* 2002 May;51(2):115-28.
Fox DT, Morris LX, Nystul T, Spradling AC (2008) Lineage analysis of stem cells. StemBook. Cambridge (MA).

Frankland PW, Bontempi B. The organization of recent and remote memories. *Nat Rev Neurosci.* 2005 Feb;6(2):119-30.

Ganz J, Kaslin J, Freudenreich D, Machate A, Geffarth M, Brand M. Subdivisions of the adult zebrafish subpallium by molecular marker analysis. *J Comp Neurol.* 2012 Feb 15;520(3):633-55.

Ganz J, Kroehne V, Freudenreich D, Machate A, Geffarth M, Braasch I, Kaslin J, Brand M. Subdivisions of the adult zebrafish pallium based on molecular marker analysis. *F1000Res.* 2014 Dec 17;3:308.

Gao P, Sultan KT, Zhang XJ, Shi SH. Lineage-dependent circuit assembly in the neocortex. *Development.* 2013 Jul;140(13):2645-55.

Gelman DM, Martini FJ, Nóbrega-Pereira S, Pierani A, Kessaris N, Marín O. The embryonic preoptic area is a novel source of cortical GABAergic interneurons. *J Neurosci.* 2009 Jul 22;29(29):9380-9. doi: 10.1523/JNEUROSCI.0604-09.2009.

Gil-Perotin S, Haines JD, Kaur J, Marin-Husstege M, Spinetta MJ, Kim KH, Duran-Moreno M, Schallert T, Zindy F, Roussel MF, Garcia-Verdugo JM, Casaccia P. Roles of p53 and p27(Kip1) in the regulation of neurogenesis in the murine adult subventricular zone. *Eur. J. Neurosci.* 34 (2011) 1040-1052.

Gil-Perotin S, Marin-Husstege M, Li J, Soriano-Navarro M, Zindy F, Roussel MF, Garcia-Verdugo JM, Casaccia-Bonnefil P. Loss of p53 induces changes in the behavior of subventricular zone cells: implication for the genesis of glial tumors. *J. Neurosci.* 26 (2006) 1107-1116.

Giresi PG, Lieb JD. Isolation of active regulatory elements from eukaryotic chromatin using FAIRE (Formaldehyde Assisted Isolation of Regulatory Elements). *Methods* 48, 233–239 (2009).

Good PJ (1995) A conserved family of elav-like genes in vertebrates. *Proc Natl Acad Sci U S A* 92: 4557-4561.

Grandel H, Kaslin J, Ganz J, Wenzel I, Brand M (2006) Neural stem cells and neurogenesis in the adult zebrafish brain: origin, proliferation dynamics, migration and cell fate. *Dev Biol* 295: 263-277.

Green J, Collins C, Kyzar EJ, Pham M, Roth A, Gaikwad S et al.. Automated high-throughput neurophenotyping of zebrafish social behavior. *J Neurosci Methods*. 2012;210:266-71.

Gunaydin LA, Deisseroth K. Dopaminergic Dynamics Contributing to Social Behavior. Cold Spring Harb Symp Quant Biol. 2014;79:221-7.

Hall WG, Oppenheim RW. Developmental psychobiology: prenatal, perinatal, and early postnatal aspects of behavioral development. 1987.*Annu Rev Psychol.* 38:91-128.

Hama H, Kurokawa H, Kawano H, Ando R, Shimogori T, Noda H, Fukami K, Sakaue-Sawano A, Miyawaki A. Scale: a chemical approach for fluorescence imaging and reconstruction of transparent mouse brain. *Nat Neurosci.* 2011 Aug 30;14(11):1481-8.

Harvey-Girard E, Giassi AC, Ellis W, et al.: Organization of the gymnotiform fish pallium in relation to learning and memory: IV. Expression of conserved transcription factors and implications for the evolution of dorsal telencephalon. *J Comp Neurol.* 2012; 520(15): 3395–3413.

Harwell CC, Fuentealba LC, Gonzalez-Cerrillo A, Parker PR, Gertz CC, Mazzola E,

Garcia MT, Alvarez-Buylla A, Cepko CL, Kriegstein AR. Wide Dispersion and Diversity of Clonally Related Inhibitory Interneurons. *Neuron.* 2015 Aug 19. pii: S0896-6273(15)00672-8.

Higashijima S, Schaefer M, Fetcho JR. Neurotransmitter properties of spinal interneurons in embryonic and larval zebrafish. *J Comp Neurol.* 2004;480:19-37.

Hinman MN, Lou H (2008) Diverse molecular functions of Hu proteins. *Cell Mol Life Sci* 65: 3168-3181.

Hiratani I, Mochizuki T, Tochimoto N, Taira M (2001) Functional domains of the LIM homeodomain protein Xlim-1 involved in negative regulation, transactivation, and axis formation in Xenopus embryos. *Dev Biol* 229: 456-467.

Hong W, Kim DW, Anderson DJ. (2014) Antagonistic Control of Social versus Repetitive Self-Grooming Behaviors by Separable Amygdala Neuronal Subsets. *Cell,* 158 (6). pp. 1348-1361.

Huang da W, Sherman BT, Lempicki RA. Systematic and integrative analysis of large gene lists using DAVID bioinformatics resources. *Nat Protoc.* 2009;4(1):44-57.

Huang X, Litingtung Y, Chiang C.. Region-specific requirement for cholesterol modification of sonic hedgehog in patterning the telencephalon and spinal cord. *Development* 2007 134: 2095-2105.

Ichikawa T, Nakazato K, Keller PJ, Kajiura-Kobayashi H, Stelzer EH, Mochizuki A, Nonaka S. Live imaging of whole mouse embryos during gastrulation: migration analyses of epiblast and mesodermal cells. *PLoS One*. 2013 Jul 8;8(7):e64506.

Imada H, Hoki M, Suehiro Y, Okuyama T, Kurabayashi D, Shimada A et al.. Coordinated and cohesive movement of two small conspecific fish induced by eliciting a simultaneous optomotor response. *PLoS One.* 2010;5:e11248.

Imayoshi I, Sakamoto M, Ohtsuka T, Takao K, Miyakawa T, Yamaguchi M, Mori K, Ikeda T, Itohara S, Kageyama R. Roles of continuous neurogenesis in the structural and functional integrity of the adult forebrain. *Nat Neurosci.* 2008 Oct;11(10):1153-61.
Inokuchi K. Adult neurogenesis and modulation of neural circuit function. *Curr Opin Neurobiol*. 2011 Apr;21(2):360-4.

Isoe Y, Okuyama T, Taniguchi Y, Kubo T, Takeuchi H (2012) p53 Mutation suppresses adult neurogenesis in medaka fish (Oryzias latipes). *Biochem Biophys Res Commun* 423: 627-631.

Ito H, Ishikawa Y, Yoshimoto M, Yamamoto N. Diversity of brain morphology in teleosts: brain and ecological niche. *Brain Behav Evol.* 2007;69(2):76-86.
Ito K, Awasaki T (2008) Clonal unit architecture of the adult fly brain. *Adv Exp Med Biol* 628: 137-158.

Ito M, Masuda N, Shinomiya K, Endo K, Ito K. Systematic analysis of neural projections reveals clonal composition of the Drosophila brain. *Curr Biol.* 2013 Apr 22;23(8):644-55.
Jacobs WB, Kaplan DR, Miller FD. The p53 family in nervous system development and disease. *J. Neurochem.* 97 (2006) 1571-1584.

Janak PH, Tye KM. From circuits to behaviour in the amygdala. *Nature.* 2015 Jan 15;517(7534):284-92.

Jarvis ED, Güntürkün O, Bruce L, Csillag A, Karten H, Kuenzel W, et al. Avian Brain Nomenclature Consortium Avian brains and a new understanding of vertebrate brain evolution. *Nat Rev Neurosci*. 2005;6:151–9.

Kagawa N. Comparison of aggressive behaviors between two wild populations of Japanese medaka, *Oryzias latipes* and *O. sakaizumii*. *Zoolog Sci.* 2014;31:116-21.

Kaidanovich-Beilin O, Lipina T, Vukobradovic I, Roder J, Woodgett JR. Assessment of

social interaction behaviors. *J Vis Exp.* 2011;doi: 10.3791/2473.

Kamei Y, Suzuki M, Watanabe K, Fujimori K, Kawasaki T, et al. (2009) Infrared laser-mediated gene induction in targeted single cells in vivo. *Nat Methods* 6: 79-81.

Kandel ER, Schwartz JH. Principles of Neural Science, Fifth Edition (Principles of Neural Science (Kandel)) Oct 26, 2012

Kao CF, Lee T (2012) Generation of Standard Wild-Type MARCM Clones for Analysis of Drosophila Brain Development. *Cold Spring Harb Protoc* 2012.

Karigo T, Kanda S, Takahashi A, Abe H, Okubo K, Oka Y. Time-of-day-dependent changes in GnRH1 neuronal activities and gonadotropin mRNA expression in a daily spawning fish, medaka. *Endocrinology.* 2012;15:3394-404.

Kaslin J, Kroehne V, Benato F, Argenton F, Brand M. Development and specification of cerebellar stem and progenitor cells in zebrafish: from embryo to adult. *Neural Dev.* 2013 May 4;8:9. doi: 10.1186/1749-8104-8-9.

Kawakami K, Abe G, Asada T, Asakawa K, Fukuda R, et al. (2010) zTrap: zebrafish gene trap and enhancer trap database. *BMC Dev Biol* 10: 105.

Ke MT, Fujimoto S, Imai T. SeeDB: a simple and morphology-preserving optical clearing agent for neuronal circuit reconstruction. *Nat Neurosci.* 2013 Aug;16(8):1154-61.

Kempermann G. New neurons for 'survival of the fittest'. *Nat Rev Neurosci*. 2012 Oct;13(10):727-36.

Kim CH, Ueshima E, Muraoka O, Tanaka H, Yeo SY, et al. (1996) Zebrafish elav/HuC homologue as a very early neuronal marker. *Neurosci Lett* 216: 109-112.

Kinoshita M, Murata K, Naruse K, Tanaka M. Medaka: Biology, Management, and

Experimental Protocols. 2009; Wiley-Blackwell.

Kinoshita M, Murata K, Naruse K, Tanaka M. Medaka: Biology, Management, and Experimental Protocols. 2009; doi: 10.1002/9780813818849.

Kitamura T, Inokuchi K. Role of adult neurogenesis in hippocampal-cortical memory consolidation. *Mol Brain*. 2014 Feb 19;7:13.

Kitamura T, Sun C, Martin J, Kitch LJ, Schnitzer MJ, Tonegawa S. Entorhinal Cortical Ocean Cells Encode Specific Contexts and Drive Context-Specific Fear Memory. *Neuron*. 2015 Sep 23;87(6):1317-31.

Kizil C, Kaslin J, Kroehne V, Brand M (2012) Adult neurogenesis and brain regeneration in zebrafish. *Dev Neurobiol* 72: 429-461.

Kobayashi K, Kamei Y, Kinoshita M, Czerny T, Tanaka M (2012) A heat-inducible CRE/LOXP gene induction system in medaka. *Genesis.* 2013 Jan;51(1):59-67

Kuroyanagi Y, Okuyama T, Suehiro Y, Imada H, Shimada A, Naruse K, Takeda H, Kubo T, Takeuchi H. Proliferation zones in adult medaka (Oryzias latipes) brain. *Brain Res.* 1323 (2010) 33-40.

LaBar KS, Cabeza R. Cognitive neuroscience of emotional memory. *Nat Rev Neurosci*. 2006 Jan;7(1):54-64.

Laegdsgaard P, Johnson C. Why do juvenile fish utilise mangrove habitats? *J Exp Mar Bio Ecol.* 2001;257:229-253.

Lara-Astiaso D, Weiner A, Lorenzo-Vivas E, Zaretsky I, Jaitin DA, David E, Keren-Shaul H, Mildner A, Winter D, Jung S, Friedman N, Amit I. Immunogenetics.

Chromatin state dynamics during blood formation. *Science*. 2014 Aug 22;345(6199):943-9.

Lee D, Karchin R, Beer MA. Discriminative prediction of mammalian enhancers from DNA sequence. *Genome Res*. 2011 Dec;21(12):2167-80.

Lee T, Luo L (2001) Mosaic analysis with a repressible cell marker (MARCM) for Drosophila neural development. *Trends Neurosci* 24: 251-254.

Legué E, Riedel E, Joyner AL. Clonal analysis reveals granule cell behaviors and compartmentalization that determine the folded morphology of the cerebellum. *Development*. 2015 May 1;142(9):1661-71. doi: 10.1242/dev.120287. Epub 2015 Apr 1.

Li J, Ghiani CA, Kim JY, Liu A, Sandoval J, DeVellis J, Casaccia-Bonnefil P. Inhibition of p53 transcriptional activity: a potential target for future development of therapeutic strategies for primary demyelination. *J. Neurosci.* 28 (2008) 6118-6127.

Li Y, Lu H, Cheng PL, Ge S, Xu H, Shi SH, Dan Y. Clonally related visual cortical neurons show similar stimulus feature selectivity. *Nature.* 2012 May 2;486(7401):118-21.

Lightfoot G, Jones N. The relationship between the size of 0+ roach, *Rutilus rutilus*, their swimming capabilities, and distribution in an English river. *Folia Zool.* 1996;44:355-60.

Lin JC, Cepko CL. Biphasic dispersion of clones containing Purkinje cells and glia in the developing chick cerebellum. *Dev Biol.* 1999 Jul 15;211(2):177-97.

Lindsey BW, Darabie A, Tropepe V. The cellular composition of neurogenic periventricular zones in the adult zebrafish forebrain. *J Comp Neurol.* 2012 Jul 1;520(10):2275-316.

Luhmann HJ, Fukuda A, Kilb W. Control of cortical neuronal migration by glutamate and GABA. *Front Cell Neurosci.* 2015 Jan 30;9:4.

Luo L, Callaway EM, Svoboda K (2008) Genetic dissection of neural circuits. *Neuron* 57: 634-660.

Maekawa F, Tsukahara S, Kawashima T, Nohara K, Ohki-Hamazaki H. The mechanisms underlying sexual differentiation of behavior and physiology in mammals and birds: relative contributions of sex steroids and sex chromosomes. *Front Neurosci.* 2014;doi: 10.3389/fnins.2014.00242.

Mak GK, Enwere EK, Gregg C, Pakarainen T, Poutanen M, Huhtaniemi I, Weiss S.(2007) Male pheromone-stimulated neurogenesis in the adult female brain: possible role in mating behavior. *Nat Neurosci*. 2007 Aug;10(8):1003-11.

Mangiamele LA, Keeney AD, D'Agostino EN, Thompson RR. Pheromone exposure influences preoptic arginine vasotocin gene expression and inhibits social approach behavior in response to rivals but not potential mates. *Brain Behav Evol.* 2013;81(3):194-202.

Martinez-Ferre A, Martinez S. Molecular regionalization of the diencephalon. *Front Neurosci.* 2012 May 25;6:73.

Mason W. Ontogeny of Social Behavior. In: Marler P, Vandenbergh JG, editors. Social Behavior and Communication. New York: Plenum Press; 1979. p. 1-28.

Mayer C, Jaglin XH, Cobbs LV, Bandler RC, Streicher C, Cepko CL, Hippenmeyer S, Fishell G. Clonally Related Forebrain Interneurons Disperse Broadly across Both Functional Areas andStructural Boundaries. *Neuron.* 2015 Aug 19. pii: S0896-6273(15)00633-9.

Medina L, Abellán A, Vicario A, Desfilis E. Evolutionary and developmental

contributions for understanding the organization of the basal ganglia. *Brain Behav Evol.* 2014;83(2):112-25. doi: 10.1159/000357832. Epub 2014 Apr 24.

Meletis K, Wirta V, Hede SM, Nister M, Lundeberg J, Frisen J. p53 suppresses the self-renewal of adult neural stem cells. *Development* 133 (2006) 363-369.

Miao G, Hayashi S. Manipulation of gene expression by infrared laser heat shock and its application to the study of tracheal development in Drosophila. *Dev Dyn.* 2015 Mar;244(3):479-87.

Ming GL, Song H. Adult neurogenesis in the mammalian brain: significant answers and significant questions. *Neuron.* 2011 May 26;70(4):687-702.

Montiel JF, Vasistha NA, Garcia-Moreno F, Molnár Z. From sauropsids to mammals and back: New approaches to comparative cortical development. *J Comp Neurol.* 2016 Feb 15;524(3):630-45. doi: 10.1002/cne.23871. Epub 2015 Aug 20.

Moreno N, González A, Rétaux S. Development and evolution of the subpallium. *Semin Cell Dev Biol.* 2009 Aug;20(6):735-43.

Muldal AM, Lillicrap TP, Richards BA, Akerman CJ. Clonal relationships impact neuronal tuning within a phylogenetically ancient vertebrate brain structure. *Curr Biol.* 2014 Aug 18;24(16):1929-33.

Nakamura S, Kobayashi K, Nishimura T, Higashijima S, Tanaka M (2010) Identification of germline stem cells in the ovary of the teleost medaka. *Science* 328: 1561-1563.

Nakazawa N, Taniguchi K, Okumura T, Maeda R, Matsuno K (2012) A novel Cre/loxP system for mosaic gene expression in the Drosophila embryo. *Dev Dyn* 241: 965-974.

Northcutt RG: Connections of the lateral and medial divisions of the goldfish telencephalic pallium. *J Comp Neurol*. 2006; 494(6): 903–943.

Northcutt RG: Forebrain evolution in bony fishes. *Brain Res Bull*. 2008; 75(2–4): 191–205.

O'Connell LA, Hofmann HA. Evolution of a vertebrate social decision-making network. *Science*. 2012 Jun 1;336(6085):1154-7.

O'Connell LA, Hofmann HA. The vertebrate mesolimbic reward system and social behavior network: a comparative synthesis. *J Comp Neurol*. 2011 Dec 15;519(18):3599-639.

Ochiai T, Suehiro Y, Nishinari K, Kubo T, Takeuchi H. A new data-mining method to search for behavioral properties that induce alignment and their involvement in social learning in medaka fish (*Oryzias latipes*). *PLoS One*. 2013;8:e71685.

Ohtsuki G, Nishiyama M, Yoshida T, Murakami T, Histed M, Lois C, Ohki K. Similarity of visual selectivity among clonally related neurons in visual cortex. *Neuron*. 2012 Jul 12;75(1):65-72.

Okuyama T, Suehiro Y, Imada H, Shimada A, Naruse K, Takeda H, Kubo T, Takeuchi H. Induction of c-fos transcription in the medaka brain (*Oryzias latipes*) in response to mating stimuli. *Biochem. Biophys. Res. Commun.* 404 (2011) 453-457.

Okuyama T, Yokoi S, Abe H, Isoe Y, Suehiro Y, Imada H et al.. 2014. A neural mechanism underlying mating preferences for familiar individuals in medaka fish. *Science*. 2014;343:91-4.

Oosumi Noriko (著) 脳の発生・発達―神経発生学入門 (脳科学ライブラリー) 2010, [単行本]

Ostrovsky A, Cachero S, Jefferis G. Clonal analysis of olfaction in Drosophila: image registration. *Cold Spring Harb Protoc*. 2013 Apr 1;2013(4):347-9.

Otsuna H, Hutcheson DA, Duncan RN, McPherson AD, Scoresby AN, Gaynes BF, Tong Z, Fujimoto E, Kwan KM, Chien CB, Dorsky RI. High-resolution analysis of central nervous system expression patterns in zebrafish Gal4 enhancer-trap lines. *Dev Dyn.* 2015 Jun;244(6):785-96.

Peretto P, Paredes RG. Social Cues, Adult Neurogenesis, and Reproductive Behavior. In: Mucignat-Caretta C, editor. Neurobiology of Chemical Communication. Boca Raton (FL): CRC Press/Taylor & Francis; 2014. Chapter 13. Available from: http://www.ncbi.nlm.nih.gov/books/NBK200979/

Pfenning AR, Hara E, Whitney O, Rivas MV, Wang R, Roulhac PL, Howard JT, Wirthlin M, Lovell PV, Ganapathy G, Mouncastle J, Moseley MA, Thompson JW, Soderblom EJ, Iriki A, Kato M, Gilbert MT, Zhang G, Bakken T, Bongaarts A, Bernard A, Lein E, Mello CV, Hartemink AJ, Jarvis ED. Convergent transcriptional specializations in the brains of humans and song-learning birds. *Science.* 2014 Dec 12;346(6215):1256846.

Phelps SM, Rand AS, Ryan MJ. . A cognitive framework for mate choice and species recognition.2006. *Am Nat.* Jan;167(1):28-42.

Puelles L, Kuwana E, Puelles E, Bulfone A, Shimamura K, Keleher J, Smiga S, Rubenstein JL. Pallial and subpallial derivatives in the embryonic chick and mouse telencephalon, traced by the expression of the genes Dlx-2, Emx-1, Nkx-2.1, Pax-6, and Tbr-1. *J Comp Neurol.* 2000 Aug 28;424(3):409-38.

Rakic P. Evolution of the neocortex: a perspective from developmental biology. *Nat Rev Neurosci.* 2009 Oct;10(10):724-35.

Rooke JE, Theodosiou NA, Xu T. Clonal analysis in the examination of gene function in Drosophila. *Methods Mol Biol.* 2000;137:15-22.

Saghatelyan A, de Chevigny A, Schachner M, Lledo PM. Tenascin-R mediates

activity-dependent recruitment of neuroblasts in the adult mouse forebrain. *Nat. Neurosci.* 7 (2004) 347-356.

Sahay A, Scobie KN, Hill AS, O'Carroll CM, Kheirbek MA, Burghardt NS, Fenton AA, Dranovsky A, Hen R. Increasing adult hippocampal neurogenesis is sufficient to improve pattern separation. *Nature*. 2011 Apr 28;472(7344):466-70.

Saito K, Watanabe S. Deficits in acquisition of spatial learning after dorsomedial telencephalon lesions in goldfish. *Behav Brain Res*. 2006 Sep 25;172(2):187-94.

Sakamoto M, Imayoshi I, Ohtsuka T, Yamaguchi M, Mori K, Kageyama R. Continuous neurogenesis in the adult forebrain is required for innate olfactory responses. *Proc Natl Acad Sci U S A*. 2011 May 17;108(20):8479-84.

Sarela AI, Verbeke CS, Ramsdale J, Davies CL, Markham AF, Guillou PJ. Expression of survivin, a novel inhibitor of apoptosis and cell cycle regulatory protein, in pancreatic adenocarcinoma. *Br. J. Cancer* 86 (2002) 886-892.

Sasado T, Tanaka M, Kobayashi K, Sato T, Sakaizumi M, NaruseK. The National BioResource Project Medaka (NBRP Medaka): An Integrated Bioresource for Biological and Biomedical Sciences. *Exp. Anim*. 59 (2010) 13-23.

Sato T, Takahoko M, Okamoto H (2006) HuC:Kaede, a useful tool to label neural morphologies in networks in vivo. *Genesis* 44: 136-142.

Schmidt R, Strähle U, Scholpp S. Neurogenesis in zebrafish - from embryo to adult. *Neural Dev*. 2013 Feb 21;8:3.

Scott EK, Mason L, Arrenberg AB, Ziv L, Gosse NJ, Xiao T, Chi NC, Asakawa K, Kawakami K, Baier H. Targeting neural circuitry in zebrafish using GAL4 enhancer trapping. *Nat Methods*. 2007 Apr;4(4):323-6.

Seki Tatsunori (著), Sawamoto Kazunobu (著). Neurogenesis in the adult brain 1 Neurobiology [ハードカバー] 2010

Seri B, Garcia-Verdugo JM, Collado-Morente L, McEwen BS, Alvarez-Buylla A. Cell types, lineage, and architecture of the germinal zone in the adult dentate gyrus. *J. Comp. Neurol.* 478 (2004) 359-378.

Sherr CJ, Roberts JM. Inhibitors of mammalian G1 cyclin-dependent kinases. *Genes Dev.* 9 (1995) 1149-1163.

Shimizu A, Shimizu N (2012) Dual promoter expression system with insulator ensures a stringent tissue-specific regulation of two reporter genes in the transgenic fish. *Transgenic Res.* 2013 Apr;22(2):435-44.

Snoeren EM, Ågmo A. The role of odors and ultrasonic vocalizations in female rat (Rattus norvegicus) partner choice. *J Comp Psychol.* 2014;128:367-77.

Song L, Crawford GE. DNase-seq: a high-resolution technique for mapping active gene regulatory elements across the genome from mammalian cells. *Cold Spring Harb. Protoc*. 2010 pdb.prot5384 (2010).

Storer NY, Zon LI. Zebrafish Models of p53 Functions. Cold Spring Harb. *Perspect Biol*. 2 (2010) a001123.

Strange BA, Witter MP, Lein ES, Moser EI. Functional organization of the hippocampal longitudinal axis. *Nat Rev Neurosci*. 2014 Oct;15(10):655-69.

Suehiro Y, Kinoshita M, Okuyama T, Shimada A, Naruse K, et al. (2010) Transient and permanent gene transfer into the brain of the teleost fish medaka (Oryzias latipes) using human adenovirus and the Cre-loxP system. *FEBS Lett* 584: 3545-3549.

Suehiro Y, Yasuda A, Okuyama T, Imada H, Kuroyanagi Y, Kubo T, Takeuchi H. Mass

spectrometric map of neuropeptide expression and analysis of the gamma-prepro-tachykinin gene expression in the medaka (*Oryzias latipes*) brain. *Gen. Comp. Endocrinol.* 161 (2009) 138-145.

Sugahara F, Aota S, Kuraku S, Murakami Y, Takio-Ogawa Y, Hirano S, Kuratani S. Involvement of Hedgehog and FGF signalling in the lamprey telencephalon: evolution of regionalization and dorsoventral patterning of the vertebrate forebrain. *Development*. 2011 Mar;138(6):1217-26.

Sur M, Rubenstein JL. Patterning and plasticity of the cerebral cortex. *Science.* 2005 Nov 4;310(5749):805-10.

Suzuki M, Toyoda N, Takagi S. Pulsed irradiation improves target selectivity of infrared laser-evoked gene operator for single-cell gene induction in the nematode C. elegans. *PLoS One*. 2014 Jan 20;9(1):e85783.

Szele FG, Cepko CL. A subset of clones in the chick telencephalon arranged in rostrocaudal arrays. *Curr Biol*. 1996 Dec 1;6(12):1685-90.

Takayanagi Y, Yoshida M, Bielsky IF, Ross HE, Kawamata M, Onaka T et al.. Pervasive social deficits, but normal parturition, in oxytocin receptor-deficient mice. *Proc Natl Acad Sci USA*. 2005;102:16096–101.

Talos F, Abraham A, Vaseva AV, Holembowski L, Tsirka SE, Scheel A, Bode D, Dobbelstein M, Bruck W, Moll UM. p73 is an essential regulator of neural stem cell maintenance in embryonal and adult CNS neurogenesis. *Cell Death Differ.* 17 (2010) 1816-1829.

Taniguchi Y, Takeda S, Furutani-Seiki M, Kamei Y, Todo T, Sasado T, Deguchi T, Kondoh H, Mudde J, Yamazoe M, Hidaka M, Mitani H, Toyoda A, Sakaki Y, Plasterk RH, Cuppen E. Generation of medaka gene knockout models by target-selected mutagenesis. *Genome Biol* 7 (2006) R116.

Than-Trong E, Bally-Cuif L. Radial glia and neural progenitors in the adult zebrafish central nervous system. *Glia*. 2015 Aug;63(8):1406-28.

Vopalensky P, Ruzickova J, Pavlu B, Kozmik Z (2010) A lens-specific co-injection marker for medaka transgenesis. *Biotechniques* 48: 235-236.

Wan Y, Otsuna H. Chien CB, Hansen C. An interactive visualization tool for multi-channel confocal microscopy data in neurobiology research. 2009. *IEEE Trans. Vis. Comput. Graph.* 15, 1489-1496

Ward A, Axford S, Krause J. Cross–species familiarity in shoaling fishes. *Proc. R. Soc. B*. 2003;270:1157-61.

Westerfield M (2000) The zebrafish book. A guide for the laboratory use of zebrafish (Danio rerio).

Wilson SW, Rubenstein JL. Induction and dorsoventral patterning of the telencephalon. *Neuron*. 2000 Dec;28(3):641-51.

Wittbrodt J, Shima A, Schartl M (2002) Medaka - A model organism from the Far East. *Nature Reviews Genetics* 3: 53-64.

Wu JH, Han YT, Yu JY, Wang TW. (2013) Pheromones from males of different familiarity exert divergent effects on adult neurogenesis in the female accessory olfactory bulb. *Dev Neurobiol.* 2013 Aug;73(8):632-45.

Wu Z, Autry AE, Bergan JF, Watabe-Uchida M, Dulac CG. Galanin neurons in the medial preoptic area govern parental behaviour. *Nature.* 2014 May 15;509(7500):325-30.

Wyart C, Del Bene F, Warp E, Scott EK, Trauner D, et al. (2009) Optogenetic dissection

of a behavioural module in the vertebrate spinal cord. *Nature* 461: 407-410.

Xu G, Deng N, Zhao Z, Judeh T, Flemington E, Zhu D. SAMMate: a GUI tool for processing short read alignments in SAM/BAM format. *Source Code Biol Med.* 2011 Jan 13;6(1):2.

Yang B, Treweek JB, Kulkarni RP, Deverman BE, Chen CK, Lubeck E, Shah S, Cai L, Gradinaru V. Single-cell phenotyping within transparent intact tissue through whole-body clearing. *Cell.* 2014 Aug 14;158(4):945-58.

Yasumasu S, Iuchi I, Yamagami K (1989) Purification and partial characterization of high choriolytic enzyme (HCE), a component of the hatching enzyme of the teleost, Oryzias latipes. *J Biochem* 105: 204-211.

Yizhar O, Fenno LE, Davidson TJ, Mogri M, Deisseroth K (2011) Optogenetics in neural systems. *Neuron* 71: 9-34.

Yokoi S, Okuyama T, Kamei Y, Naruse K, Taniguchi Y, Ansai S et al.. An essential role of the arginine vasotocin system in mate-guarding behaviors in triadic relationships of medaka fish (*Oryzias latipes*). *PLoS Genet.* 2015;11:e1005009.

Yu HH, Awasaki T, Schroeder MD, Long F, Yang JS, He Y, Ding P, Kao JC, Wu GY, Peng H, Myers G, Lee T. Clonal development and organization of the adult Drosophila central brain. *Curr Biol*. 2013 Apr 22;23(8):633-43.

Yu YC, Bultje RS, Wang X, Shi SH. Specific synapses develop preferentially among sister excitatory neurons in the neocortex. *Nature*. 2009 Mar 26;458(7237):501-4.

Yu YC, He S, Chen S, Fu Y, Brown KN, et al. (2012) Preferential electrical coupling regulates neocortical lineage-dependent microcircuit assembly. *Nature* 486: 113-117.

Zervas M, Blaess S, Joyner AL. Classical embryological studies and modern genetic

analysis of midbrain and cerebellum development. *Curr Top Dev Biol.* 2005;69:101-38.

Zupanc GK (2008) Adult neurogenesis and neuronal regeneration in the brain of teleost fish. *J Physiol Paris* 102: 357-373.

Zupanc GK, Hinsch K, Gage FH. Proliferation, migration, neuronal differentiation, and long-term survival of new cells in the adult zebrafish brain. *J. Comp. Neurol.* 488 (2005) 290-319.

Zupanc GK, Horschke I. Proliferation zones in the brain of adult gymnotiform fish: a quantitative mapping study. *J. Comp. Neurol.* 353 (1995) 213-233.

Zupanc GK, Sirbulescu RF. Adult neurogenesis and neuronal regeneration in the central nervous system of teleost fish. Eur. *J. Neurosci.* 34 (2011) 917-929.

Zupanc GK. Adult Neurogenesis and Neuronal Regeneration in the Teleost Fish Brain. *J. Physiol. Paris* 102 (2008) 357-373.

Acknowledgement

I would like to express my deepest and sincere gratitude to my supervisors, Dr. Takeo Kubo (Professor, the University of Tokyo) and Dr. Hideaki Takeuchi (Associate professor, Okayama University) for providing me with the best environment to research with freedom, brilliant inspiration, continuous encouragement, enthusiasm, and personal guidance. Their logical way of thinking and their great efforts to train my presentation skill have had a remarkable influence on my attitude toward "science" in my entire career.

I would like to express my gratitude to Dr. Hiroyuki Takeda (Professor, the University of Tokyo), Dr. Kei Itoh (Associate Professor, Institute of Molecular and Cellular Biosciences, The University of Tokyo), Dr. Yasuhiro Kamei (Associate Professor, National Institute for Basic Biology), Dr. Shigenori Nonaka (Associate Professor, National Institute for Basic Biology), Dr Ryohei Nakamura (Assistant Professor, the University of Tokyo), Dr, Teruhiro Okuyama (Post-Doc, MIT) for not only collaborations but also giving me constructive comments and warm encouragements.

I would like to thank GPLLI (Graduate Program for Leaders in Life Innovation) for giving me some wonderful chances to study abroad, broaden my academic relationships, and financial supports.

I would like to thank my kind and brilliant lab members for encouraging me and supporting me through my PhD program.

Finally, I would like to express my endless thankfulness to my dearest parents. They have always encouraged me, raised me, taught me, supported me, and loved me anytime. I dedicate this doctoral thesis to them.